Abstract

Utrophin upregulation and microRNAs – two avenues of Duchenne muscular dystrophy therapy research

Akshay Bareja, Exeter College, University of Oxford

Submitted for the degree of Doctor of Philosophy, Michaelmas Term, 2010

Characterized by the severe progressive wastage of skeletal muscle, Duchenne muscular dystrophy (DMD) is a crippling X-linked recessive disease that is caused by the absence of the protein dystrophin. This thesis aimed to critically evaluate the potential of different therapeutic options to combat this disease. *Utrophin* is a paralogue of *dystrophin*. The *Fiona* mouse is an *mdx* (dystrophin-deficient) transgenic mouse that overexpresses the full-length utrophin protein in skeletal muscle, and various studies have shown that it does not display a dystrophic phenotype. However, these studies have only been performed on sedentary mice. In this work it is demonstrated that utrophin's protective effect is partially diminished after a sustained period of exercise-induced stress, highlighting for the first time a functional difference between dystrophin and utrophin. This thesis also presents results of two *mdx* mouse drug trials testing the ameliorative effects of the administration of the drugs GW501516 and C1100, which show that treatment with both drugs results in partial amelioration of the dystrophic phenotype. GW501516 administration results in a beneficial fast-to-slow fibre type switch and an *in vivo* increase in utrophin protein levels. We have also shown that C1100 treatment results in a significant increase in utrophin A promoter activity *in vitro*, and the mechanism of action of this drug on this promoter has been deciphered. The global dysregulation of microRNAs in skeletal muscle of *mdx* and *dko* (dystrophin- and utrophin-deficient) mice was evaluated by microarray analysis to identify microRNAs involved in the dystrophic pathological cascades. The results of detailed expression analyses of miR-31, miR-206 and miR-503 are presented, and two therapeutically-relevant predicted targets of miR-503 were validated. Overall, this thesis evaluates the potential of different and possibly complementary therapeutic options to combat DMD.

Declaration

The work presented in this thesis was performed in the Department of Physiology, Anatomy and Genetics, University of Oxford, between 2007 and 2010. Except where acknowledgement is made, all the work presented is my own and has not been submitted for any other degree in this or any other university or institute of learning.

Acknowledgements

I am deeply indebted to Professor Dame Kay Davies for supporting me at every stage of my DPhil degree, right from helping me obtain my scholarship to proofreading my thesis manuscript. She has helped me develop my ideas and critically assess my results, all while displaying immense levels of patience. I also could not have done this degree without the munificence of the Oxford University Press and Exeter College, who provided me with a Clarendon bursary and Kokil Pathak scholarship respectively.

Dr. Rebecca Fairclough has taught me almost every laboratory technique I know and has spent many hours discussing new papers and plans for future experiments. I have thoroughly enjoyed working with her and the rest of the "utrophin group", which includes Sarah Squire, Allyson Potter and Dave Powell. Ben Edwards, Arran Babbs, Dr. Peter Oliver, Dr. Esther Becker, Dr. Emmanuelle Bitoun and Dr. Aurelie Goyenvalle have always been available to give advice when experiments went wrong and have patiently answered all my inane questions.

No thesis submitted from this lab is complete without acknowledging the baking skills of Dr. Carmen Coxon. She has also provided me with invaluable advice on science and life in general.

The work presented in Chapter 6 was performed in collaboration with Dr. Sheena Lee, who performed the microarray analysis. I am also grateful to Tom Roberts and Dr. Matthew Wood for sharing their expert knowledge of microRNAs.

Sharing an office with Arran, Ally, Sarah, Dave, Ben, Viv and Tom has made the last three years go by astonishingly quickly. I cannot imagine having had a more enjoyable and laughter-filled three years.

I have had the good fortune of having met and befriended many wonderful people during my time in Oxford, and will miss them all when I leave. I would also like to thank my parents and grandmother. Finally, I would like to thank Professor Sarah Gurr for having provided me with support and encouragement right from my first day as an undergraduate.

Table of contents

List of figures and tables

List of abbreviations

%CNFs	Percentage of centrally-nucleated fibres
3’ UTR	3’ untranslated region
AAV	Adeno-associated virus
AChR	Acetylcholine receptor
ANOVA	One-way analysis of variance
AO	Antisense oligonucleotide
APS	Ammonium persulfate
CaM	Calmodulin
CK	Creatine kinase
DAPC	Dystrophin associated protein complex
DMD	Duchenne muscular dystrophy
D-MEM	Dulbecco’s Modified Eagle’s Medium
DMSO	Dimethyl sulfoxide
ECM	Extracellular matrix
EDL	Extensor digitorum longus
F-actin	Filamentous actin
FCS	Fetal calf serum
GABP	GA-binding protein
GRMD	Golden retriever dog model
IBD	Inflammatory bowel disease
IF	Intermediate filament
IGF	Insulin-like growth factor
IP	Intraperitoneal
IPA	Ingenuity Pathway Analysis
L_f	Fibre length
LGMD	Limb girdle muscular dystrophy

L_o	Optimum length
MCK	Muscle creatine kinase
MCS	Multiple cloning site
MEF	Myocyte enhancer factor
Mgst1	*Microsomal glutathione S-transferase 1*
MHC	Myosin heavy chain
miRNA	MicroRNAs
MRF	Myogenic regulatory factor
MSC	Marrow-derived mesenchymal stem cell
MT	Myoblast transplantation
MTJ	Myotendinous junction
Myb	*Myeloblastosis oncogene*
NFAT	Nuclear factor of activated T cells
NMJ	Neuromuscular junction
nNOS	Neuronal nitric oxide synthase
NO	Nitric oxide
PBS	Phosphate buffered saline
P_{CT}	Probability of conserved targeting
Pen-strep	Penicillin-Streptomycin solution
PGC-1α	PPAR-γ coactivator-1α
pol II	RNA polymerase II
PPAR	Peroxisome proliferator-activated receptor
Pre-miRNA	Precursor-microRNA
Pri-miRNA	Primary-microRNA
qPCR	Quantitative PCR
RISC	RNA-induced silencing complex
RNAi	RNA interference

RT	Room temperature
$RT_{1/2}$	Half-relaxation time
SDM	Site-directed mutagenesis
SDS	Sodium dodecyl sulphate
siRNA	Small interfering RNA
Soc6	*Suppressor of cytokine signalling 6*
TA	Tibialis anterior
TBS-T	Tris-buffered saline with 1% tween
TEMED	Tetramethylethylinediamine
TTP	Time to peak
T-tubules	Transverse tubules

1 Introduction

1.1 Duchenne Muscular Dystrophy

Duchenne muscular dystrophy (DMD) is an X-linked recessive disease that afflicts one in every 3,300 males. It is caused by the absence of the protein dystrophin. DMD patients exhibit symptoms around 3-5 years of age of abnormal gait, calf muscle pseudohypertrophy (O'Brien and Kunkel, 2001) and the characteristic Gowers sign (weakness of the proximal muscles, particularly those of the lower limb) (Manzur and Muntoni, 2009). Respiratory complications, including sleep-disordered breathing and apnoea, arise during the teenage years resulting in headaches, nausea, fatigue and poor appetite. Patients are usually wheelchair-bound by 12 years of age (Nowak and Davies, 2004). Dilated cardiomyopathy of varying severity affects close to 90% of patients above the age of 18 years, and is currently responsible for the death of approximately 20% of all DMD patients. The development of scoliosis is coincident with permanent wheelchair use, rapidly progressing during puberty and adversely affecting respiratory function (Manzur and Muntoni, 2009). Many patients die of respiratory failure in their twenties (O'Brien and Kunkel, 2001). Becker muscular dystrophy is a milder disease caused by the reduced expression of dystrophin or expression of a partially functional protein (Davies and Nowak, 2006).

1.1.1 Dystrophin and the Dystrophin Associated Protein Complex

Dystrophin is a 427-kDa protein that is comprised of four domains: the N-terminal domain (which binds actin), the rod domain (which consists of 26 spectrin-like repeats), a cysteine-rich domain and a C-terminal domain (Koenig et al., 1988).

Skeletal muscle is made up of thousands of muscle fibres (myofibres), each of which is surrounded by a plasma membrane (sarcolemma) and an overlying basal lamina. Dystrophin is expressed in skeletal muscle at the sarcolemma and is enriched at the myotendinous junction (or MTJ, which is the junction of muscle fibres and tendons) and the neuromuscular junction (or NMJ, which is the junction of a motor neuron with a muscle fibre) (Khurana et al., 1991). Dystrophin binds to filamentous (F)-actin (a

constituent member of the cytoskeleton) via its N-terminus and a cluster of basic repeats 11-17 in its rod domain (Amann et al., 1999), and binds dystroglycan via its cysteine-rich domain, and α-dystrobrevin and α-syntrophin via its C-terminal domain. Dystroglycan, α-dystrobrevin and α-syntrophin are all members of the dystrophin associated protein complex (DAPC). Figure 1.1 illustrates the mechanical link dystrophin creates between the internal cytoskeleton and the external extracellular matrix (ECM) (Davies and Nowak, 2006).

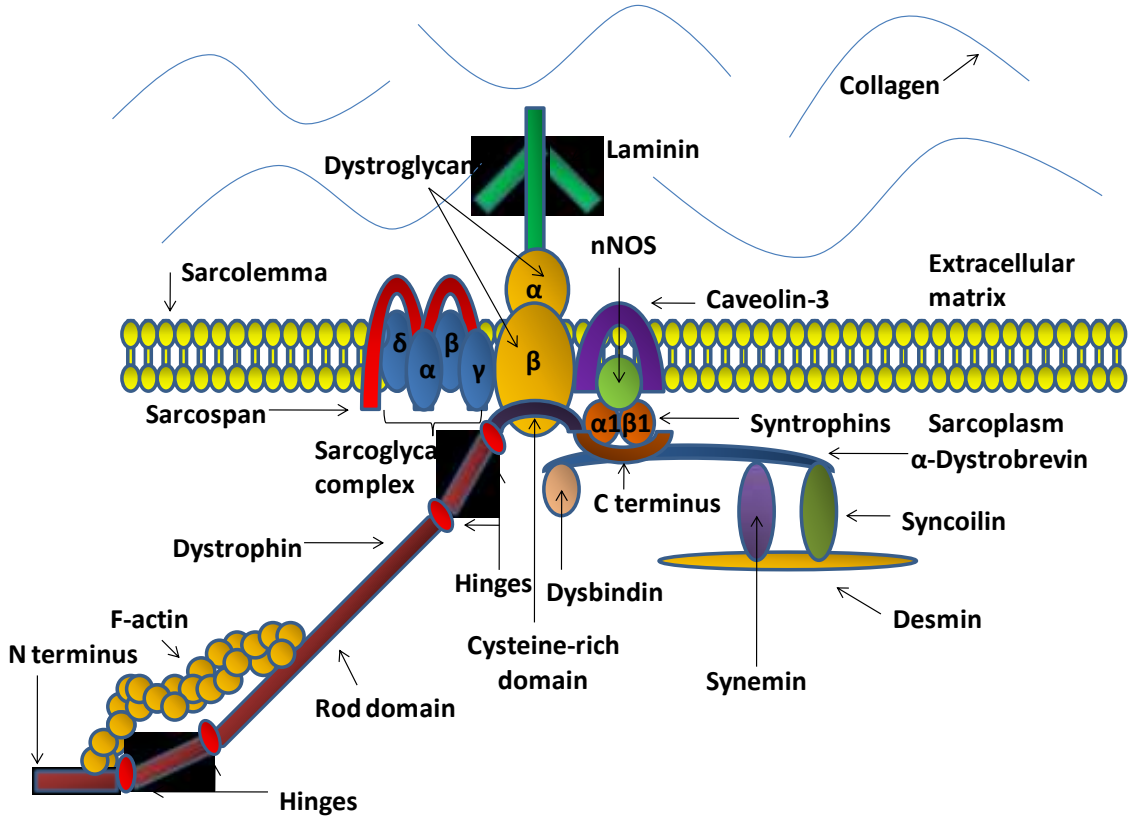

Fig. 1.1 The dystrophin-associated protein complex in skeletal muscle. Adapted from (Davies and Nowak, 2006).

The main function of dystrophin is to stabilize the sarcolemma. Due to the elasticity and flexibility of its large central rod domain consisting of triple helical repeats, dystrophin has been proposed to protect the myofibre from contraction-induced stress(Grum et al., 1999). It has also been shown to form a mechanically strong link between the sarcolemma and the internal cytoskeleton via its interaction with gamma-actin filaments (Rybakova et al., 2000). In addition to its mechanical role, dystrophin has also been

proposed to be involved in signalling pathways, such as inhibiting muscle atrophy pathways (Glass, 2005).

Besides dystrophin, many of the other constituents of the DAPC have been shown to have important structural or signalling roles. Most members of the DAPC can be divided into three subcomplexes – the dystroglycan complex, the sarcoglycan complex and the cytoplasmic complex (which includes the dystrobrevins and the syntrophins). The dystroglycan complex consists of covalently-linked α- and β-subunits which are post-translationally derived from a common mRNA transcript (Williamson et al., 1997). α-dystroglycan binds to ECM proteins such as laminin, agrin and perlecan (Campanelli et al., 1994; Ervasti and Campbell, 1993; Talts et al., 1999) and β-dystroglycan binds to both dystrophin and α-dystrobrevin.(Royuela et al., 2003). Dystroglycan-null mice are embryonic lethal, and display a marked impairment in the formation of the basement membrane (Williamson et al., 1997). Skeletal muscle-specific knockout of dystroglycan in mice results only in mild dystrophy despite the loss of the DAPC complex. This mild phenotype has been attributed to efficient regeneration as a result of satellite cells (myogenic stem cells located beneath the basement membrane of muscle cells) that still express dystroglycan (Cohn et al., 2002). No human disease has so far been linked to dystroglycan mutations. The dystroglycans are subject to significant post-translational modification, particularly glycosylation. Decreased glycosylation in α- but not β-dystroglycan has been shown to be the cause of a range of muscular dystrophies (Brockington et al., 2001; Jimenez-Mallebrera et al., 2009; Kobayashi et al., 1998; Longman et al., 2003).

The sarcoglycan complex consists of six glycosylated subunits (α, β, γ, δ, ε and ζ), of which only the first four show muscle-specific expression. Each protein has a membrane-spanning domain, an extracellular domain (N-terminal in the case of α-sarcoglycan, and C-terminal in the case of β-,γ- and δ-sarcoglycan), and an intracellular domain. The sarcolgycan complex does not bind directly to dystrophin but binds to β-dystroglycan and sarcospan. The sarcoglycan complex is proposed to have both a mechanical role, because the absence of this complex results in the weakening of the bonds between dystrophin and β-dystroglycan and between β- and α-dystroglycan, and a signalling role,

because of the presence of intramolecular -S-S-bonds in each subunit, which is indicative of receptor function. Mutations in any one subunit have been shown to not only result in the absence of or reduced expression of that subunit but also reduced expression of the entire complex (Ozawa et al., 2005). Mutations in the α-, β-, γ- and δ-subunits have been shown to cause limb girdle muscular dystrophy (LGMD) types 2D, 2E, 2C and 2F respectively (Lim et al., 1995; McNally et al., 1996; Nigro et al., 1996a; Nigro et al., 1996b; Piccolo et al., 1995; Roberds et al., 1994).

α-dystrobrevin and the syntrophins are key members of the cytoplasmic complex. α-dystrobrevin binds to dystrophin, syntrophin and the intermediate filament (IF) proteins synemin, dysbindin, and syncoilin. There are many alternatively spliced forms of α-dystrobrevin, of which only α-DB-1 and α-DB-2 are expressed in muscle. *adbn*$^{-/-}$ mice only have a mild skeletal and cardiac-muscle disease phenotype with the rest of the DAPC remaining intact. The phenotype of these mice resembles that of the dystrophin-deficient *mdx* mice, with fewer centrally-nucleated fibres (which is an index of the levels of degeneration and regeneration). Unlike *mdx* mice, however, the DAPC in these mice remains intact and only displays a marked reduction in the expression of neuronal nitric oxide synthase (nNOS), which is known to have important signalling roles. Therefore, α-dystrobrevin appears to play more of a signalling role than a structural one (Grady et al., 1999). Mutations in α-dystrobrevin have been shown to result in dilated hypertrophic cardiomyopathy in human patients (Ichida et al., 2001). Syntrophin binds to signalling proteins like nNOS, sodium channels and serine/threonine kinases. It links these molecules to the ECM via dystrophin and to the actin cytoskeleton. *syn*$^{-/-}$ mice do not display a muscular dystrophy phenotype but have abnormal NMJs with reduced levels of acetylcholine receptor (AChR) and acetylcholinesterase. These mice also show no expression of nNOS at the postsynaptic membrane and the sarcolemma (Adams et al., 2000).

The DAPC forms associations with the intermediate filament proteins dysbindin, synemin and syncoilin, all of which were discovered as novel binding partners of α-dystrobrevin. The DAPC also forms an indirect association with the muscle-specific IF protein desmin. Desmin is localized at the Z-disk of the sarcomere and has been shown to

be attached to this structure via its interaction with the sarcomeric protein nebulin (Tonino et al., 2010). Although not necessary for the development of skeletal, cardiac and smooth muscles, desmin has been shown to be required for the maintenance of these tissues (Li et al., 1996). Mutations in this protein have also been shown to result in cardiac and skeletal myopathy in human patients (Goldfarb et al., 1998; Mu et al., 1998). Dysbindin is a coiled-coil-containing protein whose binding to α-dystrobrevin has been proposed to be another means of localizing this protein to the muscle sarcolemma (Benson et al., 2001). Synemin physically interacts with both α-dystrobrevin and desmin, thereby providing an additional link between the DAPC and the sarcomere (Mizuno et al., 2001). Syncoilin, which is highly expressed in both cardiac and skeletal muscle (Newey et al., 2001), also binds to both α-dystrobrevin and desmin (Poon et al., 2002). However, the absence of syncoilin in mice does not lead to changes in either the expression or localization of α-dystrobrevin or desmin (McCullagh et al., 2008). Skeletal muscle from *sync*$^{-/-}$ mice is largely normal, only displaying a reduction in the capacity to generate maximum isometric force compared to wild-type controls (Zhang et al., 2008).

Caveolin-3 and nNOS are two other important members of the DAPC. Caveolin-3 is the major component of caveolae, which are specialized lipid rafts. Caveolin-3 binds to the same site of β-dystroglycan as dystrophin. It is also located at transverse (T)-tubules (deep invaginations of the plasma membrane into the muscle cell), which explains why caveolin-3 null mice display T-tubule defects (Galbiati et al., 2001). It also functions to inhibit nNOS (Venema et al., 1997). nNOS is an enzyme that produces nitric oxide (NO), which is known to have cytoprotective and anti-inflammatory effects. The aberrant expression of nNOS in DMD muscle is therefore thought to contribute to pathology. The overexpression of nNOS against an *mdx* background results in partial amelioration of disease phenotype (Wehling et al., 2001).

1.1.2 Pathophysiological consequences of dystrophin absence

The absence of dystrophin, and hence the impaired recruitment of the members of the DAPC to the sarcolemma, sets up a pathophysiological cascade with numerous adverse downstream effects. Since the primary function of dystrophin is to stabilize the sarcolemma, its absence renders the sarcolemma vulnerable to damage-inducing factors

(Hoffman and Dressman, 2001). As the affected organism grows in size, increased amounts of stress are imposed on the sarcolemma as a result of increased load and force generation. The resulting membrane instability has many deleterious consequences. Transient tears in the membrane promote the unregulated influx of Ca^{2+} ions into the sarcoplasm which is thought to have toxic effects primarily via its effect on mitochondrial genes. These transient breaks are also thought to allow cytotoxic macrophages to infiltrate the myofibres (Ichim et al., 2010). The continuous degeneration and regeneration of muscle tissue as a result of stress factors has been suggested to be responsible for elevated levels of fibrosis as exemplified by excess collagen deposition (Morrison et al., 2000). The lack of dystrophin, and hence α-syntrophin, results in the downregulation and relocalization of nNOS at the sarcolemma. nNOS activity is thought to counter the vasoconstrictive response of the muscle, particularly during periods of exercise. The dysregulation of blood flow as a result of its absence is therefore thought to result in functional ischaemia (Hoffman and Dressman, 2001). One study suggests that the absence of dystrophin results in the downregulation of Akt, which normally functions to inhibit MuRF1 and MAFbx, which are factors that are involved in muscle atrophy (Acharyya et al., 2005). This study also showed that a loss of dystrophin expression leads to aberrant glycosylation of β-dystroglycan and β-sarcoglycan, both of which are key members of the DAPC.

1.2 Utrophin

Utrophin (originally known as dystrophin-related protein) is an autosomal protein encoded by a gene on chromosome 6 in humans and chromosome 10 in mice (Buckle et al., 1990). Initial sequencing of the 13-kb full-length transcript highlighted numerous similarities between utrophin and dystrophin, prompting the suggestion that they are derived from a common ancestral gene (Tinsley et al., 1992). Evolutionary analysis indicated that utrophin and dystrophin arose from a duplication event early in vertebrate evolution, making them paralogues of each other (Pearce et al., 1993; Roberts and Bobrow, 1998). The full-length protein has 3,433 amino acids with a predicted molecular mass of 395 kDa (compared to 3,678 amino acids and 427 kDa for dystrophin). The primary structure of utrophin is very similar to that of dystrophin, with the N-terminal

and C-terminal domains displaying significant structural similarity (Blake et al., 2002). Unlike dystrophin, utrophin displays ubiquitous expression in the body, displaying strong expression in skeletal, cardiac and smooth muscle cells, Schwann cells of the peripheral nerves, and the lungs and kidney. Unlike dystrophin, which is expressed throughout the sarcolemma of adult skeletal muscle cells, utrophin is only expressed at the NMJ and MTJ. However, utrophin is expressed across the entire sarcolemma in developing and regenerating muscle (Khurana et al., 1991; Pons et al., 1993).

Due to the similarity between the major functional domains of dystrophin and utrophin, they share many of the same binding partners. The C-terminus of utrophin has been shown to bind to members of the DAPC, such as α-dystrobrevin-1 (Peters et al., 1998) and β-dystroglycan, although the mode of contact is different from that of dystrophin's (Ishikawa-Sakurai et al., 2004). Also like dystrophin, utrophin binds to cytoskeletal F-actin. However, as in the case of β-dystroglycan-binding, the mode of contact is different. Although both bind to actin via their N-termini, utrophin also binds to actin via its first 10 spectrin-like repeats, whereas dystrophin binds via a more distant domain involving spectrin repeats 11-17. It has been proposed that this makes the actin-dystrophin-sarcolemma linkage more elastic and flexible than the corresponding linkage involving utrophin (Prochniewicz et al., 2009).

1.2.1 A comparison of the promoters of dystrophin and utrophin

The full-length dystrophin transcript is expressed in muscle, brain and cerebellar Purkinje cells under the influence of different promoters (O'Brien and Kunkel, 2001). These promoters drive the expression of transcripts with different 5' untranslated regions and first exons (Blake and Kroger, 2000). In addition, there exist shorter transcripts expressed in the retina (Dp260) (Dsouza et al., 1995), brain and kidney (Dp140) (Lidov et al., 1995), Schwann cells (Dp116) (Byers et al., 1993) and many nonmuscle tissues (Dp71) (Rapaport et al., 1992). As with the *dystrophin* gene, the *utrophin* gene is under the regulatory influence of multiple promoters. Promoters A and B regulate the production of two alternative full-length transcripts, named utrophin A and utrophin B respectively (Burton et al., 1999). Also as with dystrophin, there exist shorter isoforms of utrophin –

Up140, Up116, Up109 and Up71 - each of whose expression is driven by an independent intron-localized promoter (Khurana and Davies, 2003).

Analysis of the human dystrophin muscle promoter revealed the existence of motifs that are known to play important roles in muscle biology, including two E-box sites (which bind helix-loop-helix transcription factors like MyoD1) an AP1 site (which has been shown to contribute to muscle-specific expression) and a myocyte enhancer factor-1 (MEF-1) site (Fracasso and Patarnello, 1998). This promoter also has a CArG element present which binds the serum response factor and dystrophin-promoter binding factor, which induces the expression of dystrophin during muscle cell differentiation (Galvagni et al., 1997). The utrophin A promoter (which orchestrates the expression of utrophin in the muscle) is located within a CpG island 5' to the utrophin locus. This promoter, unlike the dystrophin muscle promoter, lacks the commonly found eukaryotic TATA or CAAT motifs. Original mouse and human promoter analysis revealed the existence of an E-box (found in many genes involved in muscle development), an N-box (a motif found in many genes expressed at the NMJ) and numerous Sp1 binding sites (Dennis et al., 1996). Subsequent analyses highlighted the existence of other important motifs such as the nuclear factor of activated T cells (NFAT) binding site (Chakkalakal et al., 2003). This promoter drives the synapse-specific expression of utrophin. The regulation of utrophin expression in the muscle via the utrophin A promoter is described in the following section.

1.2.2 Regulation of utrophin A expression

The utrophin A promoter plays a particularly important role in regulating the expression of utrophin at the synapse. The N-box motif plays a central role in this synapse-specific expression (and was originally shown to drive the synapse-specific expression of the AChR δ-subunit gene (Koike et al., 1995). Ets-related transcriptional factors known as GA-binding protein α (GABP α) and β (GABP β) have been shown to bind to the N-box to induce utrophin A transcription. The nerve-derived trophic factor heregulin interacts with ErbB tyrosine kinase receptors to activate GABPα and GABPβ via the extracellular signal-related kinase pathway (Gramolini et al., 1999; Khurana et al., 1999). The utrophin A promoter also has sites that are targeted by the zinc finger-containing

transcription factors, Sp1 and Sp3. These factors have been shown to cooperate with GABP to activate transcription (Galvagni et al., 2001). In addition to these factors, the peroxisome proliferator-activated receptor-γ (PPAR-γ) coactivator-1α (PGC-1α), which is involved in the formation of slow-twitch fibres (Lin et al., 2002), cooperates with GABPα to activate utrophin A transcription (Angus et al., 2005).

In addition to factors that orchestrate the synaptic expression of utrophin A, there are other mechanisms that are responsible for its expression in skeletal muscle tissue. Utrophin A has been shown to be preferentially expressed in muscle containing fibres that primarily use oxidative metabolism (type I) compared to muscle containing fibres that are glycolytic (type II). Calcineurin, which plays a key role in the slow myogenic program, has been shown to increase utrophin A mRNA levels in mouse slow muscle fibres (Chakkalakal et al., 2003). Calcineurin is thought to exert this effect at least partially through the activation of the NFAT transcription factor. The utrophin A promoter has an NFAT binding site that has been shown to mediate the effects of NFAT on utrophin A transcription (Angus et al., 2005).

1.3 Animal models of DMD

1.3.1 *mdx* mouse models

There are many mouse models of DMD. Along with the original dystrophin-deficient mouse (*mdx*) mouse, there are derivative mutant models that also display the absence of expression of other key genes involved in muscle development and function, such as *MyoD*, *α-dystrobrevin*, and *integrin* (Grady et al., 1999; Guo et al., 2006; Megeney et al., 1996).

1.3.1.1 mdx *mouse*

The most widely used DMD mouse model is the *mdx* mouse, which is a naturally occurring mutant that has a premature stop codon in exon 23 of its *dystrophin* gene due to a point mutation, resulting in the complete absence of full-length dystrophin expression (Sicinski et al., 1989). Muscle degeneration follows a characteristic progression in the *mdx* mouse, beginning with a sharp increase in myofibre necrosis and

elevated serum creatine kinase levels around 3 weeks of age, which decreases in severity to a chronic low level of damage by 8 weeks of age. This persists until about 1 year of age following which there is a further reduction in the levels degeneration. Despite being the exact murine genetic analogue of human DMD patients, *mdx* mice do not display a disease phenotype that is as severe as that of DMD patients. For example, they do not show any impairment in mobility throughout their lifetime and, with the exception of the diaphragm, their skeletal muscles do not display similar levels of fibrosis. This is most likely due to the compensatory function of utrophin and the greater capacity of *mdx* muscle to regenerate than muscle from DMD patients (Grounds et al., 2008; Turk et al., 2005; Willmann et al., 2009).

Although the *mdx* mouse is similar to its human counterpart at the genetic and molecular levels, it does not display any of the gross symptoms that are characteristic of the disease, such as growth retardation, impaired mobility and kyphosis (curvature of the upper spine). This has led to some reservation about using the *mdx* mouse as an accurate model of the disease. In order to create a more accurate murine analogue of the human disease, many research groups have in recent times made use of exercise-induced stress to exacerbate the dystrophic phenotype (Luca, 2002, 2005). Exercised *mdx* mice display a more severe phenotype, characterized by a significant reduction in body mass, forelimb strength, increased centronucleated muscle fibres displaying a greater degenerating area, and higher creatine kinase levels (Luca, 2005). In contrast, wild-type mice are not affected by the same levels of stress.

1.3.1.2 mdx^{2Cv}-mdx^{5Cv} *mice*

Following the discovery of the *mdx* mouse, a series of *mdx* variants was generated using N-ethyl-nitrosourea mutagenesis (Chapman et al., 1989). These mice are phenotypically similar to *mdx* mice but display higher variation in fibre size. The *mdx*^{3Cv} mouse has an advantage over the *mdx* mouse in that it displays the absence of expression of all the dystrophin isoforms, whereas the *mdx* mouse only lacks the expression of full-length dystrophin (Vaillend and Ungerer, 1999). However, the problem with these mice is that they breed poorly and display reduced neonatal survival (Willmann et al., 2009).

1.3.1.3 mdx52 *mouse*

The *mdx52* was generated in response to the criticism that none of the *mdx* models at the time had mutations that corresponded to those found in DMD patients. To address this critique, the *mdx52* mouse was generated by disrupting exon 52 in C57BL/6J mice using the gene targeting method. This was proposed to be a better model because it has the same mutation as that seen in certain DMD patients (the deletion of exon 52), and more representative of the human condition as two-thirds of DMD patients have deletions in their dystrophin gene. Unlike the *mdx* mouse, the *mdx52* mouse displays the absence of the shorter isoforms Dp140 and Dp260 in addition to the full-length transcript (Araki et al., 1997). Despite these differences, however, these mice do not display a significant difference in phenotype compared to *mdx* mice.

1.3.2 *mdx* double knockout mice

Due to the relatively mild phenotype of the *mdx* mouse, many attempts have been made to exacerbate this phenotype by generating double knockout animals. For example, *mdx* mice have been crossed with *MyoD*$^{-/-}$ mice with the aim of generating mutants with an impaired ability to regenerate (MyoD is a muscle-specific transcription factor that plays an instrumental role in muscle differentiation). Predictably, these mice do display more pronounced dystrophy than *mdx* mice, and also suffer from severe cardiomyopathy (Megeney et al., 1999). The latter finding was surprising because MyoD is not expressed in cardiac tissue (Olson, 1993). However the authors suggest that this indicates that the observed cardiomyopathy is a direct result of widespread and extensive skeletal muscle damage. Another double knockout mouse generated with the aim of producing a mutant that more faithfully reproduces the features of DMD is the *mdx; α7 integrin*$^{-/-}$ mouse. α7β1 integrin, the main integrin expressed in skeletal muscle, is thought to form an alternative link between the cytoskeleton and ECM, thereby acting synergistically with the DAPC. In accordance with this hypothesis, the *mdx; α7 integrin*$^{-/-}$ mouse displays a very severe dystrophic phenotype and has an average lifespan of only 24-28 days (Guo et al., 2006).

Arguably the best mouse model for DMD is the *dko* (*mdx; utrn*$^{-/-}$) mouse. The *dko* mouse is a transgenic that was generated by crossing *mdx* mice with *utrn*$^{-/-}$ (utrophin-knockout)

mice (Deconinck et al., 1997b; Grady et al., 1997). This cross was performed to test the hypothesis that, due to the high level of similarity between dystrophin and utrophin, the additional absence of utrophin would exacerbate the dystrophic phenotype in *mdx* mice. *utrn*$^{-/-}$ mice do not display any signs of muscle weakness, and only show reduced folding at the NMJ (Deconinck et al., 1997a). However, *dko* display a far more severe disease phenotype that is similar to that of DMD patients. Unlike *mdx* mice, they have a significantly reduced lifespan of 4-20 weeks, and display many of the hallmark symptoms of DMD, such as severe muscle weakness, joint contractures, kyphosis and pronounced growth retardation post-weaning. In addition to these muscle defects, *dko* mice also have abnormal MTJs and NMJs that show a reduction in membrane folds. Due to the accurate recapitulation of the dystrophic progression of DMD in this mouse model, coupled with the absence of the compensatory power of utrophin, it means that the *dko* mouse can serve as a better model than the *mdx* mouse in which to test the effectiveness of therapeutic strategies. For example, this model has recently been used to test the effectiveness of an exon-skipping strategy (this strategy is discussed in section 1.4.2.2) (Goyenvalle et al., 2010).

1.3.3 *Fiona* mouse

The *Fiona* mouse is a transgenic mouse that overexpresses full-length utrophin against an *mdx* background. The utrophin transgene is under the control of the human skeletal α-actin promoter and so is expressed only in skeletal muscle (Tinsley et al., 1998). These mice are phenotypically indistinguishable from wild-type mice and show complete correction of the dystrophic phenotype, displaying even myofibre size, normal levels of muscle degeneration and regeneration, and similar levels of force production by the extensor digitorum longus (EDL) muscle compared to wild-type muscle. They have also been shown to be able to exert overall force levels that are similar to those of wild-type mice. Quantitative analysis of dystrophin and utrophin in wild-type, *mdx* and *Fiona* mice has revealed that utrophin has the ability to rescue all the dystrophic features of the *mdx* mouse even when expressed at only one-half the abundance of dystrophin in normal muscle (Ervasti, 2007).

1.3.4 Golden retriever (GRMD) dog model

The Golden retriever (GRMD) dog model is the most widely used canine model of DMD. This is the best characterized dog model of DMD, which lacks dystrophin due to incorrect splicing that results in a truncated transcript. These dogs display a phenotype that is very similar to human DMD patients (Willmann et al., 2009). The GRMD dog has been successfully used to test the therapeutic potential of mesoangioblast administration (discussed in section 1.4.1.2) (Sampaolesi et al., 2006) and exon-skipping (McClorey et al., 2006). The major problem with the use of these dogs is that they display a high degree of phenotypic variation and are expensive to breed.

1.4 Potential therapies for DMD

Numerous different therapeutic strategies have been devised to correct the various deleterious consequences of dystrophin absence. These strategies can be divided into five categories: cell therapy, gene-based therapy, growth factor modulation, the pharmacological approach, and utrophin upregulation. These strategies are briefly described and critically evaluated in the following sections.

1.4.1 Cell therapy

Cell therapy involves the delivery of cells that make new muscle to diseased areas. These can either be muscle precursor cells or stem cells that have the ability to differentiate into muscle cells. The cell therapy strategy that has experienced the most success so far has been the transplantation of myoblasts into diseased tissue.

1.4.1.1 Myoblast transplantation

Myoblasts are muscle precursor cells that can differentiate to form myofibres. Myoblast transplantation (MT) involves the derivation of myoblast cells from healthy donor skeletal muscle, expansion of these cells in culture, and administration to dystrophic tissue (Ichim et al., 2010). MT can not only result in an increase in skeletal muscle mass but it can also result in the delivery of the dystrophin gene to dystrophin-deficient muscle. The incorporation of donor myoblasts into recipient myofibres results in a phenomenon known as ‘gene complementation’, which means the expression of both

exogenous and host genes in the myofibre syncitium (Skuk, 2004). MT trials on dystrophin-deficient mice have resulted in an increase in dystrophin-positive myofibres following transplantation (Fakhfakh et al., 2010). However, there are still problems with this technique that need to be overcome. For example, intravenous and intraperitoneal (IP) injections of myoblasts in mice have so far proven to be unsuccessful, necessitating the use of intramuscular injections. The major disadvantage of this delivery method is that the myoblasts fuse mainly with the myofibres that neighbour the site of injection, resulting in restricted zones of muscle growth and recovery. Another problem with MT is the need to use immunosuppressants because the donor myoblasts are allogeneic and therefore will elicit an immune response in the host. Immunosuppressants have numerous side effects, such as inhibiting myoblast fusion and possibly killing transplanted cells (Skuk, 2004).

1.4.1.2 Stem cell therapy

It was initially thought that only satellite cells were responsible for the growth and maintenance of skeletal muscle. There are however other cells found in skeletal muscle that have myogenic potential, namely muscle-derived stem cells, muscle side-population cells and muscle-derived CD133+ progenitors. Certain stem cells derived from non-muscle have also been shown to be able to participate in myogenesis. For example, bone marrow-derived mesenchymal stem cells (MSCs) can differentiate into mesodermal cells, including myoblasts (Farini et al., 2009). MSCs have the advantages of being able to fuse with and genetically complement dystrophic muscle, possessing anti-inflammatory properties, and producing factors that enhance the activity of endogenous repair cells. However, most of the studies using MSCs in animal models did not show an appreciable improvement in muscle contractile force (Ichim et al., 2010). Another type of stem cell whose use has been proposed to be a possible therapeutic option is the mesoangioblast cell. This is a multipotent progenitor of mesodermal tissue whose transplantation in dystrophic dogs has been shown to result in the re-expression of dystrophin in myofibres and an improvement in muscle contractile force (Sampaolesi et al., 2006). Although promising, some of the interpretations of the results from this study have been questioned, such as the lack of correlation between levels of dystrophin expression and

improvement in muscle function (Davies and Grounds, 2006). The major problem with using stem cells, irrespective of their source, is that of survival and subsequent efficient migration of the cells from the site of injection to the rest of the muscle.

1.4.2 Gene-based therapies

In this thesis the term 'gene-based therapies' is applied to strategies that involve the complementation of the defective host gene with a partially or fully functional exogenous gene or the therapeutic manipulation of mRNA processing to produce partially or fully functional transcripts. These therapies can be partitioned into two categories: conventional gene replacement strategies and RNA-based approaches.

1.4.2.1 Conventional gene replacement strategies

These strategies involve the delivery of a truncated or full-length dystrophin gene to dystrophic myofibres via either plasmids or viral vectors. With a cloning capacity of 37 kb, the helper-dependent adenovirus has the capacity to carry the full-length dystrophin gene. However, long-term expression is an issue because skeletal muscle expresses very low levels of coxsackie and adenovirus receptors, which are necessary for the initial step of adenovirus infection. Two gene replacement strategies that are being actively pursued are the intramuscular injection of plasmid DNA directly into skeletal muscle and the use of adeno-associated virus (AAV) vectors to ferry truncated (yet functional) versions of dystrophin to skeletal muscle. The problem with the plasmid method is the lack of long-term expression. Although AAV vectors enable efficient systemic gene delivery to skeletal muscle, they suffer from the problem of not having the capacity to carry the full-length dystrophin gene and are only able to carry shortened micro- or mini-dystrophin genes. The administration of these shortened genes might not be enough because their protein products might not completely recapitulate all of the functions of full-length dystrophin. For example, nNOS is required for NO-mediated regulation of vasodilation, therefore its absence would result in functional ischaemia. It has been shown that the sarcolemmal targeting of nNOS is dependent on the spectrin-like repeats 16 and 17 of the rod domain (Lai et al., 2009), which means that any truncated dystrophin transgene that lacks this region is not likely to be an entirely functional replacement (Trollet et al., 2009).

1.4.2.2 RNA-based approaches

Exon-skipping is a promising RNA-based approach that can potentially be applied to the majority of (~65%) DMD patients who have out-of-frame deletions. This strategy involves the use of small molecules called antisense oligonucleotides (AOs) to correct these defects by altering the processing of these transcripts to splice out these exons with the mutations, resulting in the production of a shorter but largely functional dystrophin product. AOs alter splicing by either sterically blocking splice enhancer sequences or by altering secondary mRNA structure folding. Since the use of unmodified oligonucleotides would result in the endonucleolytic cleavage of any duplexes formed, these AOs need to be chemically modified so that they become resistant to endonucleases. Two such modifications involve the use of a 2' O-methyl-phosphorothioate backbone and a morpholino backbone (Partridge, 2010). Success with this technique has been achieved in cell culture and trials in *mdx* (Alter et al., 2006) and *dko* (Goyenvalle et al., 2010) mice have ameliorated the disease phenotypes of both mouse models. Clinical trials have also yielded positive results in DMD patients, with intramuscular injections of oligonucleotides resulting in local dystrophin expression (Kinali et al., 2009). There are currently two major human trials being conducted, one using the 2' O-methyl-phosphorothioate chemistry and the other the morpholino backbone, both targeting exon 51, whose therapeutic skipping is predicted to be applicable to 17% of all DMD patients. Successful exon skipping following intramuscular injections has been reported in both studies, and trials involving systemic delivery are currently being performed (Partridge, 2010). Two major limitations of this strategy are that different AOs will need to be designed for different deletions, and repeated administration of the AOs will be required because of their short half-life in muscle tissue (Manzur and Muntoni, 2009). Multi-exon skipping, which involves the exclusion of multiple contiguous exons, has been proposed to be a way to address the first limitation by allowing the administration of the same AO to patients with different mutational defects (Beroud et al., 2007).

1.4.3 Growth factor modulation

Two growth factors whose modulation has been proposed to have therapeutic value in DMD patients are the insulin-like growth factor-1 (IGF-1) and myostatin. Transgenic *mdx* mice engineered to express IGF-1 in a muscle specific manner displayed a noticeable increase in muscle mass and force generation capability (Barton et al., 2002), with reduced susceptibility to damage (Ridgley et al., 2009). Treatment of *mdx* mice with IGF-1 resulted in partial protection from damage-inducing exercise (De Luca et al., 2003).

Myostatin is a member of the TGF-β superfamily that inhibits muscle growth and differentiation. Transgenic mice with a disrupted myostatin gene are significantly larger and have significantly more skeletal muscle mass than their wild-type counterparts (McPherron et al., 1997). Blockage of myostatin expression has therefore been proposed to be a possible therapeutic option. A recent study showed that the delivery of a natural inhibitor of myostatin, myostatin propeptide, via AAV serotype 8 (AAV8) vectors resulted in increased muscle growth and lower levels of fibrosis and creatine kinase in treated *mdx* mice. However, a treadmill test revealed that treated *mdx* mice exhibited reduced endurance compared to untreated controls (Qiao et al., 2008).

1.4.4 Pharmacological approach

Researchers adopting the pharmacological approach test the ameliorative effects of naturally occurring and synthesized drugs. Some major strategies are the reduction of inflammation, correcting calcium homeostasis imbalance and increasing muscle mass. The major advantage of the pharmacological approach is the ease of systemic delivery. However, therapeutic drugs often are able to correct only one aspect of the disease phenotype, and some compounds have adverse side-effects when administered for a significant period of time. This section provides a brief description of the current pharmacological management of DMD progression, namely corticosteroids, the aminoglycoside gentamicin and the synthetic drug PTC124.

1.4.4.1 Corticosteroids

Corticosteroids have for many years been known to have beneficial effects. These include anabolic effects, reduction of inflammation and stimulation of myoblasts. Currently, the glucocorticoids prednisone, prednisolone, and deflazacort (the oxazoline derivative of prednisone), are the only drugs used to treat DMD patients. However, these agents have side effects, which include impaired carbohydrate tolerance (Angelini, 2007) and weight gain (Biggar et al., 2006).

1.4.4.2 Gentamicin

Studies have shown that mammalian cells treated with high concentrations of aminoglycoside antibiotics like gentamicin promote readthrough of premature stop codons by interfering with the ribosome's ability to recognize these stop signals (Manuvakhova et al., 2000). Gentamicin treatment could therefore be applied to DMD patients (5-15% of all patients (Khurana and Davies, 2003) with nonsense mutations in their dystrophin genes. A six-month trial of gentamicin on DMD patients resulted in a significant increase in dystrophin expression in skeletal muscle (with the highest level approaching 13-15% of normal expression in one individual) and decreased levels of creatine kinase. However, one of the individuals developed an immune response to the newly-expressed dystrophin protein (Malik et al., 2010). Additional problems with gentamicin include its lack of potency and possible toxic effects (Welch et al., 2007).

1.4.4.3 PTC124

PTC124 is a synthetic drug that has been shown to have the ability to induce readthrough of premature but not normal stop codons (Welch et al., 2007). It was selected following high-throughput screens of ~800,000 low molecular weight compounds screened for their ability to mediate UGA nonsense mutation suppression. The assay used in these screens involved stable cell lines containing firefly luciferase genes harbouring nonsense codons. Increase in luciferase expression following treatment was therefore indicative of readthrough ability. Treatment of *mdx* mice with PTC124 resulted in a significant increase in dystrophin expression in skeletal muscle and partial (yet significant) recovery of muscle contractile force (Welch et al., 2007). Some of the results from this study have

however been recently called into question. More detailed analysis of the luciferase assay used indicated that PTC124 stabilizes firefly luciferase, and this stabilization has been suggested to be responsible for the apparent increase in luciferase expression following treatment (Auld et al., 2009).

1.4.5 Utrophin upregulation

As discussed in section 1.3.3, utrophin upregulation has been shown to rescue all the dystrophic parameters of the *mdx* mouse, thus making this a promising potential therapy for DMD. A study using a gene-therapy approach to deliver dystrophin and utrophin minigenes to *mdx* muscle using adenovirus vectors showed that this delivery resulted in improved muscle histopathology and force-generating capacity for both genes. However, utrophin gene transfer resulted in significantly higher transgene persistence and reduced inflammation compared to dystrophin because the truncated utrophin protein was able to avoid the immune response. In this respect, utrophin delivery has a significant advantage over dystrophin delivery because it is not recognized as "foreign" by the host immune system (Ebihara et al., 2000). As discussed in section 1.4.2.1, there are many technical hurdles associated with conventional gene replacement therapy, which makes the strategy of administering a small pharmacological compound that induces global utrophin expression a more attractive option. It has been shown that the global overexpression of utrophin does not have detrimental effects in the *mdx* mouse, suggesting a drug that does result in a body-wide increase in utrophin should not have toxic side-effects (Fisher et al., 2001). Two compounds whose administration has been shown to result in utrophin upregulation in dystrophic tissue are heregulin and L-arginine. As discussed in section 1.2.2, heregulin has a natural role to play in the synapse-specific upregulation of utrophin expression. A study on *mdx* mice treated intraperitoneally with a small peptide encoding a functional fragment of the heregulin protein for three months resulted in a significant upregulation of utrophin (2.7-fold) and a concomitant decrease in muscle pathology and improvement in muscle contractile properties (Krag et al., 2004). As discussed in section 1.1.2, reduction in nNOS expression has been shown to be a contributing factor in the progression of dystrophy in DMD, suggesting that the correction of this misexpression should result in an

amelioration of phenotype. In support of this hypothesis, transgenic *mdx* mice overexpressing nNOS display a partially corrected phenotype (Wehling et al., 2001). L-arginine is a substrate whose administration results in an increase in nNOS activity. A study on the treatment of *mdx* mice with L-arginine revealed lower levels of necrosis and creatine kinase. This study also revealed a 2-3-fold increase in utrophin expression in the muscle. However, the mechanism via which L-arginine administration results in this upregulation is unknown and since increased nNOS activity is known to reduce inflammation and vasodilation, it is difficult to establish how much of the improved phenotype can be attributed to utrophin upregulation (Voisin et al., 2005).

A promising strategy used to find small molecules that upregulate utrophin is high-throughput screening, which involves screening a library of compounds on a reporter cell line for their ability to activate the utrophin A promoter. The cell line used is the dystrophin-deficient mouse muscle-derived H2K-*mdx* cell line that has been stably transfected with a promoter/reporter fusion construct. This construct encompasses 9.4 kb of sequence directly upstream of the transcription start site used by promoter-A, linked to a firefly luciferase reporter gene (Khurana and Davies, 2003). This cell line has been used to screen a library of drug-like small compounds from Summit plc. Positive hits are then administered to *mdx* mice to test for amelioration of the dystrophic phenotype and upregulation of utrophin A in muscle tissue. The compound from this screen used in this thesis was the drug C1100.

PPARδ (also known as PPARβ), along with the other PPARs, is a transcription factor that belongs to the nuclear receptor superfamily (Pettersson et al., 2007). Activation of PPARδ leads to a fast-to-slow muscle fibre type switch (Narkar et al., 2008). Myofibres can be broadly divided into four groups – type I (oxidative slow-twitch fibres); type IIa (mixed oxidative-glycolytic fast-twitch); type IIb (glycolytic fast-twitch); and type IIx (Narkar et al., 2008). The fact that utrophin A upregulation is orchestrated by the same pathways that control the slow myofibre program (Chakkalakal et al., 2004), led to the hypothesis that PPARδ upregulation might result in utrophin A upregulation. This hypothesis has since been confirmed (Miura 2007). One of the aims of this thesis was to test the possible ameliorative effects of the PPARδ agonist GW501516 (Pettersson et al.,

2007) on the *mdx* mouse, and to test its effect on the utrophin A promoter *in vitro*. GW501516 has been shown to have a potent effect on PPARδ resulting in the enhanced expression of type I fibre genes in mouse skeletal muscle (Wang et al., 2004).

1.5 The potential therapeutic benefits of microRNA manipulation

MicroRNAs (or miRNAs) are a class of small (~22 nucleotide-long) evolutionarily-conserved noncoding RNAs that over the past two decades have been shown to have important regulatory roles in plants and animals. The discovery that *lin-4*, a gene whose function is to control the timing of *C.elegans* larval development, does not code for protein but instead produces two small RNAs (22-nt- and 61-nt- long) gave birth to the field of miRNA research (Lee et al., 1993). In 2001, three landmark papers published showed that *lin-4* was not an unusual gene, but was instead a member of a class of similar genes, potential orthologues of which were suggested to exist in the *Drosophila* and human genomes (Lagos-Quintana et al., 2001; Lau et al., 2001; Lee and Ambros, 2001). Over the last decade the list of miRNAs has expanded to 677 in human and 491 in mouse (Betel et al., 2008). These miRNAs are predicted to have thousands of mRNA targets which is why they have become the subject of intense current research (Orom and Lund, 2010). While some models predict that miRNAs control the activity of approximately 30% of all protein-coding genes (Filipowicz et al., 2008), a recently developed model suggests that >60% of human protein-coding genes could be targeted by miRNAs (Friedman et al., 2009).

1.5.1 miRNA biogenesis

The majority of miRNA genes exist as independent transcriptional units (Bartel, 2004) but a significant minority overlap annotated genes (35% of mammalian miRNA loci, of which 90% are located in introns) (Griffiths-Jones et al., 2006). miRNA genes are transcribed by RNA polymerase II, and so are transcribed in the same way as mRNAs. Primary (Pri)-miRNAs are long transcripts that are derived from either independent miRNA genes or mRNA introns. These pri-miRNAs are cleaved in the nucleus by the Drosha RNase III endonuclease to produce ~60-70nt stem loop intermediates known as

precursor (pre)-miRNAs. These pre-miRNAs are then exported to the cytoplasm by Ran-GTP and the export receptor Exportin-5. Once in the cytoplasm, the pre-miRNA is recognized by another RNase III endonuclease, Dicer, which cleaves it to produce a short RNA duplex. This duplex is unwound by a helicase to produce a functional mature miRNA strand and another strand which is generally rapidly degraded. The miRNA biogenesis pathway is illustrated in Figure 1.2 (Kim, 2005).

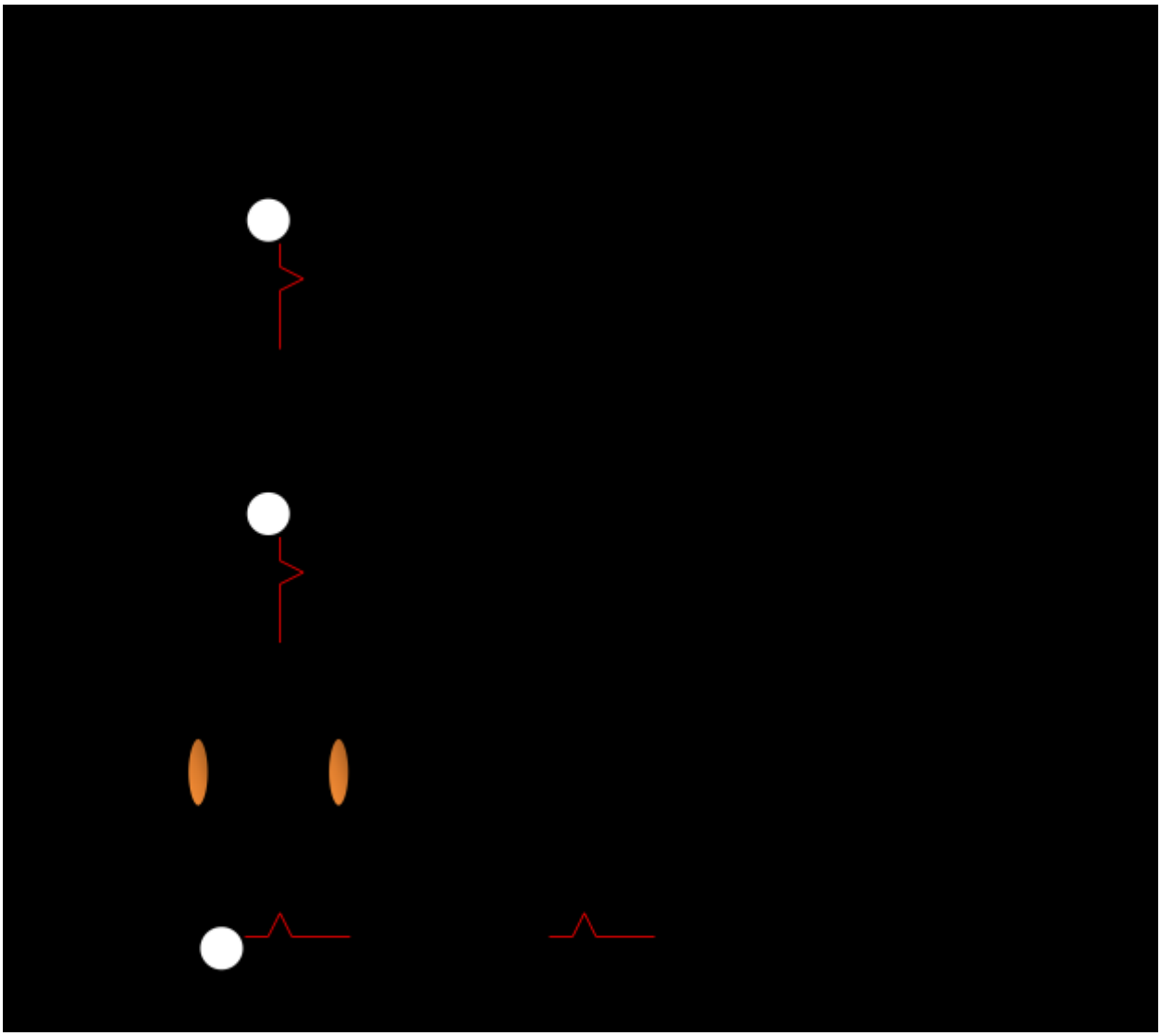

Fig. 1.2 miRNA biogenesis pathway. The miRNA gene is transcribed by RNA polymerase II (pol II) to produce the primary transcript, pri-miRNA. This transcript is processed by the enzyme Drosha to generate a pre-miRNA intermediate, which is exported to the cytoplasm by Exportin-5 and Ran-GTP, where it is cleaved by the enzyme Dicer to produce a short RNA duplex. This duplex is unwound by a helicase to

release a mature miRNA and a complementary strand that is generally degraded. Adapted from (Kim, 2005).

1.5.2 Mechanism of target-gene silencing by miRNAs

Interaction between miRNAs and their mRNA targets occurs via base-pair complementarity. This complementarity is between the miRNA and sequences in either the coding or 3' untranslated regions (3' UTRs) of target mRNAs, and is generally nearly-perfect in plants. Perfect complementarity triggers mRNA degradation in a manner that is analogous to RNA interference (RNAi) induced by small interfering RNAs (siRNAs). However, in animals, miRNAs generally regulate gene expression via imperfect base-pairing to sequences in the 3' UTR of target mRNAs. This results in either an inhibition of protein synthesis or mRNA degradation.

Two characteristic features of miRNA-mRNA interactions in animals are contiguous Watson-Crick pairing in the 5' proximal seed region (usually positions 2-8) in the miRNA and a lack of complementarity in the central part (usually positions 10 and 11) of the miRNA. This second feature is what prevents RNAi-like endonucleolytic cleavage of the target mRNA in the middle of the duplex (Pillai et al., 2007).

Like siRNAs, miRNAs become incorporated intro ribonucleoprotein complexes known as RNA-induced silencing complexes (RISCs, or in the case of miRNAs, miRISCs) before binding to target mRNAs (Bartel, 2004). Key components of miRISCs are the argonaute proteins, of which there are four kinds in mammals (Ago1 to Ago4). Ago2, also known as 'Slicer', is the only one that functions in RNAi by endonucleolytically cleaving mRNA in the middle of the mRNA-siRNA duplex, whereas all four are involved in miRNA-mediated repression.

There are currently four generally accepted possible mechanisms of miRNA-mediated mRNA repression. **(1)** Repression of translation at the initiation stage, via inhibitory interaction with the 7-methylguanosine cap at the 5' end of eukaryotic mRNA. This is thought to result in the displacement of any attached ribosomes, followed by aggregation of these mRNAs in complexes in the cytoplasm known as processing bodies, where they are either stored or degraded. **(2)** Post-initiation translational repression at either the elongation or termination stage of protein synthesis. **(3)** Proteolytic degradation of

nascent polypeptides. **(4)** 5'→3' exonucleolytic degradation of mRNA following deadenylation and decapping.

1.5.3 The roles of miRNAs in skeletal muscle development

miRNAs have been shown or suggested to play important roles in a range of major biological processes including embryonic development (Ji et al., 2009), morphogenesis of organs like the brain (Giraldez et al., 2005) and skin (Bostjancic and Glavac, 2008), and apoptosis (Jovanovic and Hengartner, 2006). miRNAs have also recently emerged as an important class of molecules involved in muscle development and function (Eisenberg et al., 2009).

During embryogenesis, trunk and limb skeletal muscle arises from somites, which are segments of paraxial mesoderm that form along the rostrocaudal axis of the embryo. Precursor cells in the mesoderm become committed to the myogenic lineage as a result of the effects of numerous positive and negative signals from the surrounding tissue (Buckingham, 2006). Specification of this lineage is initiated by the upregulation of the basic helix-loop-helix transcriptional activators MyoD and Myf5. MyoD and Myf5 are members of the myogenic regulatory factor family (MRF). The upregulation of these factors results in the formation of a pool of proliferating myoblasts. Subsequent upregulation of the secondary MRFs (MRF4 and myogenin) induces the exit of these myoblasts from the cell cycle to become terminally differentiated myocytes. These myocytes eventually fuse to give rise to multinucleated myofibres (Charge and Rudnicki, 2004). A few miRNAs have recently been shown to play key roles in myogenesis. miR-1 is an example of a well-characterized miRNA that shows muscle-specific expression. miR-1 overexpression has been shown to strongly enhance myogenesis by translationally repressing histone deacetylase 4, which normally inhibits muscle differentiation and skeletal muscle gene expression by repressing myocyte enhancer factor 2 (MEF2). The miR-1-induced release of MEF2 results in enhanced differentiation (Chen et al., 2006).

1.5.4 miRNAs in muscle disease

Considering that miRNAs have been shown to be involved in the regulation of almost every cellular process investigated so far (Filipowicz et al., 2008), it is reasonable to

hypothesize that their dysregulation would result in deleterious effects on these processes. Extensive research highlighting the links between miRNA dysregulation and disease has been conducted. The disease most thoroughly studied in this respect is cancer. For example, it has been shown that an impairment in miRNA biogenesis results in increased tumorigenesis (Kumar et al., 2007), certain miRNAs mediate the anticancer effects of the tumour suppressor protein p53 (He et al., 2007), and widespread repression of miRNAs as a result of Myc expression contributes to tumorigenesis (Chang et al., 2008).

Kunkel and colleagues used microarrays to assess the global dysregulation of miRNAs in 10 major muscular disorders, including DMD (Eisenberg et al., 2007). They showed that each disease produces a unique and characteristic set of significantly dysregulated miRNAs. In the case of DMD, they found that six signalling pathways, including TGF-β, calcium signalling pathway and Wnt, which had previously been shown to be involved in muscular disorders, were significantly targeted by the dysregulated miRNAs. A similar study was performed on skeletal muscle tissue from *mdx* mice (Greco et al., 2009). This study also produced a list of significantly dysregulated miRNAs, many of which had also been found to be dysregulated in DMD tissue.

In addition to studies of the global dysregulation of miRNAs, the dysregulation of individual miRNAs has been studied within the dystrophic context. For example, miR-206 was shown to be significantly upregulated in the diaphragms but not the limb muscles of *mdx* mice, suggesting that this differential dysregulation might partially explain why the diaphragm is more severely affected than the limbs (McCarthy et al., 2007).

1.6 Aims of this thesis

The aims of this thesis were to:

1) Assess the effects of exercise-induced stress on the *Fiona* mouse to test the proposed role of utrophin as a truly functional replacement for dystrophin.
2) Assess the effects of the drugs GW501516 and C1100 on the utrophin A promoter *in vitro* and the *in vivo* effects of their administration to *mdx* mice in terms of their ability to prevent the dystrophic phenotype and upregulate utrophin expression.
3) Explore the therapeutic potential of miRNAs by characterizing the global profile of miRNA expression in *mdx* and *dko* limb muscle, followed by a more detailed study of miR-31 and -206 expression patterns. Perform target validation for a potentially therapeutically relevant with the aim of gaining further insight into its functional roles.

2 Materials and methods

2.1 Animals

Chapter 3

Twelve four-week-old *mdx* (C57BL/10ScSn-Dmd^{mdx}/J), C57Bl/6 and *Fiona* mice were randomly split into 'sedentary' and 'run' groups of equal size. Mice in the 'run' groups were subjected to the treadmill protocol found in (Grounds et al., 2008). Briefly, mice belonging to the 'run' groups were made to run on a horizontal treadmill (Columbus Instruments, USA) at 12 m/min, twice a week, for eight weeks. The body weights of all mice were measured at the end of each week to ensure that the protocol was not having an overly detrimental effect on their health. All mice were sacrificed at the end of this protocol.

Chapter 4

Four-week old male *mdx* littermates were randomly split between two groups and treated with GW501516 (4 mg/kg) or vehicle only (phosphate buffered saline (PBS)-Tween-20 (0.1%)/5% Dimethyl sulfoxide (DMSO)) via daily IP injections for four weeks (n = 7 for each group), following which the mice were sacrificed. C57BL/6 contractile properties were measured in EDL muscle dissected from eight-week-old untreated mice (n = 7).

Chapter 5

Four-week old male *mdx* littermates were randomly split between two groups and treated with C1100 (15 mg/kg) or vehicle only (PBS-Tween-20 (0.1%)/5% DMSO) orally via gavage (administration directly into the stomach via a bendable tube attached to a syringe) daily for four weeks (n = 6 for each group), following which the mice were sacrificed.

Chapter 6

Ten-week old male *mdx* and C57Bl/10 mice (n = 4 for each) were used for the first miRNA microarray, and ten-week-old *dko* and *mdx* littermates (n = 4 for each) were used for the second miRNA microarray. In addition, ten-week-old *Fiona* mice (n = 3), three-, four-, six-, and eight-week-old *mdx* and C57Bl/10 mice (n = 3 for each age), and four-, six-, and ten-week-old *dko* and *mdx* littermates (n = 3 for each group) were used for the qPCR experiments (Figures 6.2-6.8).

Mice were sacrificed by CO_2 asphyxiation in accordance with Schedule I of the UK Animals (Scientific Procedures) Act 1986.

All animal procedures were performed in the Animal facilities of the Department of Physiology, Anatomy and Genetics, University of Oxford, Oxford, UK in accordance with UK Home Office regulations.

2.1.1 Genotyping

For genotyping, DNA was extracted from tail tips from mice younger than 10 days old and from ear clips taken from mice older than 10 days old. Tissue biopsies were digested in 500 µl lysis buffer (0.1 M NaCl, 0.5% sodium dodecyl sulphate (SDS), 10 mM Tris (pH8.0), and 25 mM ethylenediaminetetraacetic acid) with 10 µl Proteinase K (20 mg/ml, Roche) overnight at 55^{o}C. 300 µl 5 M NaCl was added the next day, followed by bench-top centrifugation at 13,200 rpm for 10 mins and transfer of the supernatant to a fresh tube. DNA was precipitated from the supernatant by adding 800µl of EtOH (100%) and centrifuging at 13,200 rpm for 6 mins. The precipitated DNA was washed in EtOH (70%), air dried, and resuspended in 50µl H_2O.

For genotyping *dko* and *mdx* littermates, two PCRs were performed with a forward primer complementary to exon 7 of mouse utrophin (pU65, GTGAAGGATGTCATGAAAG) and either a reverse primer complimentary to either intron 7 (INT, TGAAGTCCGAAAGAGATACC) or to the PGK promoter located in the Neo-knockout cassette (NEO, ACGAGACTAGTGAGACGTGC).

The cycling conditions used were as follows:

Step	Temperature	Duration
Initial denaturation	94°C	3 min
Denaturation	94°C	30 s
Annealing	52°C	30 s x35
Elongation	72°C	30 s
Final Elongation	72°C	5 min

Genotyping of *Fiona* mice was conducted by performing PCR using the primers UM101 (AGTGGACATGGATTTGGACA) and UM102 (GTTTTCATCCACAATCACCA) and the following cycling conditions:

Step	Temperature	Duration
Denaturation	94°C	30 s
Annealing	56°C	1 min x35
Elongation	72°C	1 min

2.2 *Ex vivo* measurements of muscle mechanics

Experiments were performed using EDL muscle dissected from the hind leg, as this muscle had been previously used during the optimization of this protocol. During dissection and experiments, muscles were bathed in oxygenated (95% O_2–5% CO_2) Krebs–Hensley solution composing of (mM): NaCl, 118; $NaHCO_3$, 24.8, KCl, 4.75; KH_2PO_4, 1.18; $MgSO_4$, 1.18; $CaCl_2$, 2.54; glucose, 10 (Barclay et al., 2008). Contractile properties were measured using previously described techniques (Lynch et al., 2000). Briefly, silk sutures were tied to the exposed tendons at each end of the muscle and were used to attach the proximal end of the muscle to a lever arm system connected to a force transducer (model 300B; Aurora Scientific Inc.) and the distal end to a fixed clamp. The force transducer was attached to a stimulator (model 701B; Aurora Scientific Inc.). The equipment was controlled using the signal interface model 604A (Aurora Scientific Inc.) and results were recorded by the DMC software (version 4.1.4; Aurora Scientific Inc.).

The muscle was suspended vertically and stimulated by an electric field generated by two platinum electrodes positioned in parallel on each side of the muscle. The muscle was subjected to periodic pulses of 0.2 ms in duration at 30 V, and marginally stretched after each pulse, to determine the optimum length (L_o) for production of maximum isometric twitch force. The trace of the maximum isometric twitch force was used to calculate the time to peak (TTP) and half-relaxation time ($RT_{1/2}$) values. Fibre length (L_f) was determined by multiplying the figure obtained for L_o by a fibre length to muscle length ratio of 0.45, a figure which has been previously determined (Brooks and Faulkner, 1988). A force-frequency curve was generated by dividing the force generated at 10Hz intervals from 10-100Hz during a 350 msec stimulus by the force generated at 80Hz, plotting these values against frequency. The maximum isometric force was calculated from the peak of the curve. Eccentric contractions were performed during a 0.75 sec protocol. The muscle was stimulated into tetanus at the frequency required to generate the maximum isometric force. After 0.25s of tetanic contractions the muscle was stretched at a rate of one fibre length per second for 0.15 seconds, which is equivalent to a total stretch of 15% of fibre length. Shortening of the muscle an equal distance either side of L_f was designed to enhance force development (Lynch et al., 2000). The difference in maximum force produced during tetanus between the first and the fifth eccentric contraction was expressed as a percentage of the force produced by the first contraction to calculate the percentage force drop. Forces were normalized (N/cm^2) by dividing the fibre length by the wet weight of the muscle, which was measured at the end of the experiment after tendons had been carefully removed. All data were digitized and analysed using the DMA software (version 3.2; Aurora Scientific Inc.).

2.3 Serum creatine kinase (CK)

Following CO_2 asphyxiation, blood was collected from the jugular vein into uncoated Microvette CB 300 tubes (Sarstedt Ltd) and centrifuged for 2 min at 18,000 x *g* for serum separation. Aliquots were frozen at -80 °C until processing. Serum CK levels were analysed using the CK (NAC) reagent kit in conjunction with the AU 400 Clinical Chemistry analyser (Olympus UK Ltd).

2.4 Histology and immunofluorescence

2.4.1 Preparation of sections

Following dissection, tissue was embedded in optimum cooling medium (VWR) by freezing in liquid nitrogen-cooled isopentane. A cryostat (Bright Instruments) was used to make

8 μM-thick serial sections that were either used immediately or stored at -80^{o}C until use.

2.4.2 Haematoxylin and Eosin (H & E)

8 μm cryosections were incubated for 7 mins in Ehrlich's Haematoxylin, washed, incubated for 3 mins in 0.1% Eosin, washed in increasing concentrations of acid alcohol, washed in histoclear solution and coverslips were mounted using histomount. Pictures of stained sections were taken using a light microscope and centronucleation was determined by dividing the number of centrally-nucleated fibres with non-centrally-nucleated fibres.

2.4.3 Immunohistochemistry

Myosin heavy chain (MHC) I and IIa fibre type composition was determined by first fixing cryosections in ice-cold 4% paraformaldehyde/PBS on ice for 10 mins, washing in ice-cold PBS for 5 mins, permeabilizing in ice-cold 0.3% Triton/PBS on ice for 10 mins, and washing in PBS twice for 5 mins at room temperature (RT). Slides were then blocked in 5% normal goat serum/PBS for 1 hour at RT, followed by primary incubation with mouse anti-MHC I antibody (BA-F8, 1:25, kind gift from Zhen Yan, Duke University, NC, USA) or mouse anti-MHC IIa antibody (SC-71, 1:25, kind gift from Zhen Yan, Duke University) for 2 hours RT or overnight at 4^{o}C. Slides were washed in three changes of PBS for 5 mins each, followed by secondary incubation with 1:500 goat anti-mouse-IgG-Alexaflour-488 (Molecular Probes, Leiden, Netherlands).

2.5 Protein preparation, immunoblotting and densitometry

Soluble protein was prepared from muscle samples flash frozen in liquid nitrogen immediately after dissection and stored at -80 °C until processing. For western blotting, protein was crushed with a pestle in a liquid nitrogen-cooled mortar, solubilised in 50 volumes of single-section western blot lysis buffer (4% SDS, 125 mM Tris (pH 8), 40% glycerol, 0.5 mM phenylmethylsulfonyl fluoride, 100 mM dithiothreitol) (Cooper et al., 2003), vortexed, briefly homogenised and sonicated, heated to 94 °C for 4 mins and centrifuged for 3 min at 15,000 x *g* to remove insoluble matter. For western blotting, 40 µl soluble protein was separated by SDS-polyacrylamide gel electrophoresis (Biorad) using a 5% SDS-acrylamide gel (stacking gel: 4% acrylamide mix, 125 mM Tris (pH 6.8), 0.1% SDS, 0.1% ammonium persulfate (APS), 0.1% tetramethylethylinediamine (TEMED); resolving gel: 5% acrylamide mix, 375 mM Tris pH 8.8), 0.1% SDS, 0.1% APS, 0.1% TEMED) at 50V overnight (~16 hours) at 16^{o}C, and transferred onto a polyvinyl fluoride (PVDF) membrane (GE Healthcare) at 50V overnight (~16 hours) at 4^{o}C. Membranes were blocked with 5% (w/v) milk powder in tris-buffered saline with 1% tween (TBS-T) for 1 hour at RT. The membranes were then washed in three changes of TBS-T for 10 mins, incubated with the primary antibody for 1 hour, washed as before, incubated with the secondary antibody and washed as before. Blots were developed using ECL reagent (GE Healthcare). Utrophin protein was detected using a 1:100 dilution of MANCHO 3 (kind gift from G.E. Morris, Oswestry, UK) and 1:2000 ECL HRP-conjugated anti-mouse antibody. Equal protein loading was corrected by detection of α-actinin (1:200, N-19; Santa Cruz Biotechnology, Inc) and 1:160,000 HRP-conjugated anti-goat antibody (Sigma). Densitometry was performed using the freely available web version of Image J (rsbweb.nih.gov/ij/).

2.6 Cell culture

2.6.1 Cell lines

The cell lines C2C12 (mouse skeletal myoblast) and HEK 293T (human embryonic kidney) were maintained in Dulbecco's Modified Eagle's Medium (D-MEM with GlutaMAX, Invitrogen) supplemented with 10% fetal calf serum (FCS) (PAA

Laboratories) and 1% Penicilin-Streptomycin solution (pen-strep) (Invitrogen). These cells were grown at 37^{o}C and 5% CO_2 in a humidified chamber. The cell line H2K-*mdx*-UtroA (mouse skeletal myoblast cell line stably-transfected with a 9.4 kb utrophin A promoter fragment generated in-house) was maintained in D-MEM with GlutaMAX, supplemented with 20% FCS, 1% pen-strep, 2% chick embryo extract (Sera Laboratories International) and 0.02% γ-interferon (Sigma). These cells were grown at 33^{o}C and 10% CO_2 in a humidified chamber. All cells were maintained in 75 cm^2 flasks and passaged routinely.

2.6.2 Transfection

C2C12 cells were seeded in 96-well plates at a density of 5 x 10^4 cells per well. After 24 hours, they were transfected with pUB or the derivative mutant constructs (described in section 2.10.1) and pRL-TK (a plasmid that constitutively expresses the *renilla* gene, used as an transfection control; Promega) at a ratio of 50:1 using the FuGENE transfection agent (Roche) at a ratio of 1:6 μg DNA:μL FuGENE, following manufacturer's instructions.

HEK 293T cells were seeded in 96-well plates at a density of 1 x 10^4 cells per well. After 24 hours, they were co-transfected with the psiCheck2.2 constructs (50 ng per well; described in section 2.10.2) and either the miR-503 mimic or the negative control scrambled siRNA construct (10 nM per well for both; Applied Biosystems) using Lipofectamine 2000 reagent (Invitrogen) according to manufacturer's protocol. 24 hours after transfection, cells were harvested by treatment with 1x passive lysis buffer (Promega) for 20 mins on an orbital shaker after two washes in PBS at RT. The plates were stored at -20^{o}C until further use.

2.6.3 *In vitro* drug administration

24 hours after transfection, media was removed from the C2C12 cells and either replaced with media containing the drug C1100 (which was stored in DMSO at -20^{o}C) or DMSO only. H2K-*mdx*-UtroA cells were seeded in 96-well plates at a density of 5 x 10^3 cells per well. After 24 hours, media was removed and these cells were also treated with C1100. 24 and 48 hours after treatment of C2C12 and H2K-*mdx*-UtroA cells respectively, cells

were harvested by treatment with 1x passive lysis buffer (Promega) for 20 mins on an orbital shaker after two washes in PBS at RT. The plates were stored at -20^{o}C until further use.

2.6.4 Luciferase assay

Cell extracts from C2C12 and HEK 293T cells were assayed for Firefly and Renilla luciferase activity using reagents from the dual-luciferase reporter assay kit (Promega) according to manufacturer's instructions. Light output was measured using a FLUOstar Optima plate reader (delay 2s, integration 10s; BMG Labtech). In the case of cell extracts from H2K-*mdx*-UtroA cells, the same procedure was followed but only Firefly luciferase activity was measured. All experiments were performed at least in triplicate.

2.7 miRNA/RNA extraction

Mouse muscle tissue was flash frozen immediately after dissection. Total RNA (including miRNA) was extracted from tissues using the miRNeasy kit (Qiagen), following manufacturer's instructions. RNA concentration and quality was assessed using a microvolume spectrophotometer (Nanodrop, Thermo Scientific). RNA integrity was assessed using an Agilent Bioanalyzer for microarray use.

2.8 miRNA microarray assay and analysis

The samples were processed using Agilent miRNA Complete Labelling and Hybridization Kit (Protocol Version 2.1, Agilent Technologies). Briefly, 100 ng of total RNA was dephosphorylated and then labelled with Cyanine 3-pCp.Complete drying of the sample with a vacuum concentrator followed this. Next, the samples were resuspended in nuclease-free water and hybridized on an Agilent Mouse miRNA Microarray. The slides were scanned with the high-resolution Agilent Microarray Scanner (G2305B), and images were processed with the Feature Extraction Software (Agilent Technologies). Further data were analyzed using GeneSpring (Agilent Technologies). The data were quantile normalized. A Welch *t*-test $p < 0.05$ and a fold change cut-off of 1.5 were used to select significantly changing genes. The microarray

was performed by Dr. Sheena Lee, Department of Physiology, Anatomy and Genetics, University of Oxford.

2.9 Reverse transcription and quantitative PCR (qPCR)

miRNA reverse transcription was performed using the NCode miRNA first-strand cDNA synthesis kit (Invitrogen) using 10 ng RNA template or the TaqMan MicroRNA reverse transcription kit (Applied Biosystems) using 1 ng RNA template following manufacturer's instructions. The NCode kit also included a Poly(A) tailing of miRNA step before reverse transcription, which meant that the same reverse primer could be used for quantification by qPCR of all the miRNAs.

qPCR was performed using either the NCode qRT-PCR kit (Invitrogen) or TaqMan MicroRNA assay (Applied Biosystems) on a StepOnePlus Real-time PCR machine (Applied Biosystems). The NCode kit uses the Sybr green chemistry and requires the use of custom-designed forward primers (specific to the miRNA being quantified) and a universal reverse primer for miRNA amplification and quantification. Optimum primer concentrations were determined by performing reactions for combinations of forward and reverse primer concentrations. Melt curves were analysed for primer-dimer formation and non-specific amplification.

The cycling conditions used were as follows:

Step	Temperature	Duration
Initial denaturation	95^{o}C	10 min
Denaturation	55^{o}C	15 s
Annealing/elongation	60^{o}C	10 s x40

Primer efficiency was assessed by performing qPCR on serial dilutions of cDNA. The C_t (cycle threshold, which is the cycle at which the measured fluorescence rises above background, and represents the exponential phase of the reaction) values were plotted against the log-transformed cDNA input. The slope of this curve was then used in the following equation to calculate the efficiency (E):

$$E = (10^{-1/slope} - 1) \times 100$$

E values between 90% and 105% were considered acceptable. Table 2.1 contains the sequences for the forward primers used for qPCR quantification using the NCode kit.

TaqMan MicroRNA assay kits were purchased for miR-31, miR-206, miR-503, miR-16, pri-miR-31, pri-miR-206 and pri-miR-503, and quantification was performed following manufacturer's instructions.

Target	Forward primer 5'-3'
miR-21	UAGCUUAUCAGACUGAUGUUGA
miR-29c	UAGCACCAUUUGAAAUCGGUUA
miR-31	AGGCAAGATGCTGGCATA
miR-206	UGGAAUGUAAGGAAGUGUGUGG
miR-34c	AGGCAGTGTAGTTAGCTGATTGC
miR-16	UAGCAGCACGUAAAUAUUGGCG

Table 2.1 Primers used for NCode SYBR Green qPCR.

The following cycling conditions were used:

Step	Temperature	Duration
Initial denaturation	95°C	20 s
Denaturation	95°C	1 s
Annealing/elongation	60°C	20 s x40

Relative expression using both the NCode kit and the TaqMan MicroRNA assays was calculated using the $\Delta\Delta C_t$ method, where

$\Delta C_t = C_{t\ Target} - C_{t\ Endogenous\ Control}$ and

$\Delta\Delta C_t = \Delta C_{t\ Sample} - \Delta C_{t\ Calibrator}$

where "Calibrator" refers to the designated control. The endogenous control used in all the experiments quantifying mature miRNA expression was miR-16. 18S rRNA was used as the endogenous control for pri-miR quantification. Both controls were found to

show stable expression across all the samples examined in all the experiments. Three biological and three technical replicates were used in every experiment.

2.10 Cloning

2.10.1 pUB mutant constructs

The pUB construct used in this study consists of a ~1.3 kb *Hin*d III fragment of utrophin A promoter, cloned into *Hin*d III site of pGL2 Basic (Promega) generated in-house. Derivative mutant constructs were generated by performing site-directed mutagenesis (SDM) using the QuikChange Site-Directed Mutagenesis Kit (Stratagene) according to manufacturer's instructions. 10 ng of template pUB DNA was used.

The cycling conditions used were as follows:

Step	Temperature	Duration
Initial denaturation	95°C	30 s
Denaturation	95°C	30 s
Annealing	55°C	1 min x12
Elongation	68°C	1 min/kb of plasmid length

1 μL of each reaction was transformed into 20 μL of XL-1 Blue Supercompetent cells (Invitrogen) according to manufacturer's instructions, which were then plated on LB agar plates (supplemented with ampicillin at a ratio of 1:2,500) and incubated at 37°C overnight. Colonies were picked the following day and inoculated in 5 mL cultures of LB broth (Invitrogen) supplemented with ampicillin (at a ratio of 1:2,000) overnight at 37°C. Plasmid DNA was purified the following day using a Qiagen Miniprep kit, according to manufacturer's instructions.

Table 2.2 contains the sequences of the mutagenesis primers used to generate the pUB-derived mutant constructs. The mutations induced in the Ap2-747, Ap2-850, E-box and Sp1-755 sites are the same as those induced in (Perkins et al., 2001). The N-box mutation induced is the same as the one used in (Gramolini et al., 1999), the NFAT mutation is the

same as the one used in (Angus et al., 2005), and the PPRE mutation is the same the one used in (Miura et al., 2009).

Mutation	Forward primer 5'-3'	Reverse primer 3'-5'
Ap2-747	GGAGGCGAGCCCCTTCCCATTGG GTGGGGGCGGCAAC	GTTGCCGCCCCCACCCAATGGGAA GGGGCTCGCCTCC
Ap2-850	GCAGGCCCGCAGCGTTGAGGAG GAGGAGGAGCCGCCG	CGGCGGCTCCTCCTCCTCCTCAACG CTGCGGGCCTGC
E-box	CGGGGCGCGCAGTCACGTGACT TGGGGCGCC	GGCGCCCCAAGTCACGTGACTGCG CGCCCCG
N-box	GGAACGTAGTGGGGCTGATCTTC CAGAACAAAGTTGCTGGGCCG	CGGCCCAGCAACTTTGTTCTGGAAG ATCAGCCCCACTACGTTCC
NFAT	GTGCGTTTGTGTGTGCATATTGA ACAGAAAAATAAGGTCAGCGC	GCGCTGACCTTATTTTTCTGTTCAAT ATGCACACACAAACGCAC
PPRE	CAGAAAAATAGAGCTCGCGCAA ACACTACTTGTAATAC	GTATTACAAGTAGTGTTTGCGCGAG CTCTATTTTTCTG
Sp1-755	CCTTCCCGGGGGGTGGGTTCGGC AACGCGCGACCCAGCG	CGCTGGGTCGCGCGTTGCCGAACCC ACCCCCCGGGAAGG

Table 2.2 Primers used for pUB mutagenesis.

2.10.2 pMyb+, pSocs6+, pMyb-/-, pSocs6-, pMgst1+

The pMyb+ and pSocs6+ constructs were generated by amplifying and inserting the 3' UTRs of the genes *myb* and *socs6* into the psiCheck2.2 vector which was a generous gift from Mr. Tom Roberts and Dr. Matthew Wood (Department of Physiology, Anatomy and Genetics, University of Oxford). The psiCheck2.2 vector consists of a *firefly luciferase* gene under the influence of a constitutive HSV-TK promoter, and a *renilla luciferase* gene under the influence of a constitutive SV40 promoter. Immediately downstream of the *renilla* gene is a multiple cloning site (MCS) into which can be inserted a 3' UTR sequence.

The 3' UTRs of *myb* and *socs6* were amplified using the Expand Long Template PCR System (Roche) following manufacturer's instructions. Table 2.3 contains the sequences of the PCR primers used. The forward primers and the reverse primers also contained *Xho* I and *Not* I restriction sites respectively for eventual insertion into the MCS of the psiCheck2.2 vector. 200 ng of template DNA purified from the tails of C57Bl/6 mice was used in a total reaction volume of 50 μL.

Target	Forward primer 5'-3'	Reverse primer 3'-5'
Myb 3' UTR	GAGACTCGAGGAACGCGTTCTCAGCTCGAAC	GAGAGCGGCCGCCATCTCCTCGAATATGTAACC
Socs6 3' UTR	GAGACTCGAGTGCAGGAGAAGCACTACTGAG	GAGAGCGGCCGCCAGCAGGTCTGACCTAAGATG

Table 2.3 Primers used to amplify the 3' UTR of the genes *myb* and *socs6*.

The cycling conditions used were as follows:

Step	Temperature	Duration
Initial denaturation	94°C	2 min
Denaturation	94°C	10 s
Annealing	55°C	30 s x10
Elongation	68°C	2 min
Denaturation	94°C	15 s
Annealing	55°C	30 s x25
Elongation	68°C	2 min 20 s
Final Elongation	68°C	7 min

Amplified PCR products were purified from agarose gels using the Qiagen gel purification kit, following manufacturer's instructions. Purified products were ligated with 50 ng of pGEM-T vector (Promega) at an Insert:Vector molar ratio of 1:1. Ligations were performed in a total reaction volume of 10 µl overnight in a water bath at 16°C.

1 µl of ligation reactions were transformed into 30 µl of *E. coli* TOP10 competent cells (Invitrogen) following manufacturer's instructions. Ligation and transformation efficiencies were calculated by transforming a control ligation reaction containing control insert DNA and pGEM-T vector, and another control reaction containing only cut vector. Transformed cells were plated on LB agar plates (supplemented with ampicillin at a ratio of 1:2,500 and 40 µl of 40 mg/ml X-gal) and incubated at 37°C overnight. White colonies (indicative of successful ligation) were picked the following day and inoculated in 5 mL cultures of LB broth (Invitrogen) supplemented with ampicillin (at a ratio of 1:2,000) overnight at 37°C. Plasmid DNA was purified the following day using a Qiagen Miniprep kit. SDM was then performed as described in section 2.10.1 using 10 ng of

template pGEM-T constructs containing the 3' UTRs of *myb* and *socs6* to delete sections of the predicted miR-503 seed regions. Table 2.4 contains the mutagenesis primers used.

Mutation	Forward primer 5'-3'	Reverse primer 3'-5'
Myb 3' UTR seed region 1	GAGAAATGTGTTCGCTGGTTTTAGCCTGTAG	CTACAGGCTAAAACCAGCGAACACATTTCTC
Myb 3' UTR seed region 2	GCCTGTAGTCATGCGCTAGTGTCAGG	CCTGACACTAGCGCATGACTACAGGC
Socs6 3' UTR seed region	CCCTTCCAGTCCTTTGATCCACTGTGATTC	GAATCACAGTGGATCAAAGGACTGGAAGGG

Table 2.4 Primers used for *myb* and *socs6* 3' UTR mutagenesis.

The pGEM-T construct containing the 3' UTR of *myb* was subjected to two consecutive rounds of SDM to mutate both miR-503 seed regions. Mutagenized constructs were then transformed into supercompetent cells as described in section 2.10.1. Wild-type and mutagenized inserts were cut out of the pGEM-T vectors using the restriction enzymes *Xho* I and *Not* I (New England Biolabs) in a restriction digest reaction containing 0.5 µl of each enzyme and 0.5 µg of DNA in a total reaction volume of 20 µl. Restriction digests were performed in a water bath at 37^{o}C for 1 hour and then run on an agarose gel and inserts were gel purified using a Qiagen gel purification kit. The psiCheck2.2 vector was also cut using the same enzymes (in a total reaction volume of 20 µl), and treated with 0.5 µl of calf intestinal phosphatase at 37^{o}C for 1 hour following the restriction digest, and gel purified. 100 ng of cut vector was ligated with purified insert (at an Insert:Vector molar ratio of 3:1) using T4 DNA ligase (New England Biolabs) in a total reaction volume of 20 µl at 16^{o}C overnight. 1 ul of the ligation reaction was transformed into supercompetent cells, grown overnight and plasmid DNA was purified as described in section 2.10.1.

pMgst1+ is a construct that contains the 3' UTR of the gene *mgst1* inserted into the MCS of the psiCheck2.2 vector and was a generous gift by Mr. Tom Roberts and Dr. Matthew Wood.

2.11 Statistics

Data were analysed using paired or unpaired two-tailed *t*-tests, or one-way analysis of variance (ANOVA) followed by Bonferroni post-hoc correction as indicated. Only *p*-values < 0.05 were deemed significant.

3 A study of the effect of exercise on the *Fiona* mouse model

3.1 Introduction

As described in detail in section 1.3.3., the *Fiona* mouse is an *mdx* transgenic mouse that overexpresses the full-length utrophin protein in skeletal muscle. Various studies have shown that it is completely rescued and does not display any of the dystrophic characteristics of *mdx* mice. However, these studies have only been performed on sedentary mice (Tinsley et al., 1998). The aim of the work in this chapter was to see if *Fiona* mice continued to display this rescued phenotype after an extended period of sustained exercise-induced stress, or whether they reverted to the dystrophic phenotype.

The exercise protocol used in this study is the same one referred to in section 1.3.1.1 that has successfully been used to exacerbate the dystrophic phenotype of *mdx* mice, and is now widely accepted as a standardized stress-inducing protocol (Grounds et al., 2008). Briefly, four-week-old C57BL/6 (referred to as 'C57' in this chapter), *mdx*, and *Fiona* mice were divided into two groups – 'sedentary' and 'run'. Those in the 'run' group were made to run on a treadmill at 12 $m.min^{-1}$ for 30 minutes, twice a week, for 8 weeks. After the end of the trial, muscle samples were dissected out and subjected to a range of *ex vivo* tests.

3.2 The effects of running on total body mass and EDL mass

The final body mass and EDL mass were measured for each of the mice to see if exercise had a significant impact on either of these parameters. There was no significant difference in final body weight between sedentary and run mice of any of the three genotypes. A significantly higher EDL mass was recorded for run *Fiona* mice compared to sedentary mice (Table 3.1).

A

	Total body mass (g)		
	C57	*mdx*	*Fiona*
Sedentary	21.8 ± 3.8	25.7 ± 4.1	22.2 ± 3.2
Run	23.0 ± 3.8	27.7±4.3	24.0 ± 3.3

B

	EDL mass (mg)		
	C57	*mdx*	*Fiona*
Sedentary	10.4 ± 0.5	12.9 ± 0.4	7.4±0.6
Run	10.3 ± 0.3	14.4±0.7	9.8±0.6*

Table 3.1 The effect of exercise on A) body mass and B) EDL mass. Exercise did not have a significant effect on body mass and a significant effect on EDL mass only for *Fiona* mice. * = $p < 0.05$ relative to sedentary using an unpaired two-tailed *t*-test ($n = 6$ per group).

3.3 Exercise had differential effects on the contractile properties of EDL muscle from *mdx*, *Fiona*, and C57 mice

The EDL muscle from each mouse was carefully dissected out with its tendons intact and subjected to a range of *ex vivo* tests to assess its contractile properties.

The TTP does not appear to have been significantly altered by exercise. A significant increase in $RT_{1/2}$ was observed for run compared to sedentary *mdx* mice (Table 3.2).

	Sedentary			Run		
	C57	*mdx*	*Fiona*	C57	*mdx*	*Fiona*
TTP, ms	26.2±2.2	30.7±2.2	34.3±2.0	32.0±1.8	30.7±1.6	39.6±2.7
$RT_{1/2}$, ms	65±6.6	55±4.9*	92±9.8	78.3±6.3	76.3±5.1*	88.8±3.3

Table 3.2 The effect of exercise on TTP and $RT_{1/2}$ of EDL muscle. Exercise did not have a significant effect on TTP for all three mouse groups and resulted in a significant increase in $RT_{1/2}$ for *mdx* mice. * = $p < 0.05$ relative to sedentary using an unpaired two-tailed *t*-test ($n = 6$ per group).

Exercise did not result in a significant increase in susceptibility to a series of eccentric contractions as indicated by a lack of difference in the percentage force drop between sedentary and run groups of all three genotypes (Figure 3.1A).

Exercise appears to have had detrimental effects on the force production abilities of *mdx* and *Fiona* muscles, while having spared C57 muscle. There were significant reductions in normalized maximum isometric force production in *mdx* and *Fiona* EDL muscle, but not in C57 muscle (Figure 3.1B).

Left-ward shifts in the force-frequency curves were observed in all three genotypes as a result of exercise (Figure 3.1C). However, this shift was significant only for the *Fiona* mice (at five data points).

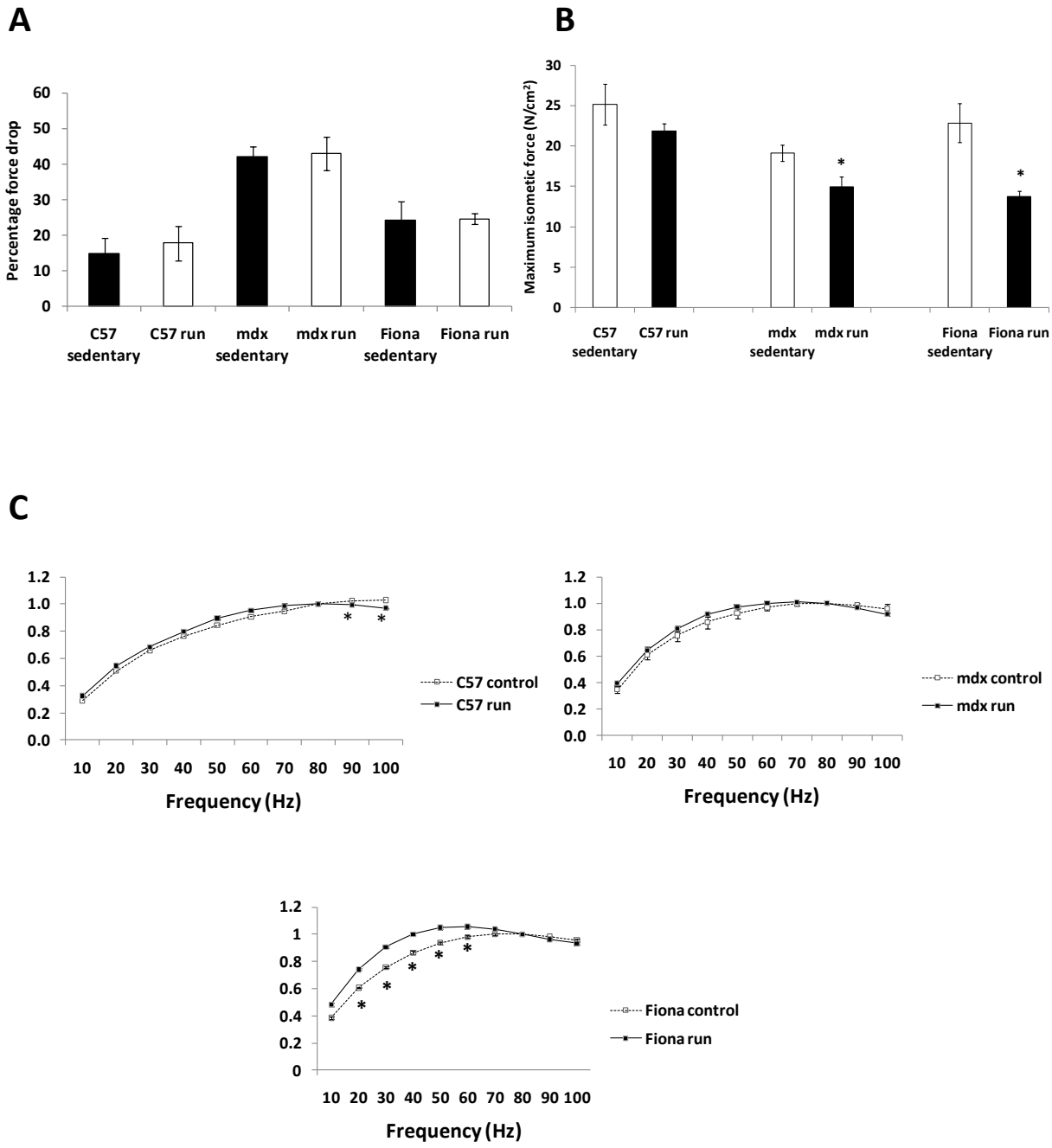

Fig. 3.1 Contractile properties of EDL muscle from run and sedentary mice. A) Exercise did not have a significant effect on percentage force drop following a series of eccentric contractions in all three mouse groups. B) EDL muscle from *mdx* and *Fiona* showed significant reduction in normalized maximum isometric force in run mice. C) A marked leftward shift was seen in the force-frequency curves as a result of exercise for all three mouse groups. * = $p < 0.05$ relative to sedentary mice using an unpaired two-tailed *t*-test ($n = 6$ per group).

3.4 Exercise had a significantly adverse effect on the histological profile of muscle from *mdx* mice only

H & E stained EDL muscle sections were used to quantify the percentage of centrally-nucleated fibres (%CNFs) and assess the gross morphology of the muscle. A significant increase in %CNFs due to exercise was observed only in the case of *mdx* mice (61.7 ± 6.2% for the sedentary *mdx* mice compared to 87.6 ± 1.3% for the run *mdx* mice; $p < 0.05$ relative to sedentary mice using an unpaired two-tailed *t*-test ($n = 6$ per group)).

EDL sections from sedentary *mdx* mice displayed characteristic dystrophic signs – increased number of CNFs, uneven fibre size and a build-up of connective tissue between muscle fibres. These signs were absent in sections from sedentary C57 and *Fiona* mice. These dystrophic signs are even more apparent in sections from run *mdx* mice, indicating the muscle-damaging impact of the exercise protocol. Sections from sedentary and run C57 mice were not noticeably different (Figure 3.2).

Although the run *Fiona* mice did not display a significant increase in %CNFs compared to sedentary mice, sections from these mice did contain isolated areas displaying signs of successive rounds of regeneration and degeneration, as indicated by centronucleation and smaller myofibres. This suggests the slightly deleterious impact of the protocol on *Fiona* mice. However, this effect was not quantifiably significant.

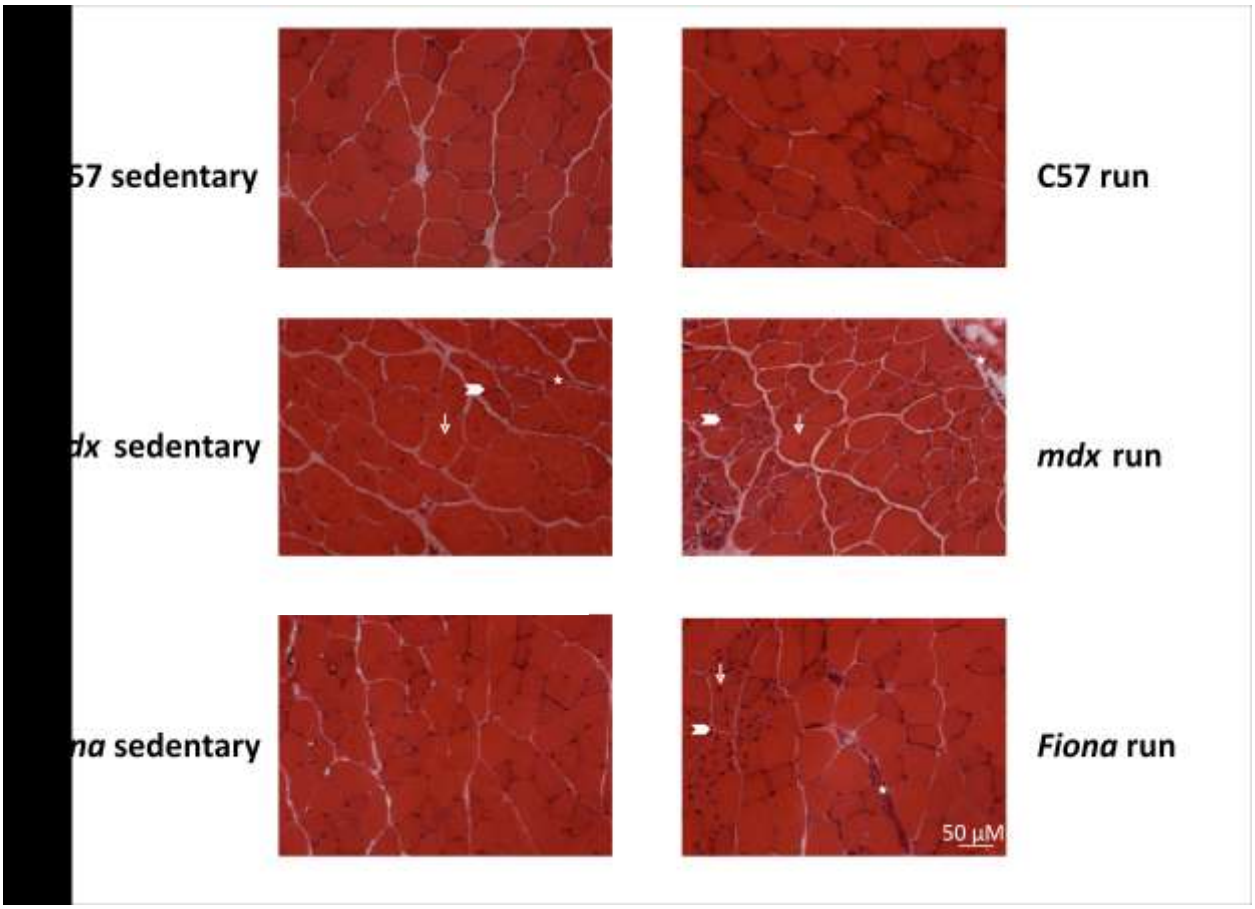

Fig. 3.2 EDL cryosections stained with H & E. *mdx* mice displayed a worsened histopathology as a result of exercise. Arrows indicate centrally-nucleated fibres, chevrons indicate uneven fibre size, and asterisks indicate build-up of connective tissue between fibres.

3.5 Exercise did not result in a significant change in blood serum CK levels in any of the three genotypes

Elevated blood serum CK levels are an index of overall muscle damage. The exercise protocol did not result in a significant increase in CK levels in any of the three genotypes, although there were mild increases in CK levels as a result of exercise for all three genotypes (Figure 3.3).

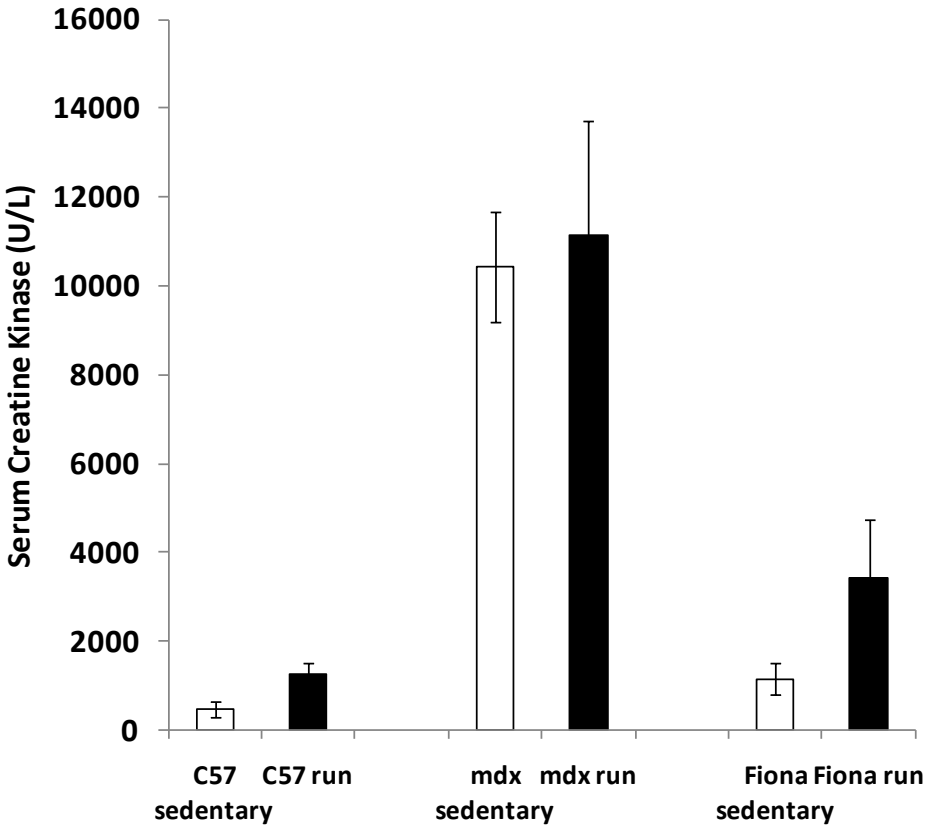

Fig. 3.3 Blood serum CK levels in run and sedentary mice. No significant difference in blood serum CK levels between run and sedentary mice (n = 6 per group).

3.6 Discussion

The overall aim of this study was to assess the impact of exercise-induced stress on the *Fiona* mouse to test the hypothesis that it continues to display its rescued non-dystrophic phenotype (Tinsley et al., 1998). *mdx* and C57 mice were included as key controls to aid in the interpretation of the results.

The results from this study show that the exercise protocol used severely alters the contractile properties of *mdx* hind limb muscle while sparing C57 muscle. These results recapitulate those found previously (Granchelli, 2000; Grounds et al., 2008; Luca, 2002, 2005). The effects on *Fiona* muscle were significantly deleterious according to some parameters but not others.

The susceptibility of the EDL muscle to contraction-induced damage was assessed by measuring the deficit in maximum isometric force following a series of five eccentric contractions. No change in percentage force drop was observed in any of the three genotypes as a result of the exercise protocol. This indicates that the protocol did not have a damaging effect on C57 EDL muscle according to this parameter, a finding that is consistent with the other results in this study. The absence of any increase in percentage force drop for EDL from run *mdx* mice could be explained by the fact that since muscles from sedentary *mdx* mice display a very high percentage force drop, any additional force drop as a result of the protocol would escape notice. The lack of increase in percentage force drop for EDL from run *Fiona* mice indicates that utrophin continues to protect the sarcolemma against stretch-induced damage (Tinsley et al., 1998).

The exercise protocol resulted in significant decreases in the normalized maximum isometric force produced by *mdx* and *Fiona* muscle, but not by C57 muscle, with the percentage decrease being greater for *Fiona* mice than for *mdx* mice. These results for the *mdx* and C57 mice are consistent with those found previously (De Luca et al., 2008; Luca, 2005) which show a significant reduction in muscle strength in *mdx* but not C57 mice as a result of the same protocol. It is worth noting that it has been shown that the normalized isometric force produced by a muscle and its resistance to contraction-induced damage are not necessarily correlative (Harper et al., 2002) so the results in this study for the *Fiona* mice are not unusual.

There were also leftward shifts in the force frequency relationships as a result of exercise for muscles of all three genotypes. However, this shift was significant at multiple data points only for *Fiona* muscle.

The changes in *Fiona* muscle properties as a result of exercise – reduction in maximum isometric force accompanied by a significant leftward shift in the force-frequency curve – mirror the dystrophic progression with age seen in *mdx* EDL muscle (Petrof et al., 1993). These results are also in keeping with a fast-to-slow fibre type switch. Skeletal muscle fibres can be divided into four types depending on the myosin heavy-chain (MHC) isoform they express (myosin II, the skeletal muscle specific myosin, consists of two heavy chains and four light chains (Schiaffino and Reggiani, 1996)). The four MHC

isoforms are – type I, type IIa, type IIb and type IIx. Muscle fibres vary considerably in terms of contractile and metabolic properties depending on the MHC isoform expressed. Muscle fibres expressing type I MHC are termed "slow twitch" and primarily use oxidative metabolism and are resistant to fatigue. The other three kinds of muscle fibres are termed "fast twitch", with those that express the type IIa isoform making use of both glycolytic and oxidative metabolism and those that express the type IIb or type IIx isoforms primarily using glycolytic metabolism (Bassel-Duby and Olson, 2006; Miura and Jasmin, 2006). Myofibres display remarkable plasticity and are able to alter the type of MHC isoform they express, thereby dramatically changing their phenotypic properties. For example, it has been shown that reinnervation of a typically slow-twitch muscle like the soleus with nerve fibres that normally stimulate fast-twitch fibres changes the properties of this muscle to a more fast-twitch phenotype. The converse has also been shown using a typically fast-twitch muscle (Bassel-Duby and Olson, 2006). Pathology has also been shown to induce fibre type change, with dramatic alterations in fibre type having been observed in muscles from both *mdx* mice and DMD patients. A progressive increase in the proportion of type I fibres has been observed in the soleus muscle (Anderson et al., 1988; Carnwath and Shotton, 1987) and the EDL muscle (Anderson et al., 1988) of *mdx* mice. There is a similarly noticeable increase in the proportion of type I fibres in DMD muscle (Marini et al., 1991). It is also worth noting that the *dko* mouse (discussed in section 1.3.2) also displays a remarkable fast-to-slow fibre type switch (Rafael et al., 2000) with an increase in expression of slow muscle fibre type genes compared to *mdx* mice (Baker et al., 2006).

The EDL is mostly composed of fast-twitch fibres that are more susceptible to damage than slow-twitch, likely because they are larger and have a lower area-to-volume ratio (Karpati and Carpenter, 1986). It is well documented that muscles composed primarily of slow-twitch fibres, such as the soleus, produce less force than those composed primarily of fast-twitch fibres, like the EDL (Lynch et al., 2001; Lynch et al., 2000). It also explains the leftward shift seen in the force-frequency relationship for *mdx* compared to wild-type mice (Petrof et al., 1993). Therefore, an attractive explanation for both the significant reductions in isometric force production by both run *mdx* and *Fiona* mice, and the significant leftward shift in the force-frequency relationship for run *Fiona* mice,

could be the preferential loss of fast-twitch fibres in the EDL muscle as a result of the protocol. Alternatively, as has been suggested for the fibre type change seen in aged *mdx* mice (Petrof et al., 1993), the exercise protocol might have resulted in transformation of existing fast fibres to a slower phenotype as a protective response to stress-induced damage as type I fibres consume less energy and are more resistant to fatigue.

Muscles composed primarily of slow-twitch fibres have longer TTP and $RT_{1/2}$ values compared to those composed primarily of fast-twitch fibres (Pastoret and Sebille, 1995). Therefore, a rise in TTP would reflect a fast-to-slow-twitch fibre switch. No increase was observed in TTP for *mdx* or C57 mice as a result of exercise. However, there was a noticeable increase (albeit non-significant) in TTP for run compared to sedentary *Fiona* mice, which is consistent with the leftward shift seen in the force-frequency curve. Increases in $RT_{1/2}$ were observed for C57 and *mdx* mice as a result of exercise (significant only for *mdx*), which is in keeping with the leftward shift seen in their corresponding force-frequency curves.

An additional explanation for the significant reductions in isometric force production by run *mdx* and *Fiona* mice could be the increased presence of embryonic and neonatal tissue as evidenced by increased levels of degeneration and regeneration seen in the H & E EDL sections from run mice. *mdx* muscle, particularly during the crisis period, experiences massive fibre degeneration and regeneration which results in the replacement of damaged myofibres by neonatal and embryonic fibres (DiMario et al., 1991) which are known to have a lower capacity for force generation (Reiser et al., 1985). However, this is a more likely explanation for *mdx* than *Fiona* mice because this increase was quantatively significant only for the former. A further reason for the significant reductions in isometric force production by run *mdx* and *Fiona* mice could be the build-up of pockets of connective tissue in run compared to sedentary mice.

A frequently used index of sarcolemmal damage is serum CK, with increased activity as a result of dystrophy (Ozawa et al., 1999). Exercise did not result in a significant increase in serum CK in any of three genotypes. Similar results for C57 and *mdx* mice have been found by other groups using the same protocol (De Luca et al., 2008). These results must

however be interpreted with caution as this parameter is not always correlated with histology and could therefore be masking membrane damage that might be present.

The results from this study indicate that the skeletal-muscle specific overexpression of utrophin in *mdx* mice is sufficient to protect the sarcolemma from stress-induced damage caused by the exercise protocol used. However, this protocol appears to have altered the fibre type properties of the muscle and caused a significant reduction in force production.

There are many possible reasons why stress-inducing exercise could have a more deleterious impact on skeletal muscle from *Fiona* mice compared to muscle from C57 mice. Although dystrophin and utrophin bind to the same proteins, it has been shown that they bind to them is significantly different ways. Although they both bind to F-actin via their N-termini, utrophin binds with a lower affinity via this domain (Levine et al., 1990; Winder et al., 1995). Dystrophin also binds to actin via the spectrin-like repeats 11-17 of its rod domain (Amann et al., 1998), whereas utrophin additionally binds to actin via the first ten spectrin-like repeats of its rod domain (Rybakova and Ervasti, 2005). Thus, dystrophin binds to actin via two separate domains, whereas utrophin binds to actin via one extended contiguous domain. This has been proposed to allow a more elastic response of the actin-dystrophin-sarcolemma linkage to muscle stretches compared to utrophin (Rybakova et al., 2006). Utrophin also has reduced lateral contact with actin filaments compared to dystrophin, with one full-length utrophin molecule being able to bind to 14 actin monomers when saturated (Rybakova et al., 2002) versus 24 actin monomers that can be occupied by a single full-length dystrophin molecule when saturated (Rybakova et al., 1996). In light of these differences, perhaps the *Fiona* mouse is less resistant to exercise-induced damage than the C57 mouse because the actin-utrophin-sarcolemma linkage is less effective at transmitting the increased contractile forces generated by the myofibrils as a result of the exercise protocol to the ECM and adjacent muscle fibres.

Utrophin also displays a weaker association with β-dystroglycan than does dystrophin (Imamura et al., 2000). Although they both bind to β-dystroglycan via the ZZ domains of their C-termini, utrophin binds more weakly by about 2-fold (Ishikawa-Sakurai et al., 2004). This perhaps suggests that utrophin is more likely than dystrophin to weaken or

sever its connection with the rest of the DAPC (and hence the sarcolemma) under conditions of stress-induced damage.

Dystrophin and utrophin have also been shown to bind to different isoforms of syntrophin, with dystrophin binding mostly to α1- and β1-syntrophin and utrophin binding to β1- and β2-syntrophin (Peters et al., 1997). The authors of this study suggest that the recruitment of different syntrophin isoforms could result in the expression of different signalling proteins at the sarcolemma. This predicted difference might result in different levels of susceptibility to stress-induced damage.

Finally, results in this study were included in a paper that highlighted the differential susceptibility of the sarcolemma to stress-induced damage depending on whether dystrophin or utrophin was expressed (Li et al., 2010). We suggested that wild-type mice (which express physiological normal levels of dystrophin) are more resistant to damage-inducing exercise than *Fiona* mice because dystrophin is able to successfully recruit nNOS (via the spectrin-like repeats 16 and 17 within its rod domain (Lai et al., 2009)) whereas utrophin is not. The absence of nNOS at the sarcolemma of *Fiona* mice is thought to result in functional ischemia as a result of exercise.

In conclusion, this is the first study that highlights a functional difference between dystrophin and utrophin. Due to the inability of utrophin to recruit nNOS to the sarcolemma, therapies based on the upregulation of utrophin will likely have to be accompanied by treatments that maintain muscle perfusion, particularly during periods of exercise.

4 Therapeutic effects of the drug GW501516 on the *mdx* mouse

(Note: this work was performed in collaboration with Sarah Squire, Allyson Potter, David Powell and Rebecca Fairclough).

4.1 Introduction

In the previous chapter the ability of utrophin to maintain its protective role following an extended period of exercise-induced stress was assessed. Although utrophin does not perform as well as dystrophin during a protracted bout of exercise-inducing stress, it nonetheless partially retains its protective function, as evidenced by only a mild increase in centronucleation and comparable protection of the sarcolemma against eccentric contractions to utrophin in sedentary mice. Therefore, although results from the previous chapter suggest that the upregulation of utrophin expression might not be entirely sufficient as a therapeutic strategy, the fact that supraphysiological levels of utrophin have potent therapeutic effects in the sedentary *mdx* mouse, some of which are retained in the exercised mouse, indicates that the quest for a means of upregulating utrophin expression should be earnestly pursued.

The use of natural or synthesized small molecules as a therapeutic option, known as the pharmacological approach, and its advantages were discussed in section 1.4.4. In section 1.4.5, the use of small molecules, namely heregulin and L-arginine, to successfully upregulate utrophin in the *mdx* mouse was discussed. The targeting of pathways that orchestrate the fast-to-slow myofibre switch as a means of upregulating utrophin expression was also discussed in this section, and it is this strategy that is specifically pursued in this chapter.

As mentioned in section 1.2.2, utrophin expression in adult skeletal myofibres is normally largely restricted to the postsynaptic membrane of the NMJ, both at the mRNA transcript (Gramolini et al., 1997) and the protein (Ohlendieck et al., 1991) levels. However, there are conditions under which this expression can extend to the rest of the sarcolemma. For example, utrophin displays extrasynaptic expression in slow myofibres (Chakkalakal et al., 2003; Gramolini et al., 2001) and this is thought to be the direct result of the increased oxidative capacity and mitochondrial content of these fibres.

Importantly, slow muscle fibres have been shown to be more resistant to damage in both DMD patients and *mdx* mice. Type IIb fibres experience both degeneration and extensive regeneration before degeneration appears in type I fibres of DMD patients (Webster et al., 1988). Also, EDL (a typically fast muscle) from *mdx* mice has been shown to be more susceptible to a series of *in vitro* isometric contractions than control muscle, but no difference in the response of the soleus (a typically slow muscle) from *mdx* and control mice to this protocol was observed (Moens et al., 1993). In addition to the reason mentioned in section 3.6 as to why slow fibres are more resistant to damage than fast fibres (lower area-to-volume ratio), it is reasonable in light of the studies mentioned to propose that sarcolemmal expression of utrophin is another reason for this. This proposal has stimulated research attempting to decipher the mechanisms that orchestrate the sarcolemmal utrophin expression observed in slow fibres.

A number of pathways have been identified that control fast-to-slow fibre switch and the resultant increase in utrophin expression. One of these is the calcineurin-NFAT pathway mentioned in section 1.2.2. Calcineurin is a phosphatase that is under the regulatory control of calcium. It exists as a heterodimer that consists of two parts – CNA (catalytic subunit) and CNB (Ca^{2+}-binding regulatory subunit). It exerts its influence on gene expression by dephosphorylating the serine-rich region near the N-terminus of NFAT, a molecule that normally resides in the cytoplasm of unstimulated cells. This dephosphorylation results in the unmasking of two nuclear localization sequences and subsequent import into the nucleus where it binds to the promoters of target genes (including utrophin (Angus et al., 2005)). Importantly, constitutive expression of calcineurin under the influence of the muscle-specific muscle CK (MCK) enhancer results in an increase in the proportion of type I fibres in the hind limb muscles of these transgenic mice, and pharmacological inhibition of calcineurin leads to a decrease in the proportion of type I fibres and reduced expression of enzymes involved in oxidative metabolism. Also, prolonged, low-amplitude Ca^{2+} signals (a feature of slow fibres) results in the maintenance of NFAT in the nucleus whereas high-amplitude Ca^{2+} transients (a feature of fast fibres) do not (Olson and Williams, 2000). Calcineurin inhibition has also been shown to result in a significant decrease in utrophin mRNA levels in mouse skeletal muscle. Increased calcineurin expression results in increased

utrophin expression via the binding of NFAT to an NFAT-binding site in the utrophin A promoter (Chakkalakal et al., 2003). Transgenic *mdx* mice that constitutively overexpress calcineurin in skeletal muscle display an ameliorated phenotype, whose muscles are less susceptible to contraction-induced injury and express higher levels of utrophin (Stupka et al., 2006).

In addition to the calcineurin-NFAT pathway, PGC-1α has also been shown to promote the formation of slow fibres. Transgenic mice that express PGC-1α at physiological levels under the influence of an MCK promoter (which is preferentially activated in type II fibres) display a fast-to-slow fibre switch. The absence of calcineurin has been shown to inhibit this PGC-1α-mediated fibre type switch, indicating cooperation between the calcineurin pathway and PGC-1α (Lin et al., 2002). PGC-1α has also been shown to upregulate utrophin expression at the NMJ by acting synergistically with GABPα (Angus et al., 2005). Heregulin-stimulated phosphorylation of PGC-1α and GABP results in the formation of a complex that enhances the transcription of a range of genes important for NMJ function, including utrophin. The muscle-specific overexpression of PGC-1α under the influence of an MCK promoter in transgenic *mdx* mice results in an increase in utrophin expression and a concomitant amelioration of phenotype (Handschin et al., 2007). A number of pathways converge onto the PGC-1α promoter in skeletal muscle. In addition to being influenced by calcineurin activity, PGC-1α is also under the direct influence of CaMKIV and MEF2 (Handschin et al., 2003). Both calcineurin-NFAT and PGC-1α are under the influence of Ca^{2+}/calmodulin (CaM) signalling. Transgenic *mdx* mice expressing a small peptide inhibitor for CaM (CaMBP) under the influence of the troponin I slow promoter display a worsened phenotype, slow-to-fast fibre type switch and reduced utrophin expression (Chakkalakal et al., 2006).

An additional pathway that has recently been shown to promote the slow myofibre program involves PPARδ. It has been shown that the muscle-specific overexpression of PPARδ results in a significant increase in the oxidative capacity of skeletal muscle, partially mimicking the effects of endurance exercise (Luquet et al., 2003). Another mouse engineered to express PPARδ under the influence of the human skeletal actin promoter was able to run twice the distance of wild-type littermates and displayed an

increase in the number of type I muscle fibres. Treatment of mice with a PPARδ agonist GW501516 (the same agonist used in this study), resulted in the enhanced expression of type I fibre genes (Wang et al., 2004).

Wild-type mice treated with GW501516 have been shown to display an increase in the number of slow fibres along with the capacity to run significantly longer than untreated control mice when combined with exercise training. The purpose of the study described in this chapter was to test the ability of GW501516 to ameliorate the dystrophic phenotype of *mdx* mice via the increase of utrophin expression.

In this trial, four-week-old *mdx* mice were treated with either GW501516 or vehicle only via daily IP injections for four weeks. The reason for selecting four-week-old mice was that mice younger than four weeks of age displayed poor tolerance to daily injection in the animal facility used at the time. Untreated eight-week-old C57Bl/6 mice were included as wild-type controls.

4.2 GW501516-treated EDL muscle showed partial improvement in contractile properties

To assess the effects of GW501516 treatment on the contractile properties of the EDL muscle, this muscle was dissected out and subjected to the same tests mentioned in section 3.3. A significant reduction in the percentage force drop following eccentric contractions was observed in the GW501516-treated *mdx* group (38.8 ± 2.69%) compared to 58.0 ± 9.25% in *mdx* treated with vehicle alone (Figure 4.1A). The comparable figure obtained from eight week-old untreated C57 mice was 7.89 ± 2.74%. Despite this apparent reduction in the susceptibility of the EDL muscle to stretch-induced damage, no concurrent improvement in absolute force was seen (Figure 4.1B). The normalized isometric force was 18.8 ± 2.51 N/cm^2 in the GW501516-treated *mdx* group, compared to 20.8 ± 1.41 N/cm^2 in the group treated with vehicle alone. Eight week old C57 EDL muscle produced an average normalized isometric force of 44.5 ± 3.32 N/cm^2. There was no significant decrease in TTP observed in *mdx* mice as a result of treatment (Figure 4.1C) but there was a significant decrease in $RT_{1/2}$ (Figure 4.1D). A rightward

shift in the force versus frequency curve as a result of treatment was observed, indicating that the GW501516-treated muscle required less stimulation to produce the same force compared to *mdx* EDL treated with vehicle alone (Figure 4.1E). Despite this rightward shift following GW501516 treatment, it should be noted that a significant difference in force produced at a particular stimulation frequency was only obtained at 10 and 30 Hz for GW501516-treated EDL. In contrast, when the force produced over the same range of frequencies by eight-week old C57 EDL is compared with *mdx* treated with vehicle only, a significant difference was obtained at five stimulation frequencies between 10-60Hz.

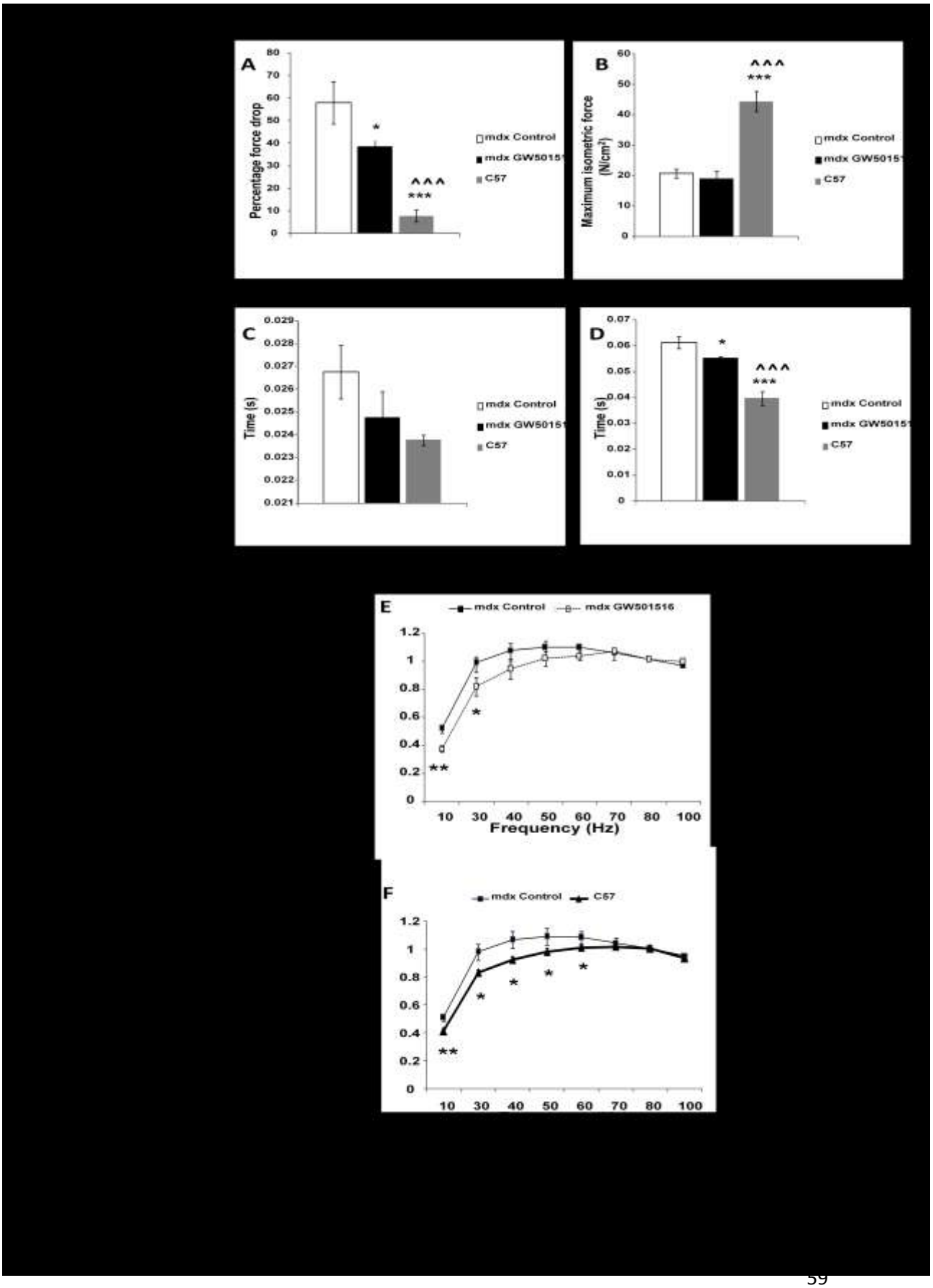
A
Percentage force drop
80
70
60
50
40
30
20
10
0
*
^^^
***
mdx Control
mdx GW501516
C57
B
Maximum isometric force (N/cm²)
60
50
40
30
20
10
0
^^^
***
mdx Control
mdx GW501516
C57
C
Time (s)
0.029
0.028
0.027
0.026
0.025
0.024
0.023
0.022
0.021
mdx Control
mdx GW501516
C57
D
Time (s)
0.07
0.06
0.05
0.04
0.03
0.02
0.01
0
*
^^^
***
mdx Control
mdx GW501516
C57
E
mdx Control
mdx GW501516
1.2
1
0.8
0.6
0.4
0.2
0
**
*
10 30 40 50 60 70 80 100
Frequency (Hz)
F
mdx Control
C57
1.2
1
0.8
0.6
0.4
0.2
0
**
*
*
*
*
10 30 40 50 60 70 80 100

Fig. 4.1 Contractile properties of EDL muscle from GW501516-treated *mdx*, control *mdx* and C57 mice. A) Significant decrease in percentage force-drop from treated vs. control *mdx* mice. B) No significant change in normalized maximum isometric force from treated vs. control *mdx* mice. C) No significant change in TTP from treated vs. control *mdx* mice. D) Significant decrease in $RT_{1/2}$ from treated vs. control *mdx* mice. E) Noticeable rightward shift in force-frequency curve from treated vs. control *mdx* mice. F) Noticeable leftward shift in force-frequency curve from control *mdx* vs. C57 mice. * = $p < 0.05$, ** = $p < 0.01$ and *** = $p < 0.001$ relative to control *mdx*; ^^^ = $p < 0.001$ relative to treated *mdx* using an unpaired two-tailed *t*-test ($n = 7$).

4.3 GW501516 treatment did not result in a significant decrease in centronucleation or blood serum CK level in *mdx* mice

To determine whether GW501516 treatment resulted in reduced muscle damage, the %CNFs was determined for tibialis anterior (TA) and diaphragm muscles dissected from GW501516 and vehicle treated *mdx* mice. TA was selected as a typical limb muscle and the diaphragm was selected because it displays the most dystrophic phenotype of all the skeletal muscles examined. No significant decrease in the %CNFs was seen for GW51516 treatment in either of the muscle groups analysed (Figure 4.2A). Consistent with the CNF data, there was also no significant reduction in blood serum CK levels for *mdx* mice treated with GW501516 compared to vehicle (Figure 4.2B).

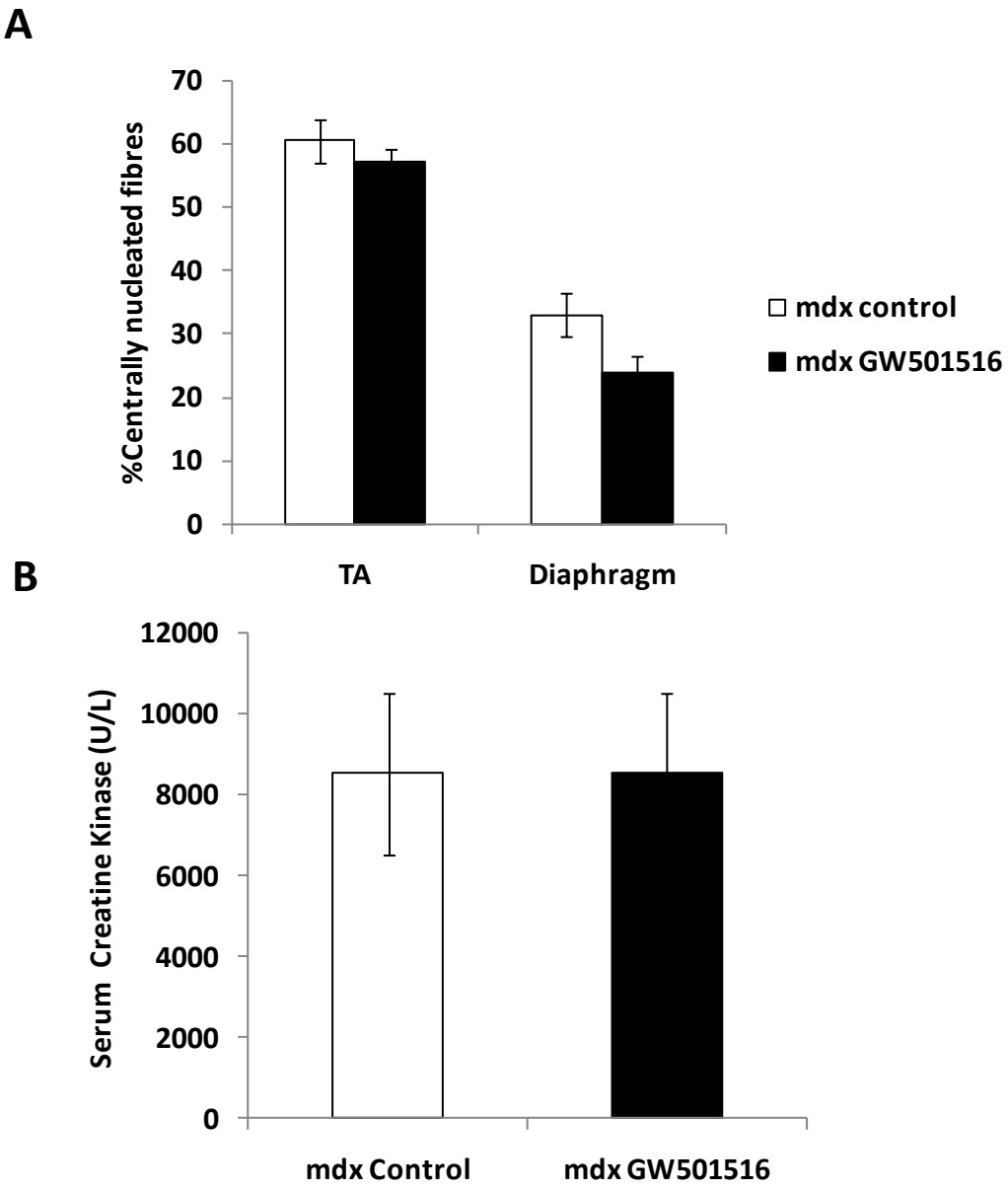

Fig. 4.2 Percentage of centrally nucleated muscle fibres and blood serum CK levels from GW501516-treated and control *mdx* mice. A) No significant difference in the %CNFs in TA or diaphragm between treated and control *mdx* mice. B) No significant difference in blood serum CK levels between treated and control *mdx* mice.

4.4 Fibre type staining indicated a slow-myofibre switch in GW501516-treated *mdx* mice

To confirm whether four-week IP injection of *mdx* mice with GW501516 was sufficient to cause a shift in fibre type composition towards increased numbers of slow fibres, TA muscle sections from GW501516 and vehicle treated *mdx* mice were stained for type I and IIa slow oxidative fibres. No staining of either MHC I or MHC IIa positive fibres was observed for any of the sections cut from each of the vehicle treated mice (Figure 4.3). In contrast, both MHC I and IIa fibres were observed in TA muscle from GW501516-treated *mdx* mice.

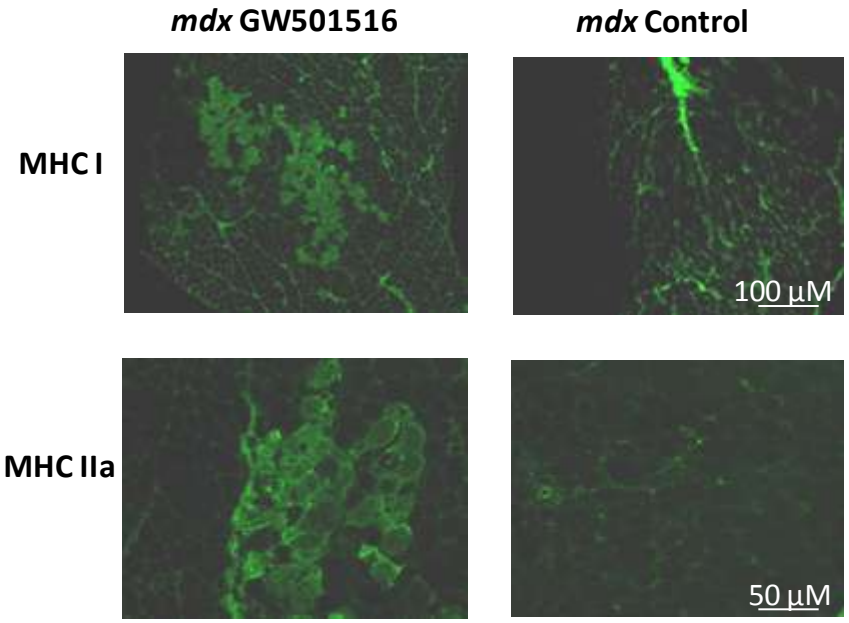

Fig. 4.3 Immunofluorescent staining for MHC I and MHC IIa fibres in TA muscles from GW501516-treated and control *mdx* mice. GW501516 treatment resulted in a noticeable increase in expression of both MHC I and IIa in TA muscle.

4.5 GW501516 treatment resulted in a significant increase in utrophin protein in *mdx* mice

To determine whether the increased numbers of slow fibres present in GW501516-treated *mdx* skeletal muscle was associated with an increase in utrophin levels, western blotting was used to quantify utrophin protein relative to the internal protein loading control α-actinin. A statistically significant increase in average utrophin protein levels was observed in GW501516 versus vehicle treated *mdx* for TA (Figure 4.4) but nor for diaphragm (Figure 4.5) muscle.

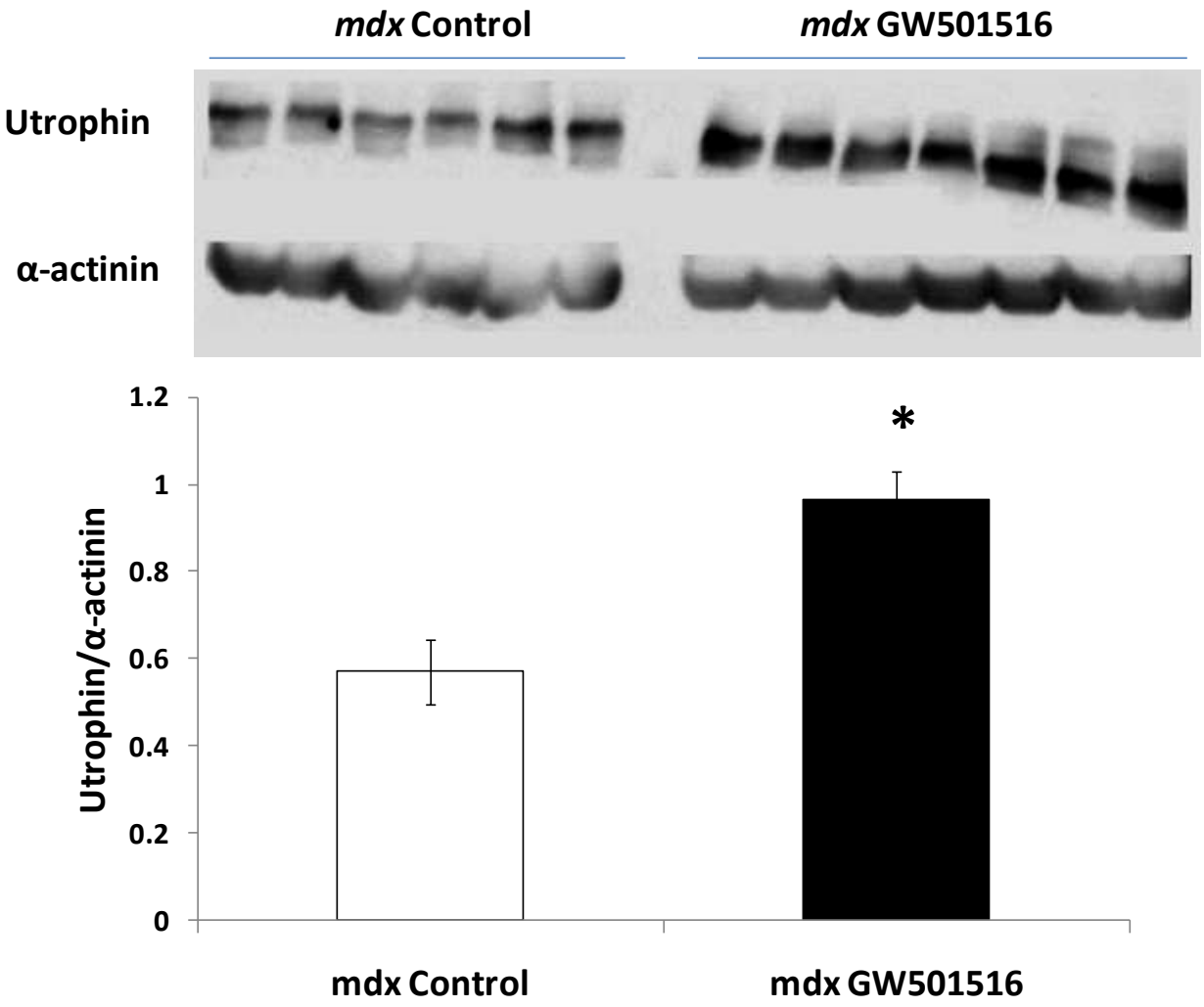

Fig. 4.4 Utrophin protein quantification in TA from GW501516-treated and control *mdx* mice. GW501516 treatment resulted in a significant increase in utrophin protein levels. * = $p < 0.05$ relative to control using an unpaired two-tailed *t*-test.

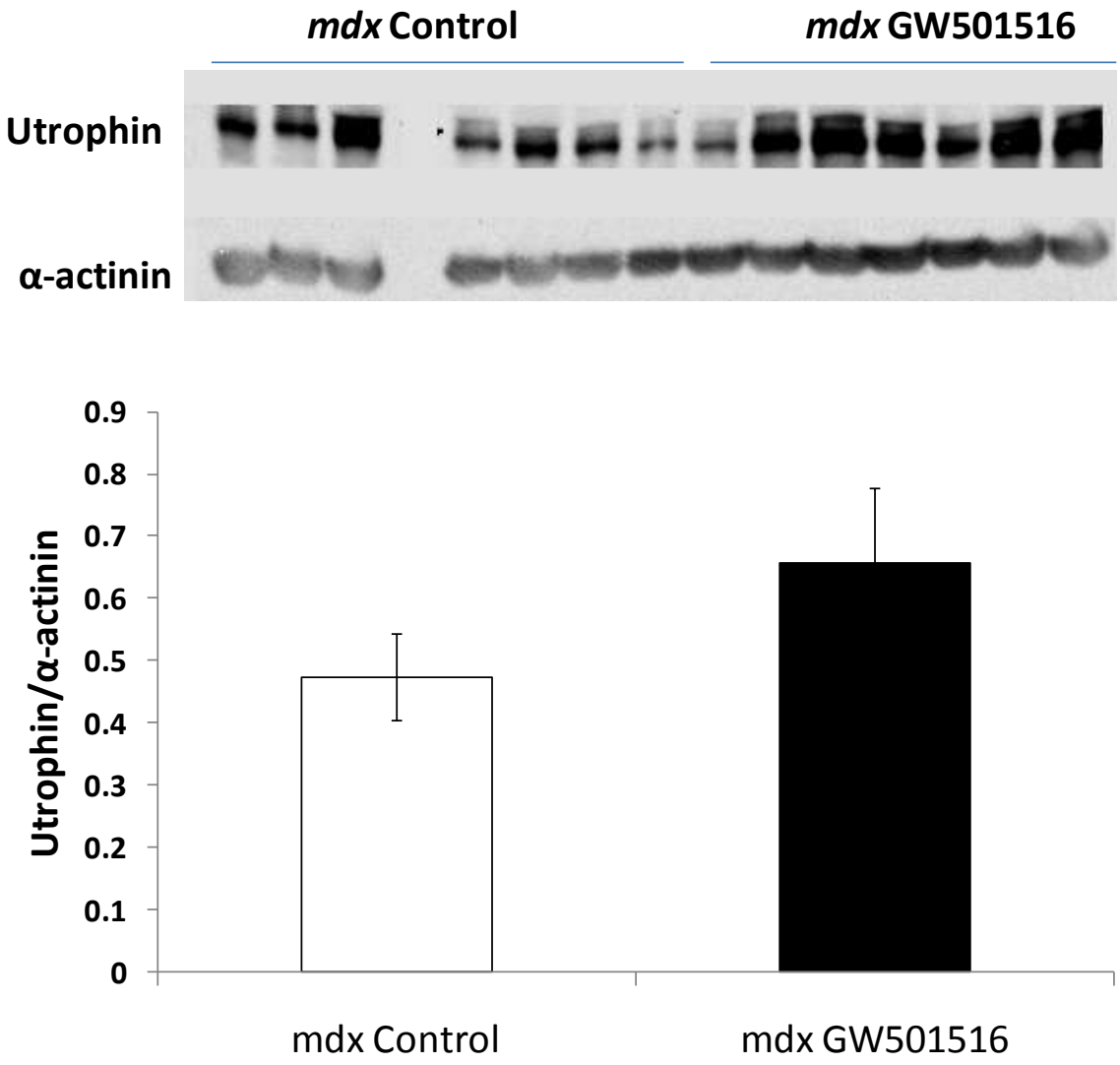

Fig. 4.5 Utrophin protein quantification in diaphragm from GW501516-treated and control *mdx* mice. GW501516 treatment did not result in a significant increase in utrophin protein levels.

4.6 Discussion

The aim of this study was to test the ability of the PPARδ agonist GW501516 to correct the phenotype of the *mdx* mouse and increase utrophin expression *in vivo*. To this end, GW501516 was administered daily via IP injections for four weeks to four-week-old

male *mdx* mice. This treatment regime resulted in the partial correction of the *mdx* dystrophic phenotype.

Treated *mdx* displayed a significant reduction in the percentage force drop following a series of five eccentric contractions but no change in isometric force production compared to untreated *mdx* mice. As discussed in section 3.6, such a finding is not without precedence. The increased resistance to contraction-induced injury could be explained by increased utrophin levels and/or shift to a slower fibre type (both discussed below). The lack of increase in isometric force as a result of treatment could be explained by the slow fibre switch. It is well established that typically slow muscles, like the soleus, produce less force than typically fast muscles, like the EDL (Lynch et al., 2000).

The leftward shift in the force-frequency curve for control *mdx* mice compared to wild-type mice is in keeping with previous observations (Petrof et al., 1993). Treatment with GW501516 results in a rightward shift of the force-frequency curve compared to untreated mice. Such a shift has also been observed in the muscles of *mdx* mice treated with L-arginine (to increase NO production, which has many therapeutic benefits). The authors suggest that this rightward shift is indicative of a correction of the Ca^{2+} imbalance known to exist in dystrophic muscle (dystrophic muscle exhibit significantly increased levels of Ca^{2+} influx (Hopf et al., 1996; Turner et al., 1991)) (Barton et al., 2005). Therefore, perhaps GW501516 treatment results in partial phenotype correction by means of the partial correction of this Ca^{2+} imbalance. In keeping with this rightward shift, the $RT_{1/2}$ was also lowered in treated compared to untreated *mdx* mice. There was, however, no change observed in the TTP as a result of treatment.

A noticeable increase in staining of type I and IIa fibres was observed in the TA muscle (a typically fast muscle) as a result of treatment. This is in keeping with the hypothesis that GW501516 treatment results in increased activity of PPARδ, which in turn drives the shift to a slower muscle phenotype. This also explains the increased resistance of treated muscle to contraction-induced injury because it has been shown by numerous groups that slow fibres are more resistant to this nature of damage than are fast fibres (Brooks, 1998; Consolino and Brooks, 2004; Dellorusso et al., 2001).

Utrophin protein expression levels were significantly increased in TA but not diaphragm (although a modest increase was observed in this muscle) as a result of treatment. This increase in expression could also explain both the increased resistance of the muscle to contraction-induced injury and the rightward shift in the force-frequency curve. This increase might be explained by the shift towards a slower muscle phenotype (slow muscles express more utrophin than fast muscles, as discussed in section 4.1) and/or the direct interaction of PPARδ with the utrophin promoter.

The therapeutic effects of GW501516 did not manifest themselves in terms of change in either levels of centronucleation or serum CK levels, as there was no difference with respect to these two parameters between treated and untreated *mdx* mice.

Shortly after the experiments described in this chapter were completed, another group published their results on the effect of GW501516 treatment on *mdx* mice (Miura et al., 2009). Although the condition of their experiment were not identical to ours (they chose to use mice aged 5-7 weeks and administered the drug via gavage treatment) it is still useful to compare the results of these two studies. There was remarkable similarity between the results of these two studies, namely an increased resistance to contraction-induced stress, an increase in utrophin expression, a fast-to-slow fibre type switch, and no change in levels of centronucleation as a result of treatment. These authors also show that GW501516 treatment resulted in the increase of utrophin expression via the interaction of PPARδ with a site in the utrophin promoter known as the PPRE half site.

Thus, GW501516 treatment resulted in the partial amelioration of the dystrophic phenotype of *mdx* mice, via an increase in utrophin expression and a fast-to-slow myofibre switch, and so presents itself as a promising candidate for use in the pharmacological treatment of DMD. Despite these promising results, there are concerns about the possible negative side-effects of GW501516. It has been suggested that since PPARδ plays a central role in important cellular functions such as adhesion, proliferation, differentiation and survival, an increase in its activity could have tumorigenic effects (Michalik et al., 2004). In keeping with this suggestion, genetic disruption of PPARδ has been shown to result in the reduced ability to form tumours in mice (Park et al., 2001). This has prompted researches to develop GW501516-derivative

partial agonists with a reduced ability to transactivate PPARδ (Pettersson et al., 2007). It will be of great interest to test the efficacy of these partial agonists on the *mdx* mouse.

5 Therapeutic effects of the drug C1100 on the *mdx* mouse.

(Note: this work was performed in collaboration with Sarah Squire, Allyson Potter, David Powell and Rebecca Fairclough).

5.1 Introduction

In the previous chapter the therapeutic potential of GW501516 on the *mdx* mouse was evaluated. Treatment of this drug resulted in a partial amelioration of the dystrophic phenotype via fast-to-slow fibre type switch and utrophin upregulation. In this chapter the therapeutic effects of the drug C1100 on the *mdx* mouse were similarly tested. As mentioned in section 1.4.5, C1100 was discovered in a drug screen performed by the company Summit plc to reveal novel utrophin-upregulating compounds. C1100 was shown to have a positive effect on the utrophin A promoter *in vitro*. In order to ensure that this drug could eventually be tested on humans, we performed experiments to decipher its mode of action via the utrophin A promoter.

In section 1.4.5 a description of the high throughput screening process used to identify promising drugs with the potential to upregulate utrophin was provided. To recapitulate, the H2K-*mdx* cell line stably transfected with a promoter/reporter fusion construct consisting of a 9.4 kb fragment containing the utrophin A promoter and a luciferase reporter gene was used to screen a library of compounds for their ability to promote the activity of the utrophin A promoter as evidenced by a significant increase in luciferase expression following treatment. A promising drug identified by this screen, C1100, was used in this chapter.

In order to understand how C1100 treatment resulted in increased utrophin A promoter activity, an unbiased strategy aiming to assess the individual contribution of all the major regulatory motifs was adopted. The promoter/reporter fusion construct used for this purpose consists of a 1.3 kb fragment of the utrophin A promoter that contains all the motifs mentioned previously, linked to a luciferase reporter gene. Derivative mutants were generated by mutating these motifs in order to evaluate the involvement of each motif in C1100-induced activation of the utrophin A promoter. A detailed description of

the important utrophin A promoter motifs not previously described is provided in the remainder of this section.

The utrophin A promoter was introduced in section 1.2.1 as a TATA- and CAAT-less promoter located within a CpG island located directly upstream of the utrophin locus (Dennis et al., 1996). The minimal, or core, promoter element was identified as a 155 bp large fragment containing recognition sites for the transcription factors Ap2, Sp1 and Sp3, which were subsequently shown to orchestrate basal transcriptional activity (Perkins et al., 2001). Upstream of this core element lie the following motifs – NFAT site, PPRE half site, E-box and N-box. Figure 5.1 shows the relative position of these regulatory motifs in the utrophin A promoter.

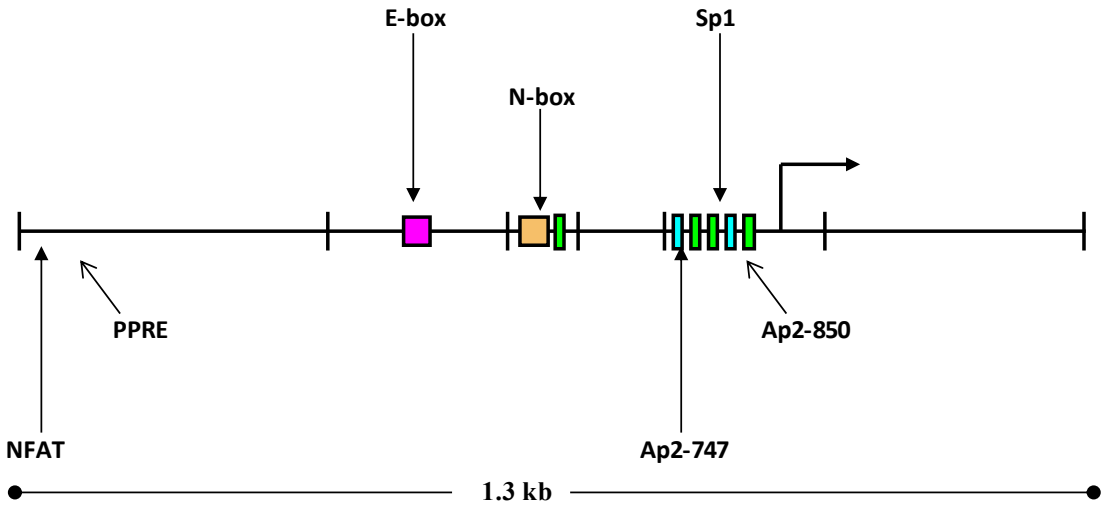

Fig. 5.1 Schematic of the 1.3 kb utrophin A promoter fragment with the position of regulatory motifs and transcriptional start site indicated.

The Sp family of zinc finger transcription factors consists of four members, Sp1-4. Of these, the role of Sp1 in regulating utrophin A transcription has been most comprehensively studied. Sp1 contains a DNA-binding domain at its C-terminal end that is made up of three Cys_2His_2-type zinc finger motifs, and a glutamine-rich activation domain at its N-terminus (Courey and Tjian, 1988; Gyrd-Hansen et al., 2002). Sp1 has been shown to have an affinity to GC rich regions (Dynan and Tjian, 1983) and regulates

the transcription of many genes. The importance of Sp1 is highlighted by the fact that Sp1-deficient mice die as embryos (Marin et al., 1997). Sp1 (along with Ap2) has been shown to be necessary for full activity of the utrophin A core promoter region (Perkins et al., 2001). Sp1 has also been shown to physically interact with GABPα, cooperatively enhancing the activity of the utrophin A promoter (Galvagni et al., 2001; Gyrd-Hansen et al., 2002).

Ap2 is a retinoic acid inducible sequence-specific DNA-binding protein capable of forming dimers to activate the transcription of target genes (Williams and Tjian, 1991), that is involved in a range of developmental processes ranging from apoptosis to cell-cycle control (Hilger-Eversheim et al., 2000). As stated previously, along with Sp1, Ap2 is essential for optimal activity of the utrophin A promoter (Perkins et al., 2001).

As discussed in sections 4.1 and 4.6, the NFAT site and the PPRE half site are recognized by NFAT and PPARδ, respectively, via which they enhance utrophin A transcription.

The E-box motif plays important roles in myogenesis and is recognized by helix-loop-helix proteins of the MyoD family (MyoD1, myogenin, myf5 and MRF4) (Perkins and Davies, 2002). A two-fold increase in utrophin A mRNA levels is observed upon differentiation of myocytes into myotubes, and this increase is mediated via the E-box (Gramolini and Jasmin, 1999; Perkins et al., 2001).

As discussed in section 1.2.2, the GABPα/β heterodimer binds to the N-box motif to induce synapse-specific expression of utrophin A.

In this mouse trial, four-week-old *mdx* mice were treated with either C1100 or vehicle only via daily gavage for four weeks. The reason for selecting four-week-old mice was that we thought that mice younger than four weeks of age would display poor tolerance to daily treatment by gavage (which was the first time this mode of administration was used) in the animal facility used at the time.

5.2 C1100-treated EDL muscle showed partial improvement in contractile properties

To evaluate the effects of C1100 treatment on the contractile properties of the EDL muscle, this muscle was dissected out and subjected to the same tests mentioned in section 3.3. C1100 treatment did not result in a significant improvement in the percentage force drop following a series of five eccentric contractions (39.02 ± 1.87% for control *mdx* mice versus 45.15 ± 3.75% for treated mice) (Figure 5.2A). Despite the absence of improvement in this parameter, treatment did result in a significant increase in the absolute force produced by the EDL. The normalized isometric force was 17.82 ± 1.25 N/cm^2 in the control *mdx* group, compared to 23.64 ± 1.57 N/cm^2 in the C1100-treated *mdx* group (Figure 5.2B). No significant changes in either TTP (Figure 5.2C) or $RT_{1/2}$ (Figure 5.2D) were observed as a result of treatment. A rightward shift in the force versus frequency curve as a result of treatment was observed, indicating that the C1100-treated muscle required less stimulation to produce the same force compared to *mdx* EDL treated with vehicle alone (Figure 5.2E). However, this shift was not statistically significant at any of the stimulatory frequencies.

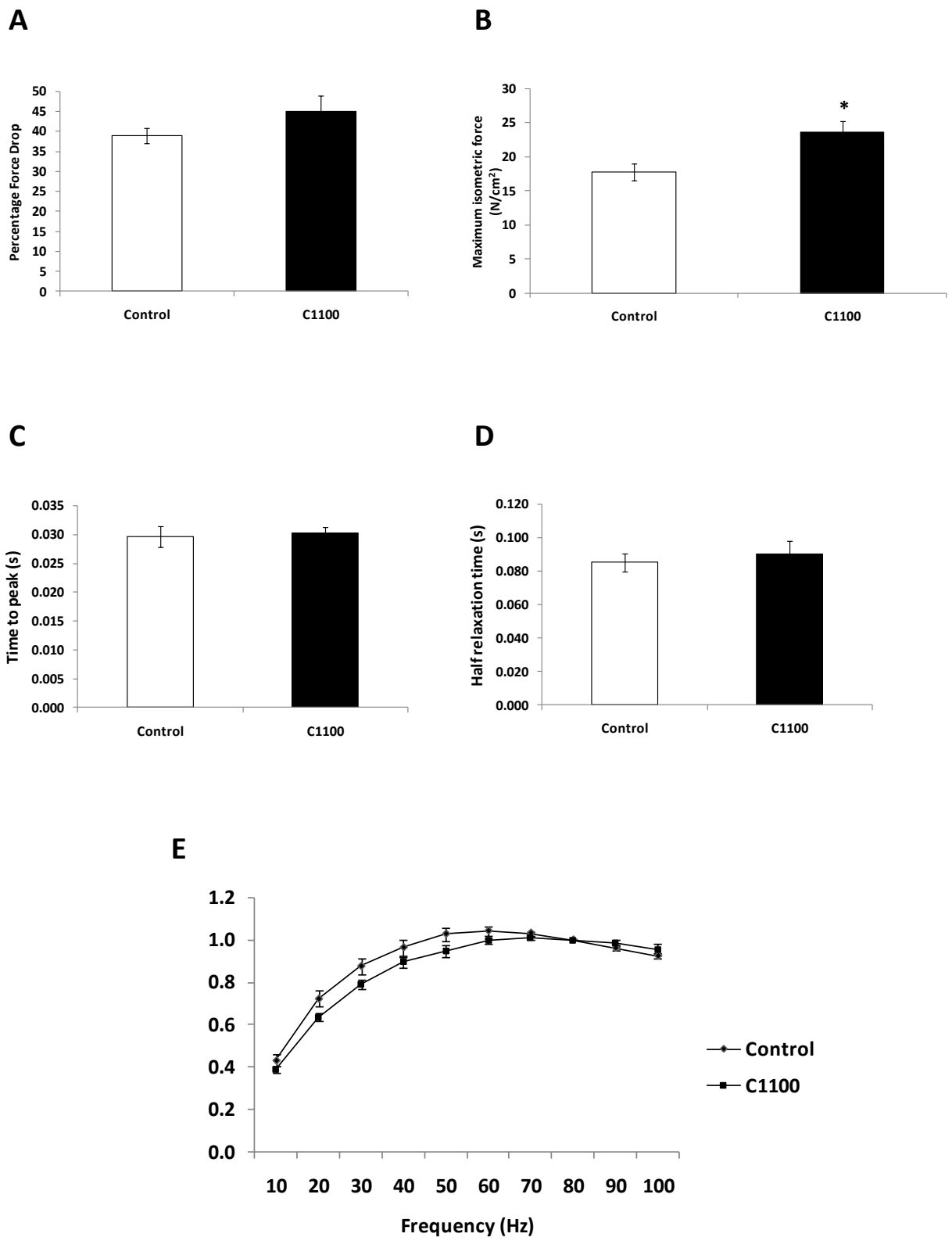
A
Percentage Force Drop
50
45
40
35
30
25
20
15
10
5
0
Control
C1100
B
Maximum isometric force (N/cm²)
30
25
20
15
10
5
0
*
Control
C1100
C
Time to peak (s)
0.035
0.030
0.025
0.020
0.015
0.010
0.005
0.000
Control
C1100
D
Half relaxation time (s)
0.120
0.100
0.080
0.060
0.040
0.020
0.000
Control
C1100
E
1.2
1.0
0.8
0.6
0.4
0.2
0.0
10 20 30 40 50 60 70 80 90 100
Frequency (Hz)
Control
C1100

Fig. 5.2 Contractile properties of EDL muscle from C1100-treated *mdx* and control *mdx* mice. A) No improvement in percentage force drop for EDL from treated vs. untreated *mdx* mice. B) Significant increase in normalized maximum isometric force for EDL from treated vs. untreated *mdx* mice. C) No significant change in TTP for EDL from treated vs. control *mdx* mice. D) No significant change in $RT_{1/2}$ for EDL from treated vs. control *mdx* mice. E) Rightward shift in force-frequency curve for EDL from C1100-treated vs. control *mdx* mice. * = $p < 0.05$ relative to control using an unpaired two-tailed *t*-test (n = 6 per group).

5.3 C1100 treatment did not result in a significant decrease in centronulceation or blood serum CK level *mdx* mice

To determine whether C1100 treatment resulted in reduced muscle damage, %CNFs was determined for TA and diaphragm muscles dissected from C1100- and vehicle-treated *mdx* mice. No significant decrease in %CNFs was seen for C1100 treatment in either of the muscle groups analysed (Figure 5.3A). Consistent with the CNF data, there was also no significant reduction in blood serum CK levels for *mdx* mice treated with C1100 compared to vehicle (Figure 5.3B).

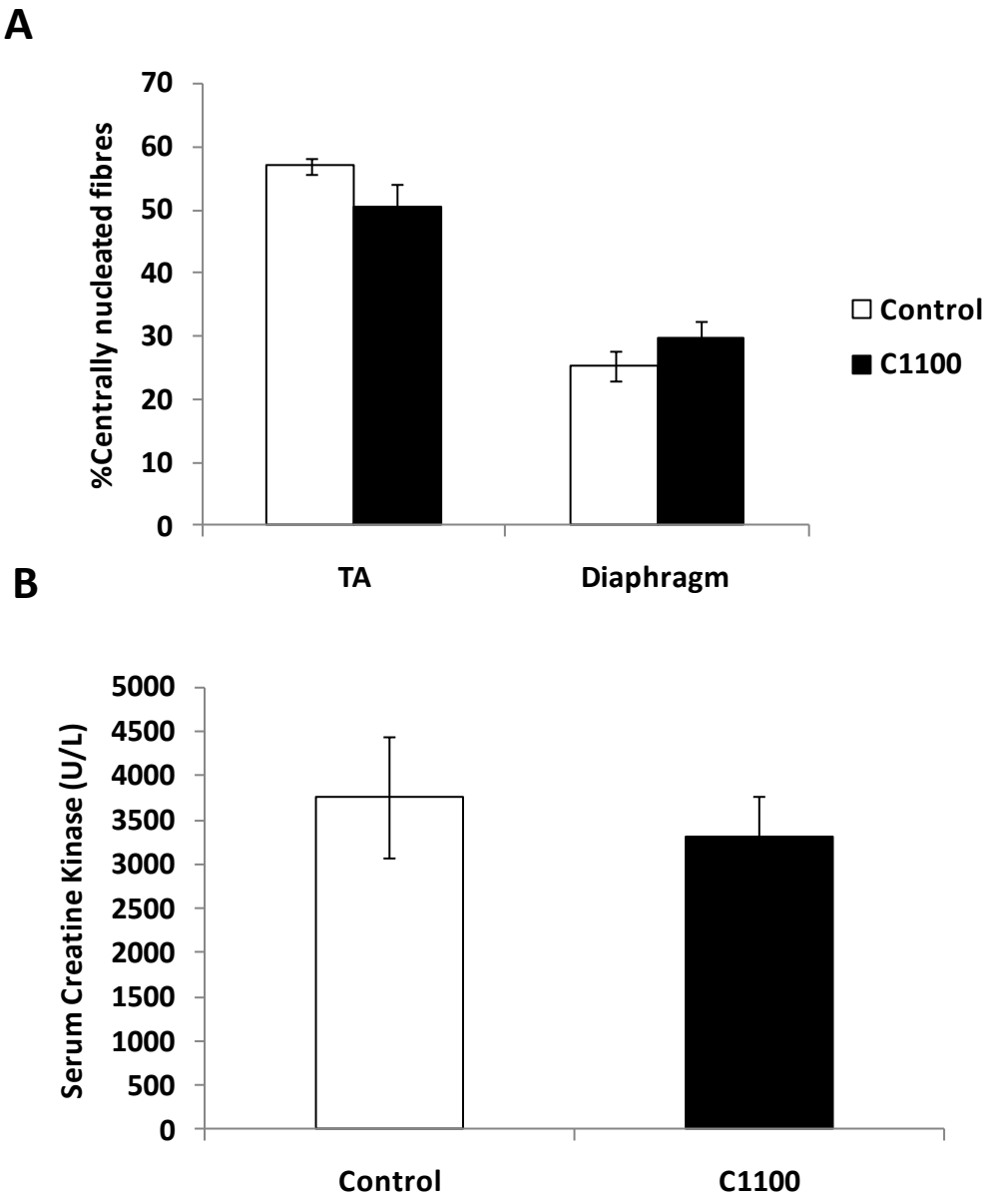

Fig. 5.3 Percentage of centrally nucleated muscle fibres and blood serum CK levels from C1100-treated and control *mdx* mice. A) No significant difference in the percentage of centrally nucleated fibres between treated and control *mdx* mice. B) No significant difference in blood serum CK levels between treated and control *mdx* mice (n = 6 per group).

5.4 C1100 treatment did not result in a significant increase in utrophin protein in *mdx* mice

To determine if C1100 treatment resulted in an increase in utrophin protein levels in skeletal muscle, western blotting was used to quantify utrophin protein relative to the internal protein loading control α-actinin. C1100 treatment did not result in a significant increase in utrophin in either the TA (Figure 5.4) or diaphragm (Figure 5.5).

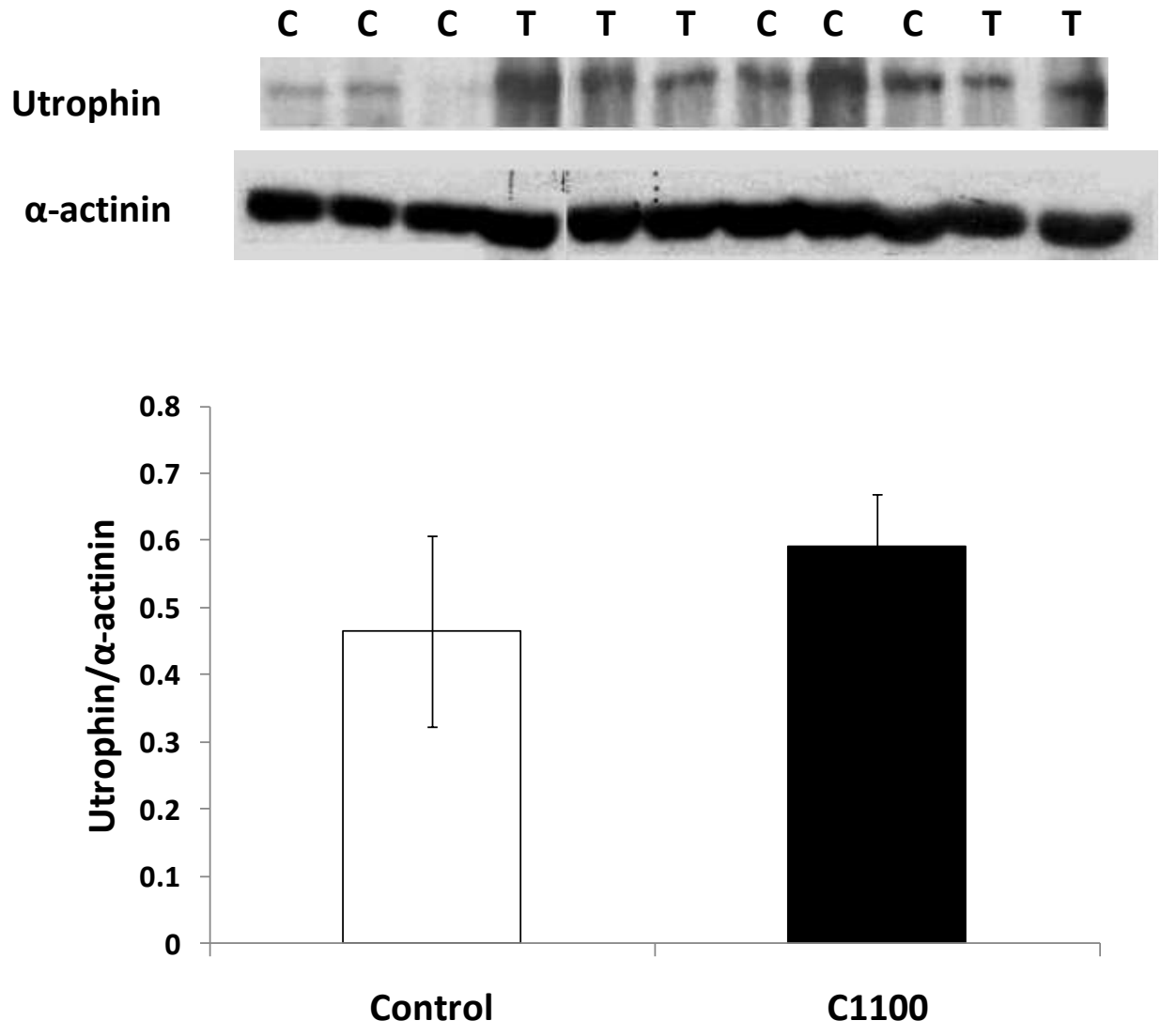

Fig. 5.4 Utrophin protein quantification in TA from C1100-treated and control *mdx* mice. C1100 treatment did not result in a significant increase in utrophin protein levels. C = control; T = treated (*n* (control) = 6, *n* (treated) = 5).

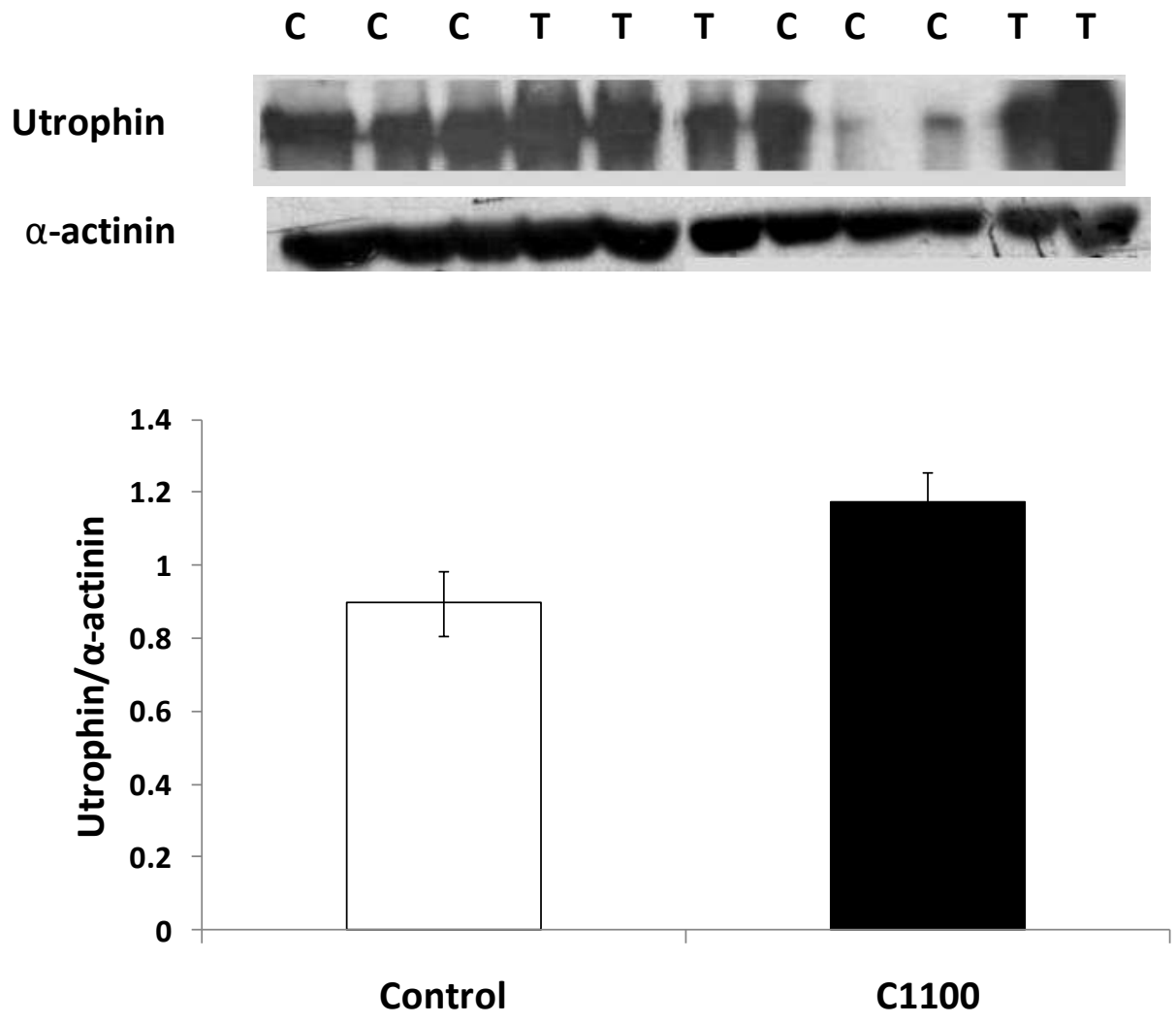

Fig. 5.5 Utrophin protein quantification in diaphragm from C1100-treated and control *mdx* mice. C1100 treatment did not result in a significant increase in utrophin protein levels. C = control; T = treated (*n* (control) = 6, *n* (treated) = 5).

5.5 C1100 treatment had an observable effect on the utrophin A promoter in the H2K-*mdx*-UtroA cell line

In order to evaluate the effect of C1100 treatment on the utrophin A promoter, myoblasts of the H2K-*mdx*-UtroA cell line were treated with a range of concentrations of C1100 twice over a 48-hour period in 96-well plates. Following this treatment period, cells were harvested and luciferase activity was assessed using a luminometer. Figure 5.6 shows that C1100 had a significantly positive effect on the 9.4 kb fragment of the utrophin A

promoter across all the concentrations used, in agreement with positive results obtained by Summit plc.

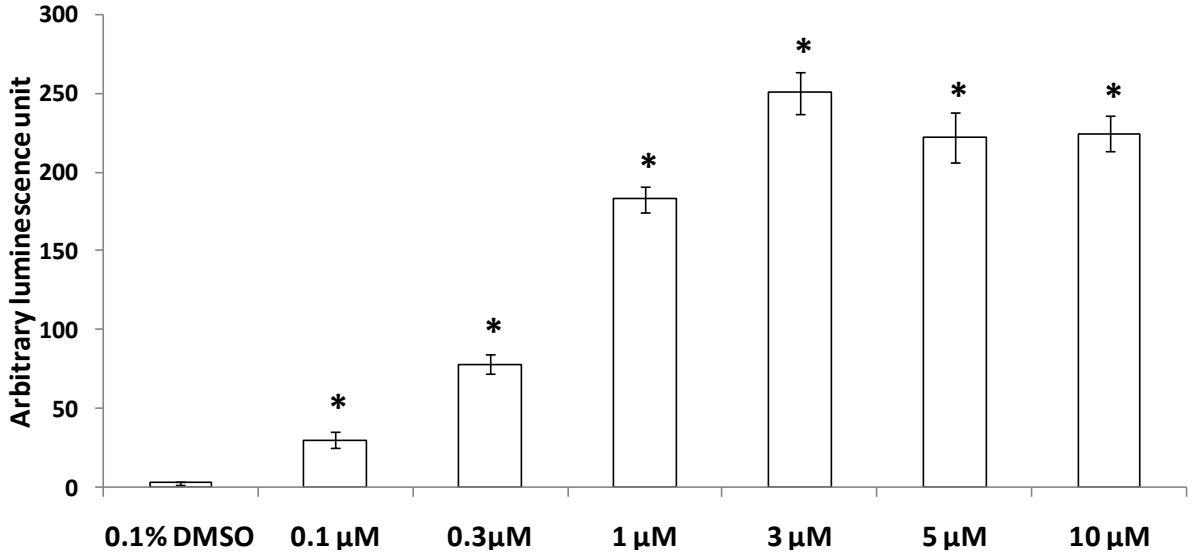

Fig. 5.6 Measurement of core utrophin A promoter (9.4 kb) activity in H2K-*mdx*-UtroA cells treated with a range of concentrations of C1100. C1100 treatment resulted in a significant increase in promoter activity at all concentrations tested. * = $p < 0.05$ relative to 0.1% DMSO treatment using ANOVA analysis followed by Bonferroni post-hoc correction. Each bar represents the average of 10-12 independent experiments.

5.6 C1100 treatment had an observable effect on the core 1.3 kb human utrophin promoter fragment in the C2C12 cell line

To test the hypothesis that C1100 treatment had as potent an effect on the 1.3 kb utrophin A promoter fragment as it did on the 9.4 kb fragment, C2C12 myoblasts were transfected with the pUB construct and treated with a range of concentrations of C1100, also in 96-well plates. After 24 hours, these cells were harvested and luciferase activity in these cells was also assessed using a luminometer. Figure 5.7 indicates that C1100 treatment resulted in a significant increase in activity of the 1.3 kb fragment of the utrophin A promoter across all the concentrations used, except at 0.1 µM and 10 µM.

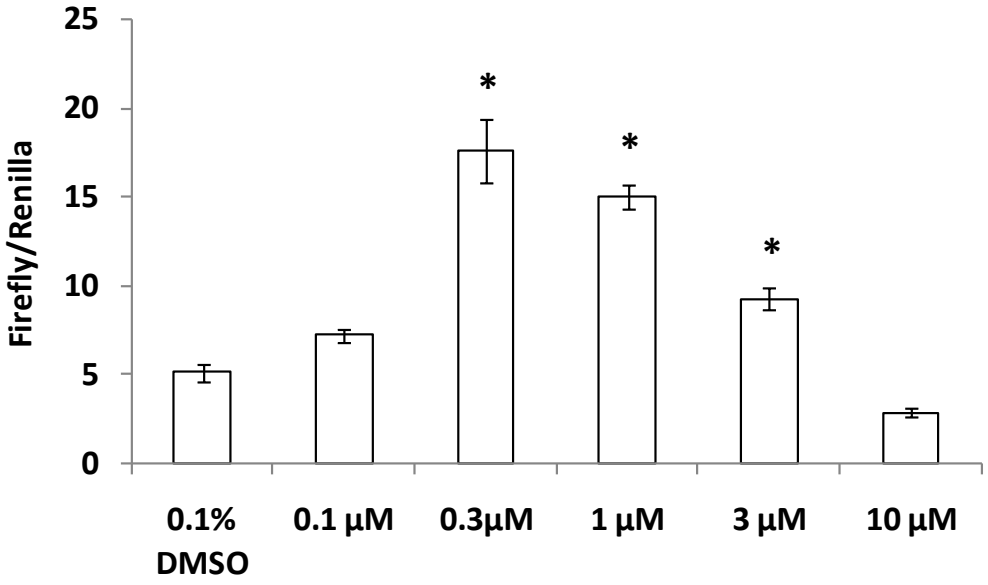

Fig. 5.7 Measurement of core utrophin A promoter (1.3 kb) activity in transfected C2C12 cells treated with a range of concentrations of C1100. C1100 treatment resulted in a significant increase in promoter activity at 0.3 µM, 1 µM and 3 µM. * = $p < 0.05$ relative to 0.1% DMSO treatment using ANOVA analysis followed by Bonferroni post-hoc correction. Each bar represents the average of 4 independent experiments.

5.7 Deciphering the mode of action of C1100 on the core 1.3 kb human utrophin A promoter fragment

To unravel the mode of action of C1100 on the 1.3 kb utrophin A promoter fragment, the pUB construct was used to generate a range of mutant constructs, each with mutations in an important regulatory motif. Figure 5.8A indicates the relative location of the motifs studied and the mutations induced. The 'Sp1' mutant refers to a mutation in Sp1-755 site. The Sp1-780 site could not be mutated despite a number of attempts, most likely because of the surrounding GC rich region. C2C12 myoblasts were transfected with all these constructs, along with the wild-type pUB, and treated with 1 µM C1100 for 24 hours. Luciferase assays were performed after this treatment period, and the results are presented in Figures 5.8B and C. These results indicate that mutating the N-box, PPRE or NFAT motif resulted in an abrogation of C1100-induced increase in utrophin A promoter activity. For practical reasons, this experiment was performed in two separate batches.

However, in each case, the wild-type pUB was included to ensure that C1100 treatment continued to have a significantly positive effect on the utrophin A promoter.

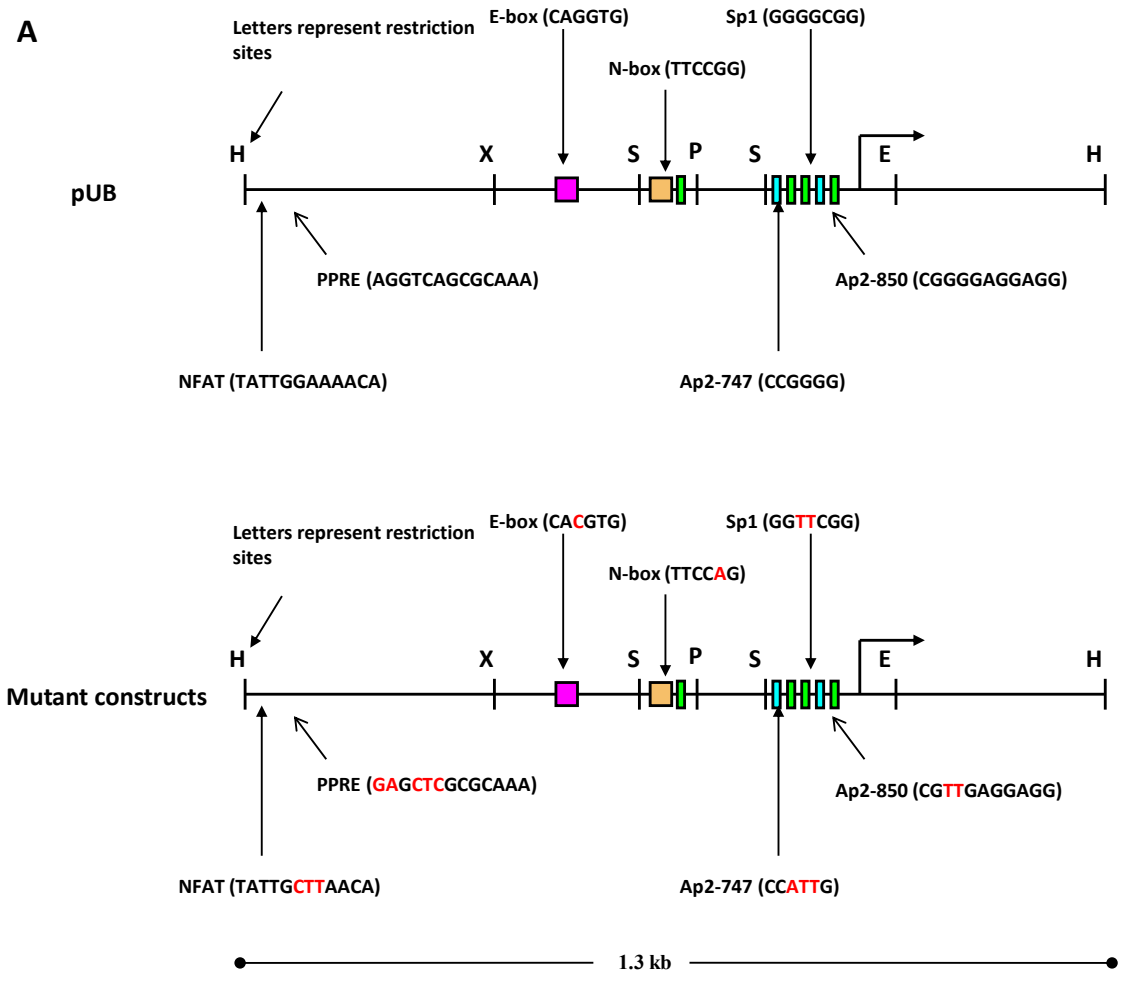
A
Letters represent restriction sites
E-box (CAGGTG)
Sp1 (GGGGCGG)
N-box (TTCCGG)
H
X
S
P
S
E
H
pUB
PPRE (AGGTCAGCGCAAA)
Ap2-850 (CGGGGAGGAGG)
NFAT (TATTGGAAAACA)
Ap2-747 (CCGGGG)
Letters represent restriction sites
E-box (CACGTG)
Sp1 (GGTTCGG)
N-box (TTCCAG)
Mutant constructs
PPRE (GAGCTCGCGCAAA)
Ap2-850 (CGTTGAGGAGG)
NFAT (TATTGCTTAACA)
Ap2-747 (CCATTG)
1.3 kb

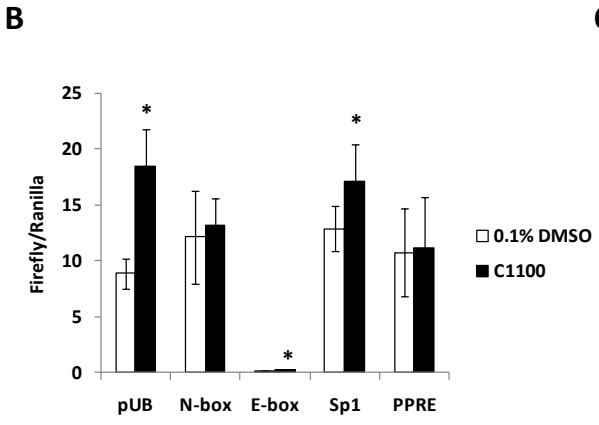
B
Firefly/Ranilla
25
20
15
10
5
0
pUB
N-box
E-box
Sp1
PPRE
0.1% DMSO
C1100

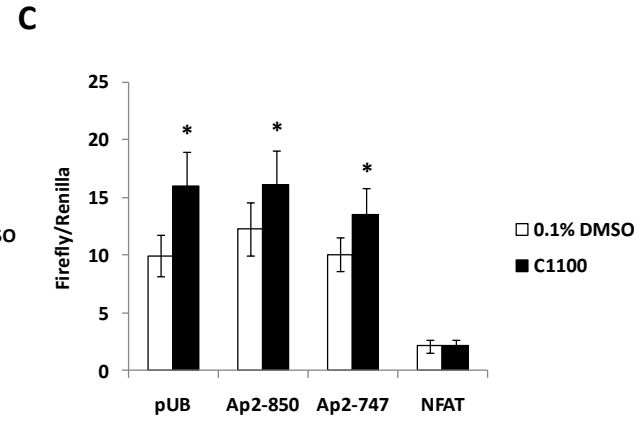
C
Firefly/Renilla
25
20
15
10
5
0
pUB
Ap2-850
Ap2-747
NFAT
0.1% DMSO
C1100

Fig. 5.8 Identification of regulatory pathways targeted by C1100 within the utrophin A promoter. A) Schematic of the 1.3 kb utrophin A promoter fragment (pUB) with the position and sequences of relevant motifs indicated. Letters in red denote nucleotides that were mutated in each motif to generate the mutant constructs used in this study. B) & C) Effect of disruption of key regulatory elements in the utrophin A promoter on C1100 drug activity in a luciferase reporter assay in C2C12 cells. The N-box, PPRE and NFAT motifs are all involved in C1100-mediated activation of the utrophin A promoter. * = $p <$ 0.05 relative to cells treated with 0.1% DMSO using a paired two-tailed *t*-test. Each bar represents the average of 4-7 individual experiments.

5.8 Discussion

As with the PPARδ agonist GW501516, whose effects on the pathology of the *mdx* mouse were evaluated, the drug C1100 was administered daily for four weeks to four-week-old male *mdx* mice. However, in this trial the drug was delivered orally via gavage. This was one of many trials testing the effects of C1100 treatment carried out in this lab. The other trials were of different lengths, using either IP injections or gavage as the treatment method. Treatment with C1100 also resulted in a partial correction of the dystrophic phenotype, however in the trial presented here this correction was not as potent as with GW501516 treatment.

Treatment with C1100 in this trial did not result in a significant decrease in the percentage force drop following a series of five eccentric contractions, indicating that C1100 treatment did not make the muscle less susceptible to contraction-induced injury. However, C1100 treatment did result in a significant increase in the maximum isometric force.

C1100 treatment resulted in a rightward shift in the force-frequency curve. Again, as discussed in section 4.6, this could be indicative of a partial redressal of the Ca^{2+} imbalance that exists in dystrophic muscle. However, this shift was not accompanied by changes in either the TTP or $RT_{1/2}$.

The therapeutic effects of C1100 did not manifest themselves in terms of change in either levels of centronucleation or serum CK levels, as there was no difference between treated and untreated *mdx* mice with respect to these two parameters.

The lack of significant improvement in the dystrophic phenotype according to most parameters is most likely attributable to a lack of change seen in the expression of utrophin as a result of treatment. Although treatment with C1100 in this trial resulted in a modest increase in utrophin protein levels in both TA and diaphragm, this increase was not significant. However, other mouse trials testing the effects of C1100 administration yielded more positive results. A trial that yielded particularly promising results also involved the daily delivery of C1100 treated for four weeks via gavage (Davies/Tinsley/Fairclough in preparation). In this study, there was a significant increase in utrophin protein levels in the diaphragm. As a result of increased fibre protection caused by this higher amount utrophin, there was also a significant reduction in %CNFs, which was indicative of reduced levels of fibre degeneration and regeneration. There was also an improvement in muscle contractile properties, as indicated by a significant increase in resistance to contraction-induced injury of the EDL muscle. A key difference between this trial and the trial described in this chapter is that treatment began at an earlier age (3 weeks instead of 4). Between 3 and 4 weeks of age, skeletal muscle in the *mdx* mouse experiences a massive bout of fibre degeneration followed by regeneration (DiMario et al., 1991). Therefore, the timing of the commencement of drug administration (before the onset of this degeneration as opposed to just after) could be a crucial factor that influences the efficacy of the drug. Unfortunately, younger mice could not have been used in the trial described in this chapter because of the suboptimal conditions of the animal facility used at the time. Subsequent trials have been conducted in a newer, cleaner facility, allowing the treatment of younger mice. Another problem encountered in the trial described in this chapter was the poor solubility of C1100 in DMSO. Subsequent trials have made use of improved formulations of the drug that display superior solubility.

C1100 was shown to have a very positive effect on utrophin A promoter activity. Figures 5.6 and 5.7 indicate that C1100 increased the activity of both the 9.4 kb promoter and the 1.3 kb promoter at a range of concentrations. The comparatively higher increase in the activity of the 9.4 kb promoter could be attributed to a range of reasons – stable transfection of this fusion construct versus the transient transfection of the 1.3 kb construct, different cell lines, the lack of dystrophin in the H2K-*mdx*-UtroA cell line

(which is expressed in the C2C12 cell line) whose expression might interfere with the utrophin A promoter via some feedback mechanism were it to be present, and the presence of elements outside the 1.3 kb region that might be involved in C1100-mediated increase of promoter activity.

The reasoning underpinning the strategy used to unravel the mechanism of action of C1100 on the utrophin A promoter was that if a mutation in a particular motif resulted in the abrogation of the positive effect of C1100, it was indicative of the involvement of that motif in the mode of action. Figures 5.8B and C indicate that the N-box, PPRE half site and the NFAT site are somehow involved in the mode of action of C1100. It is not surprising that multiple, apparently disparate, pathways might be affected by C1100 in light of many published results highlighting the interconnectedness of the various signalling cascades that feed into the utrophin A promoter.

An attractive model for the mechanism of action of C1100 could be that it acts via the Ca^{2+}/CaM signalling cascade. As discussed in section 4.1, increased cytosolic Ca^{2+} levels results in the activation of the phosphatase calcineurin, which dephosphorylates NFAT to trigger its nuclear relocalization where it binds to and activates the promoter of target genes, including *utrophin*. This would explain the involvement of the NFAT site in C1100-mediated utrophin A promoter activation. Increased Ca^{2+} have also been shown to result in a significant increase in the expression of PGC-1α (Ojuka et al., 2003). This occurs via an increase in calcineurin activity, as constitutive expression of the active form of calcineurin has been shown to induce the expression of PGC-1α, while the knockout of the calcineurin regulatory subunit results in a decrease in expression of PGC-1α (Schaeffer et al., 2004). PGC-1α synergistically activates the utrophin A promoter with GABPα/β (Angus et al., 2005), which binds to the N-box. This therefore serves as a possible explanation for the involvement of the N-box motif in C1100-mediated activation. Finally, PGC-1α has not only been shown to be a target of PPARδ (Hondares et al., 2007; Tanaka et al., 2003), but has also been shown to induce PPARδ expression (Hondares et al., 2007). As discussed in section 4.6, PPARδ activates the promoter of its target genes by binding to the PPRE half site in their promoter, therefore,

the involvement of the PPRE half site in the mode of action of C1100 suggests that C1100 induces the expression of PPARδ, possibly via the Ca^{2+}/CaM signalling cascade.

The results in this chapter indicate that C1100 has a significantly positive effect on the utrophin A promoter *in vitro*, and this effect is mediated via the NFAT, PPRE, and N-box motifs. However, treatment of *mdx* mice with this drug only had marginally positive effects. Possible reasons for this could have been an insufficient length of treatment (four weeks), inefficient mode of delivery (gavage), and/or poor solubility. As mentioned previously, a similar trial yielded much more positive results. Likely reasons for these differences is that this trial was conducted more recently than the trial described in this chapter, and so made use of a more advanced formulation of C1100 with improved solubility, and that the trial was begun at an earlier age (3 weeks instead of 4). Another likely cause for these differences could be that the trial described in this chapter was performed in a different animal facility from the one used for subsequent trials. These results indicate that C1100 is worth carrying forward for use in human clinical trials and could be used to design derivative utrophin-upregulating compounds.

6 A study of the role of microRNAs in the dystrophic process in the *mdx* and *dko* mouse models

6.1 Introduction

In the last three chapters the hypothesis that utrophin was functionally equivalent to dystrophin in terms of its ability to protect skeletal muscle from chronic stress was tested (Chapter 3), and the therapeutic potential of two small compounds, GW501516 (Chapter 4) and C1100 (Chapter 5), were evaluated, specifically via their ability to upregulate utrophin in skeletal muscle tissue. In this chapter, the consequence of the absence of dystrophin, and of the combined absence of dystrophin and utrophin, in terms of the change in the global profile of miRNA expression in mouse skeletal muscle, was assessed. The purpose of this endeavour was to evaluate the contribution of the alteration of miRNA expression to disease etiology.

Prior to the initiation of this study, the contribution of only a handful of miRNAs to the dystrophic progression in the *mdx* mouse had been studied, and the role of miRNAs in the pathology of the *dko* mouse had not been examined at all. Our aim was therefore to produce a more comprehensive picture of the contribution of all known miRNAs to the pathology of these two important mouse models. As mentioned previously, a number of miRNAs have been shown to be deregulated in the skeletal muscle of DMD patients (Eisenberg et al., 2007). However, due to obvious limitations of experiments involving humans, the contribution of these miRNAs to the dystrophic process could not be further examined *in vivo*. Therefore, detailed examination of the involvement of miRNAs in the dystrophic process of appropriate mouse models (*mdx* and *dko*) might provide further clues about their role in human disease. Also, this examination would lay the foundation for future work on therapies based on miRNA manipulation, as these therapies would have to first be tested and validated in the mouse.

The experimental strategies employed in this chapter included the use of microarrays to assess the global pattern of miRNA expression in normal and dystrophic skeletal muscle tissue, a comprehensive evaluation of the expression profiles of select miRNAs, and the

functional analysis of a chosen miRNA in terms of its interaction with predicted mRNA targets.

There is much precedence for the use of microarrays to elucidate the involvement of miRNAs in biological processes ranging from organogenesis, such as brain development (Miska et al., 2004), to disease, such as cancer (Yang et al., 2008). In section 1.5.4, the use of microarrays to evaluate the global deregulation of miRNAs in 10 major muscular disorders, including DMD, was described (Eisenberg et al., 2007). In this chapter, microarrays were performed to compare the global expression profile of mature miRNAs in TA tissue from 10-week-old male C57Bl/10 and *mdx* mice, and from 10-week-old male *mdx* and *dko* mice. The reasons for selecting this muscle were that not only does the dystrophic phenotype manifest itself in this muscle in terms of increased centronucleation and a reduced capacity of force production in *mdx* compared to wild-type mice, it is further pronounced in *dko* compared to *mdx* mice. TA from *dko* mice consists almost entirely of oxidative fibres, compared to TA from *mdx* mice, which contains a mixture of oxidative and glycolytic fibres, indicating the selective loss of glycolytic fibres in *dko* TA (Deconinck et al., 1998). These observable morphological changes are paralleled by an upregulation of slow muscle fibre type genes in TA muscles from *dko* compared to *mdx* mice (Baker et al., 2006). The reason for selecting 10-week-old tissue was that this age was deemed to be sufficiently old enough to maximize the histological (centronucleation and fibre type) differences in the TA muscle between wild-type and *mdx* mice, and between *mdx* and *dko* mice. H & E staining of TA muscle sections from the *mdx* and *dko* mice used in this study revealed an increase in centronucleation and fibrosis with age, agreeing with previous findings (Deconinck et al., 1997b). The microarray chip used in this study was the Agilent Mouse MicroRNA Microarray 8 x 15K, based on Sanger miRBase (release 12.0). This chip was used to detect the relative expression levels of 627 mature miRNAs. We chose to measure the expression of the mature miRNAs, instead of the precursor pri- and pre-miRNA species, because the mature, and not the precursor, miRNAs are proposed to have biological functions.

qPCR was used to validate some of the microarray results and to further evaluate the expression profiles of select miRNAs in different tissues and at different ages. Two systems – NCode and the TaqMan assay – were used to measure mature miRNA expression levels. Both systems are discussed in detail in the following sections. qPCR was also used to measure the expression of select pri-miRNAs to see if the observed deregulation of select miRNAs was due to transcriptional or post-transcriptional factors.

Finally, target validation for one of the significantly dysregulated miRNAs, miR-503, was performed. A range of online prediction algorithms was used to produce a list of possible targets of miR-503. Two of these targets, the *myeloblastosis oncogene* (*myb*) and *suppressor of cytokine signalling 6* (*soc6*), were selected for experimental validation due to their relevance to muscle biology and disease.

6.2 Microarray analysis produced a list of significantly dysregulated miRNAs in both *mdx* and *dko* skeletal muscle tissue

The purpose of these experiments was to assess the global expression patterns of mature miRNAs in TA tissue from *mdx* versus C57Bl/10 mice (Table 6.1A), and in tissue from *dko* versus *mdx* mice (Table 6.1B). Table 6.1 shows that many more miRNAs were significantly dysregulated in the first microarray experiment (*mdx* versus C57Bl/10) than in the second (*dko* versus *mdx*).

A

SystematicName	Fold change	Regulation
mmu-miR-31	11.9	up
mmu-miR-206	6.7	up
mmu-miR-34c	6.0	up
mmu-miR-18a	5.3	up
mmu-miR-532-5p	5.1	up
mmu-miR-34b-5p	4.9	up
mmu-miR-362-3p	3.9	up
mmu-miR-214	3.8	up
mmu-miR-221	3.6	up
mmu-miR-434-3p	3.3	down
mmu-miR-675-3p	3.3	up
mmu-miR-500	2.9	up
mmu-miR-338-3p	2.9	down
mmu-miR-674*	2.4	up
mmu-miR-299*	2.3	down
mmu-miR-199a-5p	2.2	up
mmu-miR-21	2.2	up
mmu-miR-329	2.2	down
mmu-miR-410	2.1	down
mmu-miR-223	2.1	up
mmu-miR-199a-3p	2.0	up
mmu-miR-29c*	1.9	down
mmu-miR-15b	1.7	up
mmu-miR-30c	1.7	down
mmu-miR-154	1.7	down
mmu-miR-467f	1.6	down
mmu-miR-34a	1.6	up
mmu-miR-29c	1.6	down
mmu-miR-29a	1.6	down
mmu-miR-193	1.6	up
mmu-miR-150	1.6	down
mmu-miR-342-3p	1.5	up
mmu-miR-365	1.5	up
mmu-miR-199b*	1.5	up
mmu-miR-30a	1.5	down

B

SystematicName	Fold change	Regulation
mmu-miR-379	5.4	up
mmu-miR-337-3p	4.4	down
mmu-miR-503	3.6	up
mmu-miR-26b*	3.0	down
mmu-miR-127	2.1	up
mghv-miR-M1-1	2.0	down
mmu-miR-106b	1.8	up
mmu-miR-29c	1.7	down
mmu-miR-451	1.6	down
mmu-miR-206	1.6	up
mmu-miR-500	1.6	up
mmu-miR-30c	1.5	down

Table 6.1 Significantly dysregulated miRNAs in TA tissue is A) *mdx* compared to C57Bl/10 mice and B) *dko* compared to *mdx* mice ($n = 4$).

The Ingenuity Pathway Analysis (IPA) software was used to discover what biological pathways these dysregulated miRNAs might be involved in. Each of the miRNAs listed in Table 6.1 is predicted to potentially modulate the expression of numerous mRNA targets. As mentioned in section 1.5.4, these targets can number in the thousands. Prediction programs typically employ unique algorithms but are based on a shared two-step strategy of prediction that involves the location of complementary seed sequences in the 3' UTR of target genes followed by an estimate of the evolutionary conservation of these binding sites (Griffiths-Jones et al., 2006). The program used to generate predicted

targets for IPA analysis was TargetScan. TargetScan is a frequently-used target prediction program that ranks target genes according to either total context score or the probability of conserved targeting (P_{CT}). The total context score is indicative of how favourable a particular miRNA-mRNA pairing is and is the sum of the contribution of four features – site-type, 3' pairing (with reference to the miRNA), local AU content, and the position on the 3' UTR. The more negative the context score, the more favourable the predicted pairing. P_{CT} is the probability that a particular site is conserved as a result of selection due to miRNA targeting rather than by chance alone or other causes (Friedman et al., 2009; Grimson et al., 2007).

Predicted targets of all the significantly dysregulated miRNAs from Table 6.1 produced by TargetScan were entered into the IPA software to identify biological pathways that were significantly overrepresented. Table 6.2 contains the two top-ranked pathways in each of the following categories – networks, diseases and disorders, molecular and cellular functions, physiological system development and function, and canonical pathways.

Category	*mdx* vs. C57Bl/10	*dko* vs. *mdx*
Top Networks	1) Connective Tissue Development and Function, Skeletal and Muscular Development and Function, Tissue Morphology 2) Nervous System Development and Function, Drug Metabolism, Cell-To-Cell Signalling and Interaction	1) Cancer, Cell Cycle, Embryonic Development 2) Tissue Morphology, Cardiovascular System Development and Function, Organ Development
Diseases and Disorders	1) Ophthalmic Disease 2) Cancer	1) Neurological Disease 2) Cancer
Molecular and Cellular Functions	1) Cell-To-Cell Signalling and Interaction 2) Cellular Movement	1) Cell Cycle 2) Cellular Compromise
Physiological System Development and Function	1) Nervous System Development and Function 2) Tissue Development	1) Nervous System Development and Function 2) Organ Development

Table 6.2 Top two pathways in each category for *mdx* compared to C57Bl/10 mice; and *dko* compared to *mdx* mice ($n = 4$).

6.3 Optimization of the NCode system for measuring mature miRNA expression

In order to validate some of the results from Table 6.1, the NCode qPCR system was initially used. The major advantage of this system is that it can be used to identify and quantify any miRNA. However, due to the stringent requirements of qPCR, much optimization is generally required. A common problem initially encountered was the inability to produce clean melt curves i.e. curves with only one distinct peak. Melt curves with multiple peaks are indicative of primer-dimer formation and off-target amplification. The most effective solution to this problem was found to be reducing the

elongation step of the PCR reaction from the recommended 60s to 10s (Figure 6.1). In spite of this improvement, qPCR for many of the miRNAs tested failed using the NCode system, prompting the use of another system of quantification.

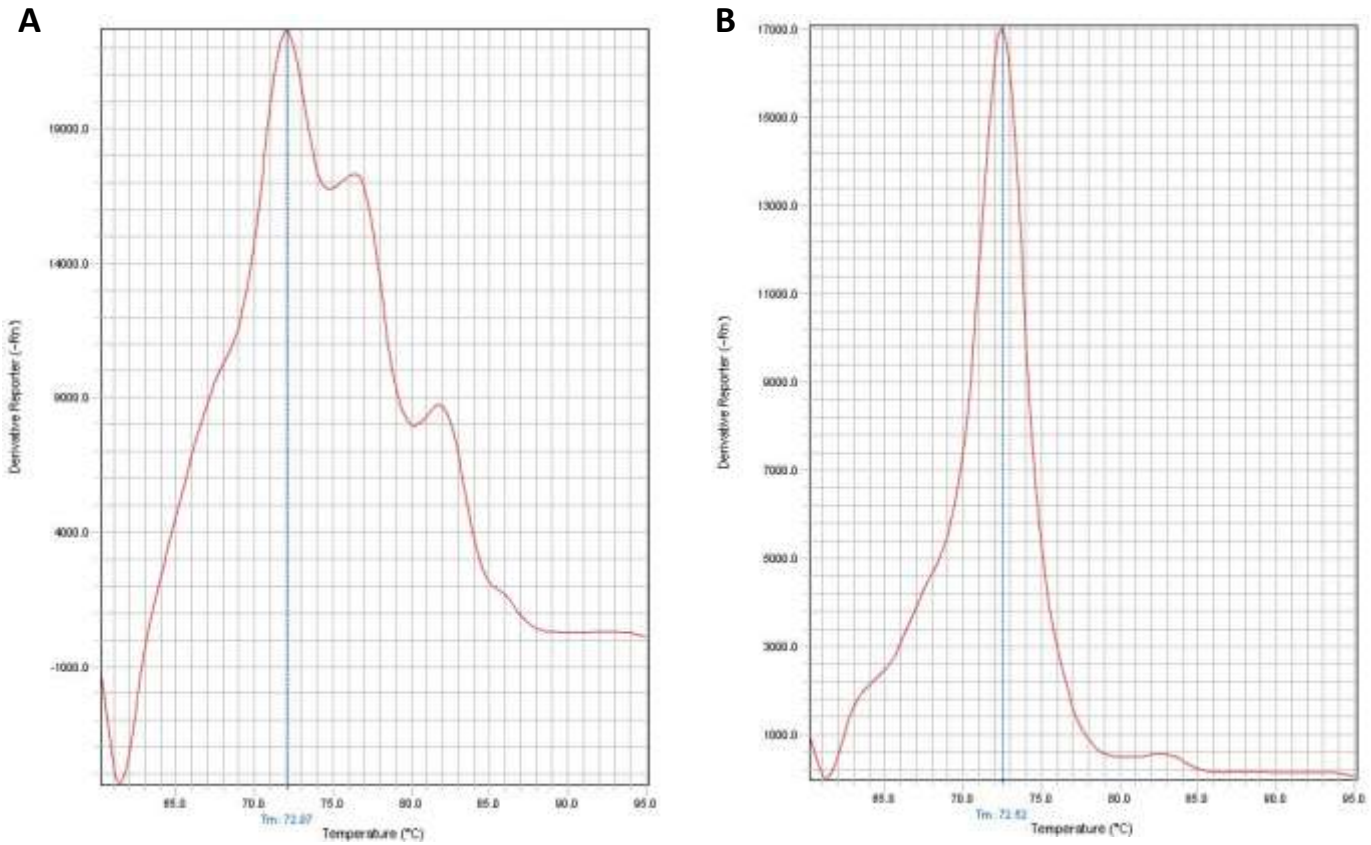

Fig. 6.1 Adjusting PCR cycling conditions to produce melt curves with single distinct peaks. Shortening of extension times from 60s (A) to 10s (B) resulted in a cleaner melt curve for miR-206.

6.4 qPCR validation of some key dysregulated miRNAs using the NCode system and TaqMan assay

Following optimisation, the NCode system was used to validate the microarray results in Table 6.1A. The expression of five miRNAs – miR-21, miR-29c, miR-31, miR-206, and miR-34c – was assessed (Figure 6.2A). These results confirm the microarray results for all the miRNAs except miR-34c.

miR-31 and miR-206 expression was also quantified using the more reliable custom-designed TaqMan assay system. This system is based on the use of custom-designed stem-loop reverse transcription primers that are unique to the miRNA whose expression is being assayed. These primers have been shown to have high efficiency and display high discriminatory power, being able to distinguish between mature miRNAs that differ by only one nucleotide (Chen et al., 2005). The disadvantage of this system is that it is relatively expensive. Use of this system also showed that miR-31 and miR-206 were significantly upregulated in TA from *mdx* versus wild-type mice (Figure 6.2B). Importantly, the fold-change increase in miR-31 expression was ~64.5-fold compared to ~5.3-fold using the NCode system and ~11.9-fold using the microarray. This is not surprising considering the higher sensitivity of the TaqMan assay. However, and surprisingly, the fold-change in miR-206 was only ~4.4-fold using the TaqMan assay compared to ~13.3-fold using the NCode system.

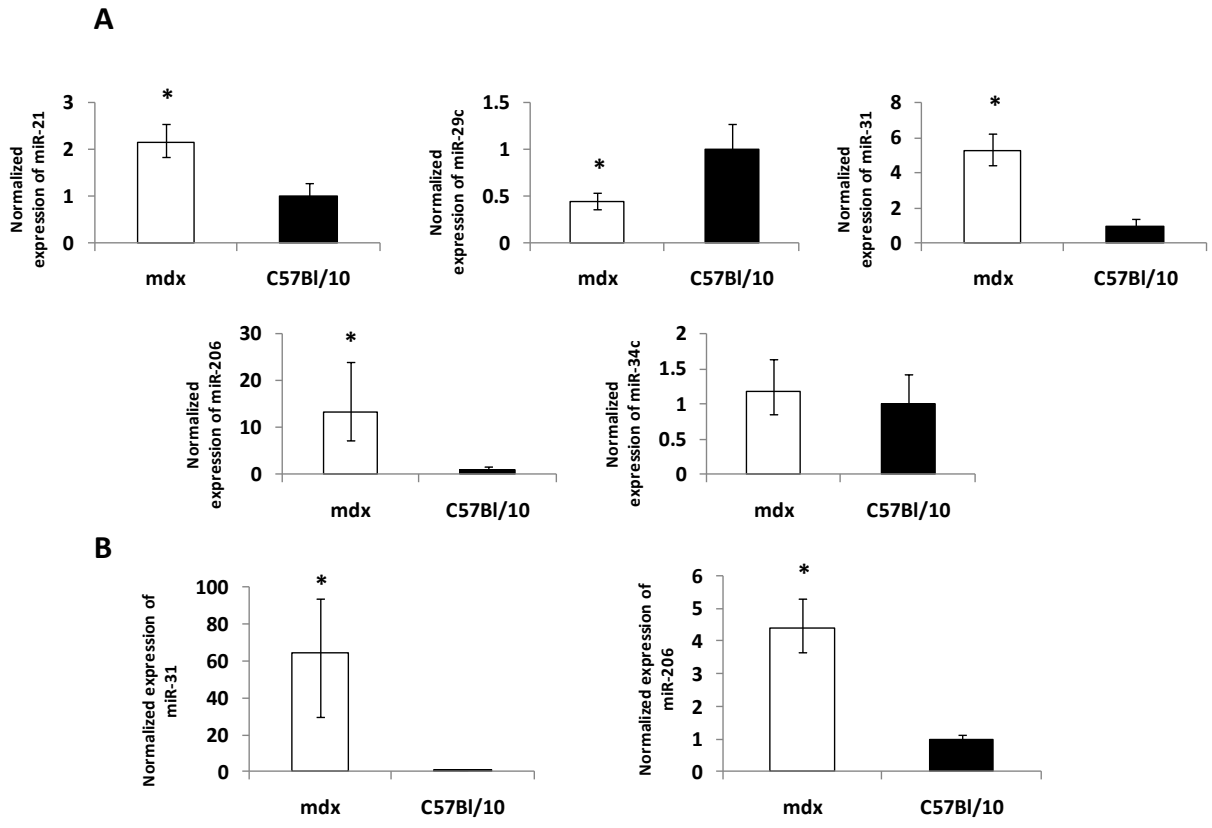

Fig. 6.2 qPCR quantification of select miRNAs in *mdx* compared to C57Bl/10 TA tissue using A) NCode system and B) TaqMan assay. These results validated some of the data

in Table 6.1, except for miR-34c, which showed no significant difference in expression between *mdx* and C57Bl/10 TA tissue. * = $p < 0.05$ relative to expression in C57Bl/10 TA tissue using an unpaired two-tailed *t*-test ($n = 3$).

6.5 pri-miR-31 and pri-miR-206 dysregulation in *mdx* TA tissue mirrored the dysregulation of their mature counterparts

The purpose of these experiments was to better understand the factors contributing to the increased expression of miR-31 and miR-206 in *mdx* muscle. As miRNA genes are initially transcribed to produce pri-miRNAs, quantification of pri-miRNA expression is indicative of the level of miRNA gene activity. Figures 6.3A and B clearly show that both pri-miR-31 and pri-miR-206 were both significantly upregulated in *mdx* muscle, indicating that the reason for the increased expression of their mature counterparts (miR-31 and miR-206) was because of perturbations at the level of transcription. In fact, the fold-changes for both pri-miR-31 (~154.3-fold) and pri-miR-206 (~15.4-fold) are much higher than the fold-changes for their mature counterparts, suggesting the differences in the expression of these two miRNA genes (between *mdx* and wild-type muscle) becomes less pronounced during the course of miRNA biogenesis.

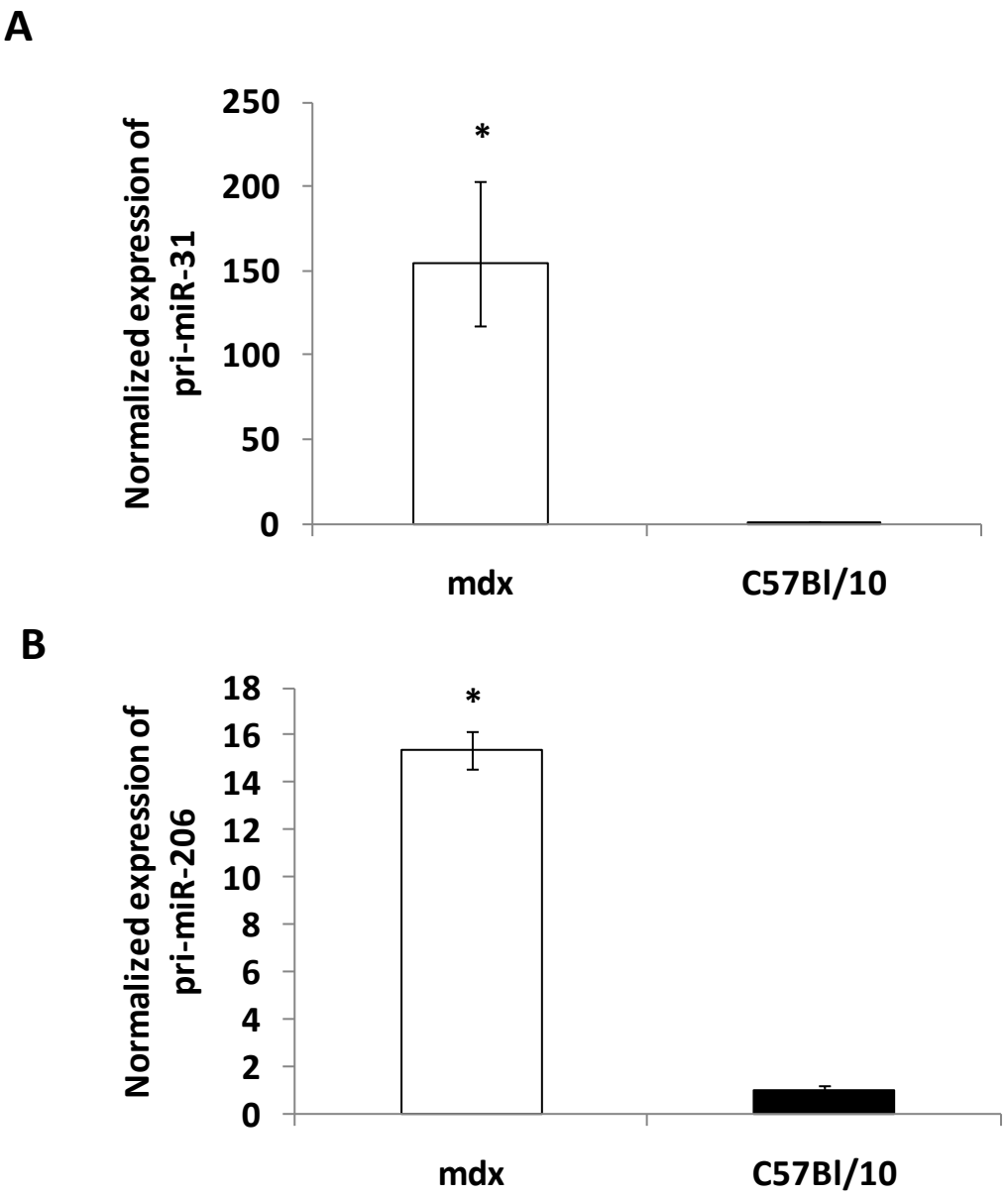

Fig. 6.3 qPCR quantification of A) pri-miR-31 and B) pri-miR-206 in *mdx* compared to C57Bl/10 TA tissue. Both pri-miR-31 and pri-miR-206 were significantly overexpressed in *mdx* compared to C57Bl/10 tissue. * = $p < 0.05$ relative to expression in C57Bl/10 TA tissue using an unpaired two-tailed *t*-test ($n = 3$).

6.6 miR-31 and miR-206 were also misexpressed at different ages in *mdx* compared to C57Bl/10 skeletal muscle tissue

miR-31 and miR-206 expression was also quantified in TA from *mdx* and wild-type mice of different ages to understand how the expression of these two miRNAs changed with age and dystrophic progression. Figures 6.4A and B show significant differences in the expression of both these miRNAs between *mdx* and wild-type muscle at all ages examined. These figures also highlight differences in the ways miR-31 and miR-206 expression change in *mdx* and wild-type muscle. While miR-31 levels remain at a reasonably steady level in wild-type muscle, they increase noticeably in *mdx* muscle with age. On the other hand, miR-206 levels appear quite stable in *mdx* muscle, but progressively decrease with age in wild-type muscle.

A

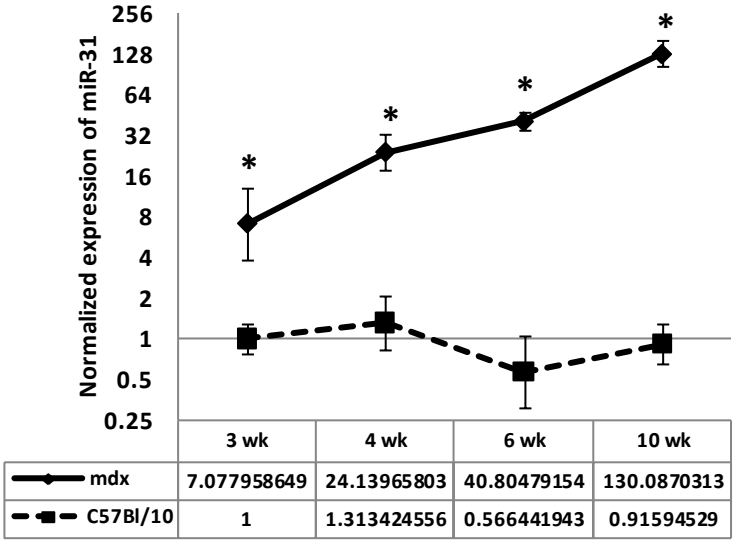

	3 wk	4 wk	6 wk	10 wk
mdx	7.077958649	24.13965803	40.80479154	130.0870313
C57Bl/10	1	1.313424556	0.566441943	0.91594529

B

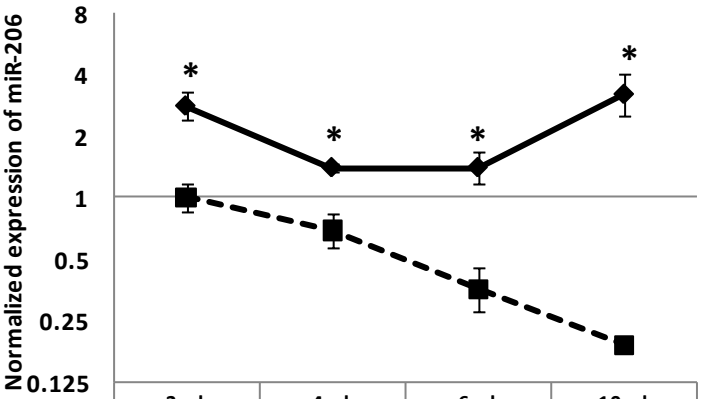

	3 wk	4 wk	6 wk	10 wk
mdx	2.808889751	1.401203665	1.401203665	3.20427951
C57Bl/10	1	0.687770909	0.354371217	0.189464571

Fig. 6.4 qPCR quantification of A) miR-31 and B) miR-206 in *mdx* compared to C57Bl/10 TA tissue at different ages. miR-31 and miR-206 were significantly overexpressed in *mdx* TA tissue at all ages examined. * = $p < 0.05$ relative to expression in C57Bl/10 TA using an unpaired two-tailed *t*-test ($n = 3$ for all time points). Note: y-axes have been $\log_2$-transformed.

6.7 miR-31 and miR-206 misexpression was corrected in *Fiona* skeletal muscle tissue

In order to test the hypothesis that miR-31 and miR-206 misexpression was directly linked to muscle dystrophy, the expression of these miRNAs was quantified in skeletal muscle from *Fiona* mice, which show complete rescue of all the dystrophic features of the *mdx* mouse. Figures 6.5A and B indicate that correction of the dystrophic phenotype results in the return of the expression of miR-31 and miR-206 to near-normal levels, as there was no significant difference in expression of either of these two miRNAs in TA from *Fiona* and wild-type mice.

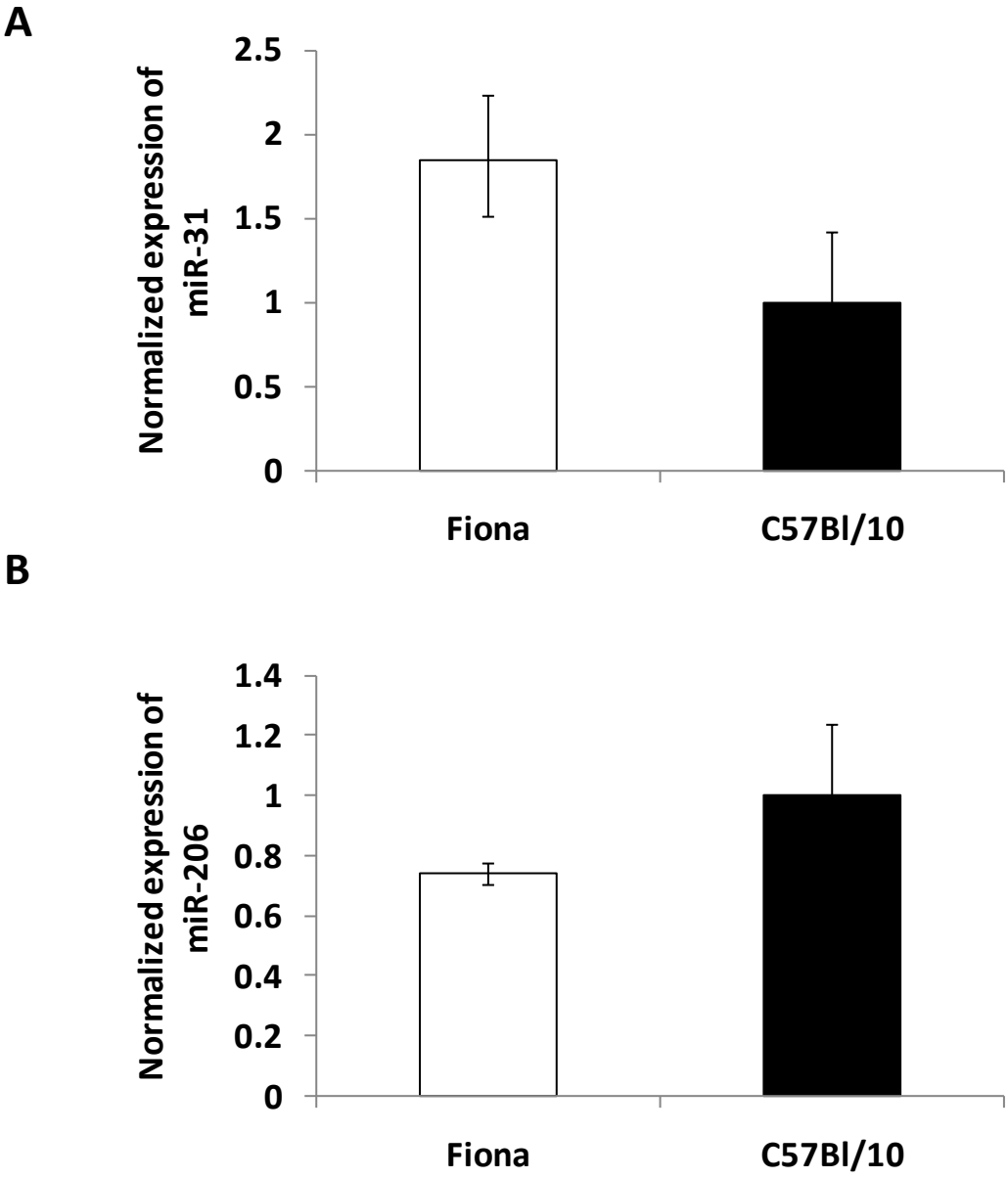

Fig. 6.5 qPCR quantification of A) miR-31 and B) miR-206 in *Fiona* compared to C57Bl/10 TA tissue. No significant difference in expression was observed for either miR-31 or miR-206 ($n = 3$).

6.8 miR-503 was misexpressed in TA and diaphragm, but not in quadriceps, of *dko* compared to *mdx* mice

Unlike with miR-31 and miR-206, there was no published information on the possible role of miR-503 in muscle biology at the time of this study. Therefore, this miRNA was selected for more comprehensive examination.

miR-503 was shown to be overexpressed 3.6-fold in TA muscle from 10-week-old *dko* mice compared to *mdx* mice (Table 6.1B). This significant overexpression was validated by performing qPCR using the TaqMan assay. Figure 6.6 shows a significant upregulation in miR-503 expression in the TA muscle of *dko* mice, albeit at a lower fold change (2.2-fold). This significant upregulation was also observed in the diaphragm muscle, thus indicating that miR-503 overexpression was not restricted to the TA muscle. However, no significant difference in expression was observed in quad muscle from *mdx* compared to *dko* mice.

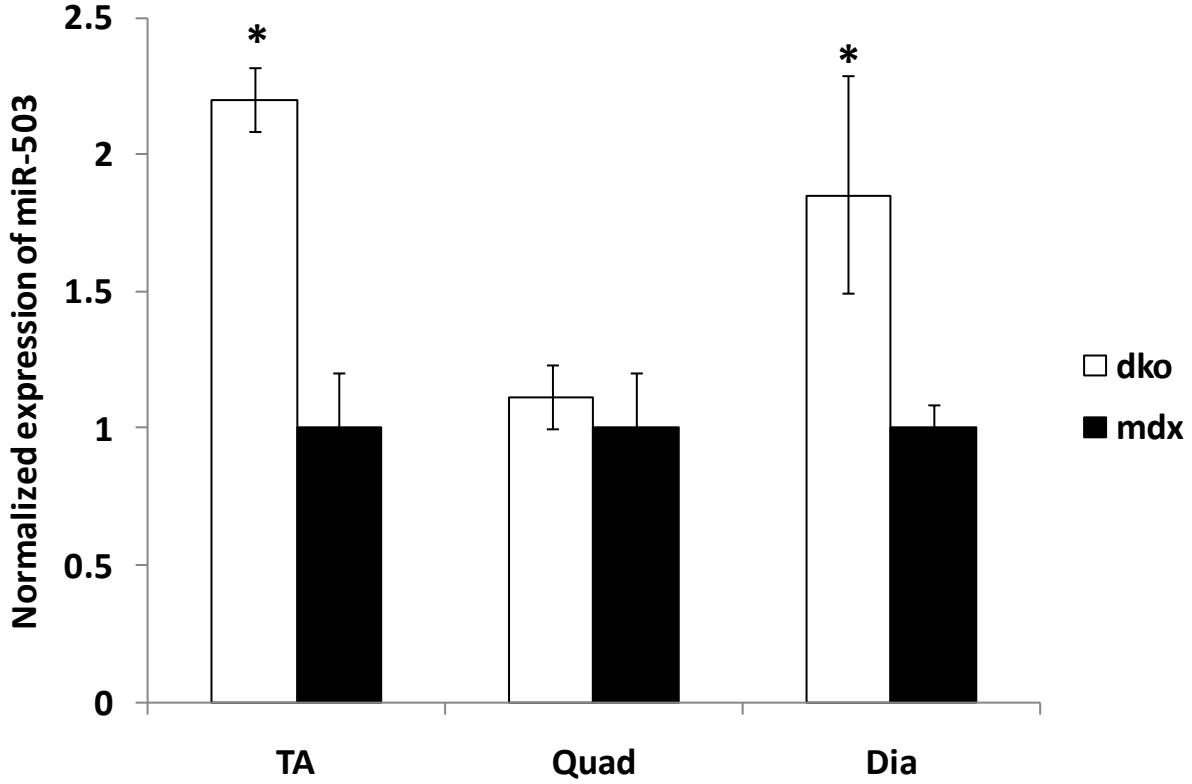

Fig. 6.6 qPCR quantification of miR-503 in *dko* compared to *mdx* TA, diaphragm and quadriceps tissue. miR-503 was significantly overexpressed in TA and diaphragm tissue from *dko* compared to *mdx* mice. * = $p < 0.05$ relative to *mdx* tissue using an unpaired two-tailed *t*-test ($n = 3$).

6.9 pri-miR-503 was not dysregulated in *dko* compared to *mdx* TA tissue

pri-miR-503 levels were quantified in order to understand the reasons for the overexpression of miR-503 in TA from *dko* compared to *mdx* mice. Figure 6.7 shows no significant difference in the expression of pri-miR-503, indicating that the reasons for the overexpression of miR-503 in *dko* muscle are post-transcriptional.

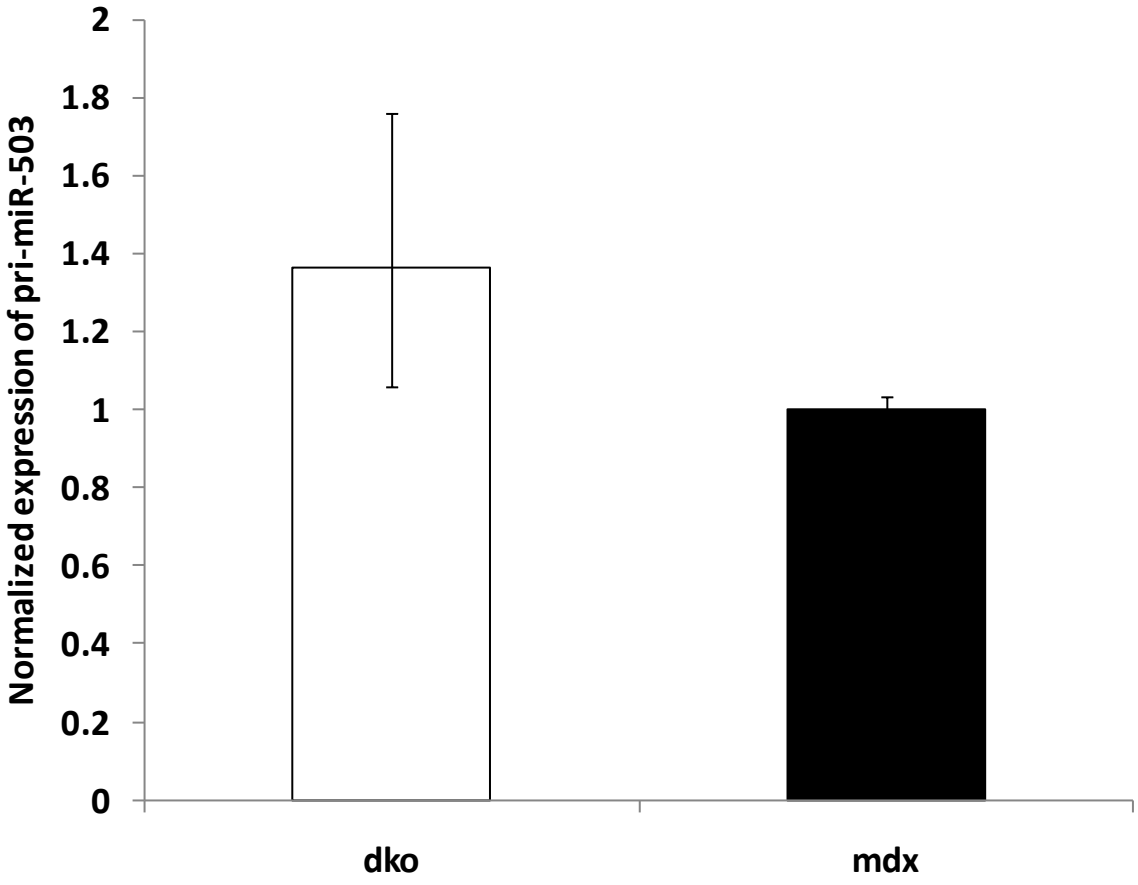

Fig. 6.7 qPCR quantification of pri-miR-503 in *dko* compared to *mdx* TA tissue. No significant difference in expression was observed ($n = 3$).

6.10 miR-503 was not misexpressed at other ages in *dko* compared to *mdx* skeletal muscle tissue

The phenotypes of both the *mdx* and *dko* mouse become more dystrophic as they age. The onset of dystrophy is earlier in the *dko* mouse (~6 days compared to ~3 weeks for the *mdx* mouse), and it becomes steadily worse until death as opposed to the *mdx* mouse that experiences an acute phase lasting from ~3 weeks to ~8 weeks of age, followed by a steady-state chronic stage that does not get worse as the mouse ages (Deconinck et al., 1997b; DiMario et al., 1991).

miR-503 expression was measured in TA tissue from both genotypes at the following ages – 4 weeks, 6 weeks, and 10 weeks. The data are plotted in Figure 6.8, and show clearly that miR-503 expression reduced with age. This reduction appears to be more pronounced in the *mdx* mouse than in the *dko* mouse, and the difference in expression became significant only at 10 weeks of age.

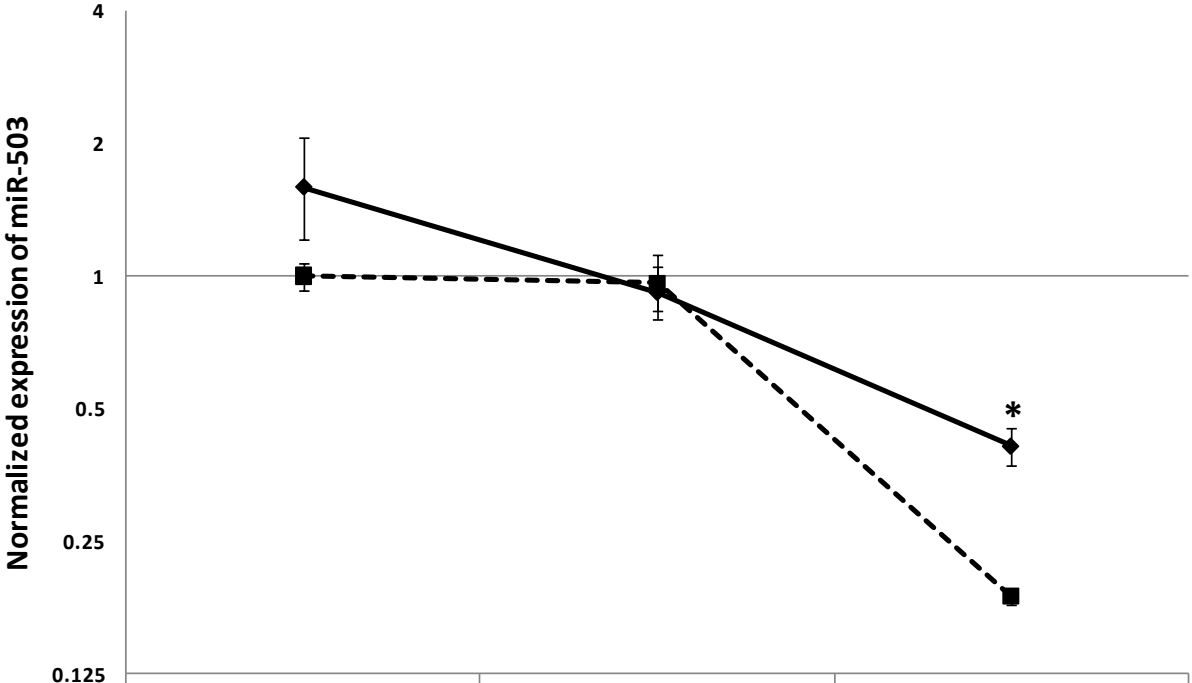

	4 wk	6 wk	10 wk
dko	1.589235949	0.91594529	0.409896999
mdx	1	0.963707118	0.186640416

Fig. 6.8 qPCR quantification of miR-503 in *dko* compared to *mdx* TA tissue at different ages. A significant difference in expression was observed only at 10 weeks of age. * = $p < 0.05$ relative to *mdx* TA using an unpaired two-tailed *t*-test ($n = 3$ for all time points). Note: y-axes have been $\log_2$-transformed.

6.11 *Myb* and *socs6* - novel validated targets of miR-503

In order to further understand miR-503's role in skeletal muscle and its possible contribution to dystrophy, the predicted targets *myb* and *soc6* were selected for experimental validation, as they not only came up as top-ranked candidates using target prediction programs, but were also hypothesized to play roles in the dystrophic progression (discussed in section 6.12).

Of the four online prediction programs used to identify interesting targets of miR-503 - TargetScan, Pictar, miRanda and DIANA-microT 3.0, *myb* came up as a predicted target using all four programs, whereas *socs6* was predicted only by TargetScan and Pictar, although both programs ranked it highly. *Socs6* has one predicted seed region (which is the region predicted to directly bind to the mature miRNA) in its 3' UTR for miR-503. The programs DIANA-microT 3.0 and Pictar predict two seed regions in the *myb* 3'UTR for miR-503, whereas TargetScan and miRanda predict only one. For the purpose of this study it was decided to consider both seed regions as functionally relevant.

The basic strategy for target validation involved the cotransfection of a miR-503 mimic and a 3' UTR dual-luciferase construct into HEK 293T cells, followed by a luciferase assay to test for knockdown of expression. The constructs consist of the 3' UTR of the predicted targets located directly downstream of the *renilla* gene in the dual-luciferase vector psiCheck2.2 (which contains both the *firefly* and *renilla* genes). Due to this configuration, the activity of the *renilla* gene (as measured by assaying for Renilla luciferase activity) is under the influence of the 3' UTR, therefore positive or negative effects on the 3' UTR will manifest themselves as changes in expression levels of this gene. The *firefly* gene acts as an internal control. Two sets of constructs were made for *myb* and *socs6* – a psiCheck2.2 vector containing the wild-type mouse 3' UTR (dubbed pMyb+ and pSocs6+ respectively) and a psiCheck2.2 vector containing the 3' UTR with deletions of the seed region(s) (dubbed pMyb-/- and pSocs6- respectively). Use of the

second set of constructs was necessary to show that any inhibitory effects exhibited by miR-503 were the result of specific interaction with the seed region(s) and not because of off-target reasons. Figure 6.9 shows the miR-503 seed sequences in the 3' UTRs of *myb* and *socs6* and the deleted regions used in the pMyb-/- and pSocs6- constructs.

In order to test the hypothesis that *myb* and *socs6* were bona fide targets of miR-503, HEK 293T cells were cotransfected with either the psiCheck2.2 dual-luciferase constructs containing the wild-type 3' UTRs (constructs pMyb+ and pSocs6+) or constructs containing 3' UTRs with the appropriate miR-503 seed regions deleted (constructs pMyb-/- and pSocs6-) and either a miR-503 mimic or a negative (scrambled siRNA) control. Figures 6.9A and B show the predicted miR-503 seed regions in the 3' UTR of *myb* and *socs6* respectively, with the deleted regions (in constructs pMyb-/- and pSocs6-) indicated.

A

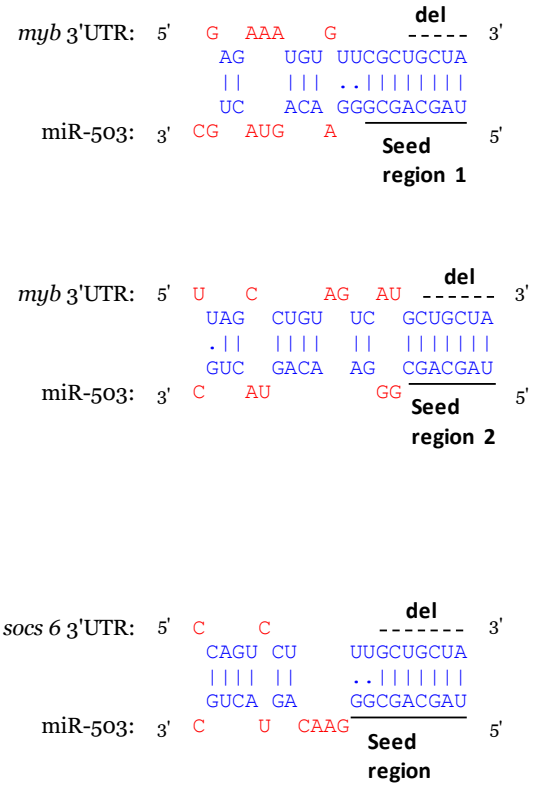

B

Fig. 6.9 Sequence alignments of miR-503 and the 3' UTR of A) *myb* and B) *socs6*. *Solid line*, seed match regions; *dashed line*, seed-deleted region. Note: miR-503 has two predicted seed regions in the 3' UTR of *myb*.

Figures 6.10A and B show clearly that miR-503 had a significantly inhibitory effect on both the *myb* and *socs6* 3' UTR compared to the negative control (in terms of a reduction in normalized luciferase activity). This inhibitory effect was relieved by mutations of the miR-503 seed regions in both 3' UTRs, highlighting the specificity of activity of miR-503 via these target seed regions. Figure 6.10C shows that cotransfection of cells with the miR-503 mimic and the parental luciferase construct (i.e. the empty psiCheck2.2 vector) did not result in a knockdown of luciferase expression. This was a useful control experiment to show that miR-503 did not have an inhibitory effect via any region of the psiCheck2.2 vector. To confirm that the inhibitory effects of miR-503 on *myb* and *socs6* expression were unique, the miR-503 mimic was cotransfected with a psiCheck2.2 contruct (pMgst1+) containing the 3' UTR of a gene that was not predicted to be a target of miR-503, *microsomal glutathione S-transferase 1* (*mgst1*). Figure 6.10D shows that miR-503 overexpression did not result in the knockdown of pMgst1+, indicating that miR-503 does not have a universally inhibitory effect on gene expression.

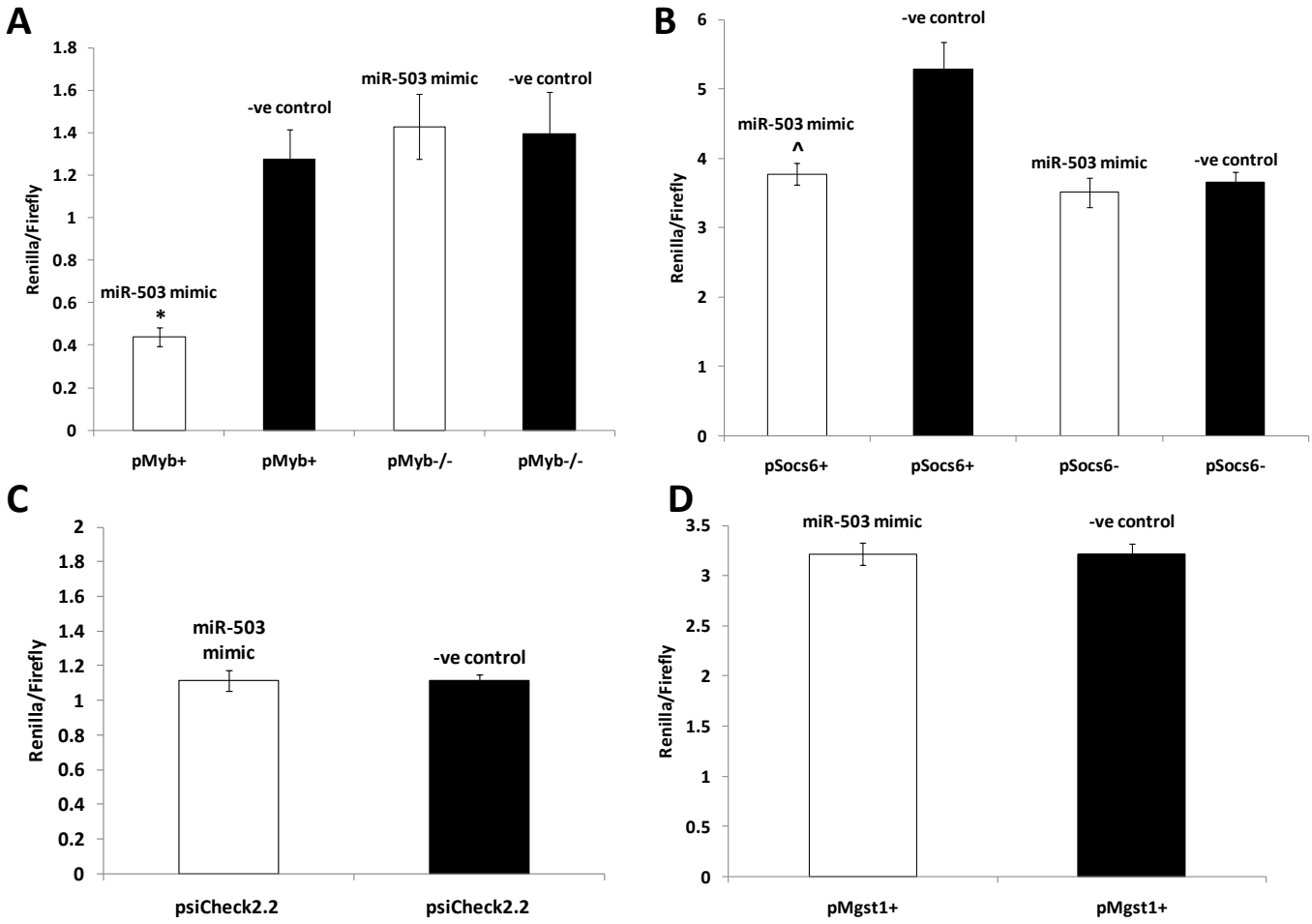

Fig. 6.10 Functional validation of *myb* and *socs6* as targets of miR-503 using the dual-luciferase assay in HEK 293T cells. miR-503 had a significant inhibitory effect on A) pMyb+ but not pMyb-/-, on B) pSocs6+ but not pSocs-, and no effect on C) the empty psiCheck2.2 vector or D) Mgst1. * = $p < 0.05$ relative to expression of pMyb+ in cells co-transfected with –ve control ; ^ = $p < 0.05$ relative to expression of pSocs+ in cells co-transfected with –ve control using a paired two-tailed *t*-test. Each bar represents the average of 3 independent experiments.

6.12 Discussion

The purpose of this study was to evaluate the contribution of miRNAs to the progression of muscular dystrophy in mouse skeletal muscle tissue as a result of the absence of dystrophin, and the combined absence of dystrophin and utrophin. In order to produce a comprehensive picture of the extent of global miRNA deregulation as a result of the absence of these proteins, miRNA microarrays were carried out. These microarrays produced two lists of miRNAs that were significantly dysregulated (Table 6.1A and B).

It is clear that more miRNAs were significantly misexpressed, and to a greater degree, in TA from *mdx* versus C57Bl/10 mice compared to TA from *dko* versus *mdx* mice. This is not surprising considering the more substantial difference in the gross morphology of skeletal muscle tissue from *mdx* and C57Bl/10 mice, compared to that found in tissue from *dko* and *mdx* mice. Importantly, there is very little overlap (bar miR-29c and miR-206) between these two lists. Whether this is indicative of different pathways being affected (and therefore possibly contributing to dystrophy) in skeletal muscle from *dko* and *mdx* mice is not possible to ascertain due to the lack of sufficient functional information about many of these miRNAs.

Predicted targets of all the significantly dysregulated miRNAs produced by TargetScan were entered into the IPA software to identify biological pathways that were significantly overrepresented. The results of this analysis for both lists of miRNAs from Table 6.1 are presented in Table 6.2. Importantly, the two top-ranked networks produced for the miRNAs in Table 6.1A suggest an involvement in skeletal, muscle, and nervous system development. Additionally, in the category 'Physiological System Development and Function', 'Nervous System Development and Function' appeared as the top candidate for both lists of miRNAs, which is not surprising considering the impairment in NMJ structure found in both *mdx* and *dko* mice.

qPCR was used to confirm some of the results produced by the microarrays. Initially, the NCode system was used because of its relative inexpensiveness (the same kit can be used to measure the expression of all miRNAs of interest as the only additional requirement is a forward primer that is specific to the miRNA being studied). Figure 6.2 shows the results of qPCR quantification of five miRNAs – miR-21, miR-29c, miR-31, miR-206, and miR-34c. These results validated the microarray results for 4 miRNAs, but not miR-34c. However, due to the problems mentioned in section 6.3, TaqMan MicroRNA assays were used for further analysis.

Figure 6.2B shows that the TaqMan assays confirmed the microarray results that miR-31 and miR-206 were significantly upregulated in *mdx* compared to wild-type TA muscle. However, these qPCR results indicate that the fold difference was much greater for miR-31. Significantly, both miR-31 and miR-206 were shown to be significantly upregulated

in DMD compared to normal muscle tissue (Eisenberg et al., 2007), perhaps pointing to a conservation in function of miR-31 and miR-206 in mouse and human skeletal muscle. miR-31 and miR-206 were selected for further analysis because they were two of the top-ranked candidates in terms of fold-change difference between *mdx* and wild-type tissue (Table 6.1A). While miR-206 has been shown to play a very important role in muscle biology, miR-31 has been shown to almost exclusively play a role in cancer. For example, miR-31 has been shown to be a reliable biomarker for the progression of inflammatory bowel disease (IBD) from normal tissue to IBD-related neoplasia (Olaru et al., 2010), increase the invasiveness of a range of colon carcinoma cell lines (Cottonham et al., 2010), and repress tumour suppressors in lung cancer (Liu et al., 2010). In spite of its almost exclusive involvement in cancer, miR-31 is worth pursuing research on within a DMD context because of the remarkable increase in its expression seen in *mdx* muscle tissue. It could also serve as a biomarker for the disease. Unlike with miR-31, a great deal is known about the role of miR-206 in muscle biology. For example, miR-206 has been shown to be significantly upregulated during the myoblast-myotube transition (Rao et al., 2006) and is a direct target of MyoD (Rosenberg et al., 2006). One of the ways in which miR-206 has been suggested to promoted muscle cell differentiation is via the downregulation of the gap junction protein connexin43 (Anderson et al., 2006). miR-206 has also been shown to be significantly upregulated in the diaphragm (McCarthy et al., 2007) and limb muscle (Yuasa et al., 2008) of *mdx* compared to wild-type mice. Also within this context, miR-206 has been shown to directly target utrophin for downregulation (Rosenberg et al., 2006), therefore presenting itself as a possible therapeutic target because the artificial downregulation of miR-206 might result in an increase in utrophin expression. Therefore, both miR-31 and miR-206 present themselves as worthy of further examination within the DMD context.

As mentioned in section 1.5.1, miRNA genes are transcribed to produce long transcripts known as pri-miRs. Therefore, measurement of the expression of pri-miRs is indicative of the level of expression of the miRNA gene. Figure 6.3 shows a very significant difference in the expression of both pri-miR-31 and pri-miR-206 in *mdx* compared to wild-type muscle, mirroring the difference seen in the expression of their mature

counterparts. This indicates that significant increase in miR-31 and miR-206 in *mdx* muscle was due to transcriptional effects.

miR-31 and miR-206 levels were also quantified in the TA of *mdx* and wild-type mice at different ages. Figure 6.4A shows that while miR-31 levels remained steady in normal muscle across the ages examined, it steadily rose in dystrophic muscle with age. This could indicate either a direct contribution of miR-31 or simply a response to dystrophic progression. Figure 6.4B shows that while miR-206 was naturally downregulated in normal muscle with age, it maintained a steady level of expression in dystrophic muscle. Perhaps miR-206 plays an important role in the early development of skeletal muscle (which is in keeping with its known role in muscle differentiation) and so is downregulated with age as it is no longer required. The persistence of miR-206 expression in dystrophic muscle might therefore contribute to the pathogenesis of the disease, as accelerated differentiation is known to be a feature of DMD muscle (Eisenberg et al., 2009).

The *Fiona* mouse was introduced in section 1.3.3 as a transgenic mouse that overexpressed utrophin in a skeletal-muscle specific manner against an *mdx* background, and shows complete correction of all the dystrophic features of the *mdx* mouse when sedentary. It would therefore be reasonable to hypothesize that miR-31 and miR-206 levels would return to normal in *Fiona* skeletal muscle. Figures 6.5A and B indicate no significant difference in the levels of miR-31 and miR-206 in *Fiona* and wild-type mice. Although miR-31 appeared to be expressed more strongly in *Fiona* muscle than wild-type muscle, this difference was not statistically significant. These results strongly suggest a positive correlation between miR-31 and miR-206 expression and the degree of dystrophy. These miRNAs could therefore serve as biomarkers to assess therapeutic success.

While the experiments of this study were being carried out, another group published results from a miRNA microarray on skeletal muscle from *mdx* and wild-type mice (Greco et al., 2009). Although they used different tissue (adductor muscle) and a different microarray (based on the TaqMan qPCR assay system performed in 96-well format) there was significant overlap between their results and ours. Most strikingly, they

also found that miR-31 was the most significantly upregulated miRNA in *mdx* tissue, and to a similar degree found in our study (71.5-fold versus ~64.45-fold). They also similarly found that miR-21, -221, -223, -206 and -34c were significantly upregulated, and miR-29a and miR-29c were significantly downregulated.

The top ranked miRNAs from Table 6.1B were each evaluated for their possible significance to muscle biology and DMD by conducting a survey of the literature and analysing the lists of predicted target produced by the online programs TargetScan, PicTar, miRanda and DIANA-microT 3.0. A literature survey at the time revealed that none of the top-ranked miRNAs had been shown to be involved in muscle biology or disease (however, miR-503 has since been shown to play an important role in myoblast differentiation (Sarkar et al., 2010)). A detailed analysis of predicted targets revealed an overrepresentation of genes with known or possible relevance to muscle biology and/or disease for miR-503 compared to the other miRNAs. Therefore, this miRNA was selected for further analysis.

As with miR-31 and miR-206, the microarray results were validated by qPCR (using the TaqMan assay). Figure 6.6 shows that miR-503 was significantly upregulated in TA from *dko* compared to *mdx* mice. In addition, miR-503 levels were measured in quadriceps and diaphragm tissue in order to see if miR-503 misexpression was specific to the TA or was also found in other skeletal muscle tissue. Figure 6.6 shows that miR-503 was also significantly upregulated in the diaphragm, but not the quadriceps, of *dko* compared to *mdx* mice, indicating that this misexpression was not TA-specific. Perhaps miR-503 is not misexpressed in the quadriceps because of the heterogeneous nature of this muscle.

Also as with miR-31 and miR-206, pri-miR-503 levels were quantified in *dko* and *mdx* TA tissue in order to understand how the dysregulation of miR-503 occurs. Figure 6.7 shows no significant difference expression of pri-miR-503 between *dko* and *mdx* TA tissue, indicating that the reasons for miR-503 dysregulation are post-transcriptional. Post-transcriptional regulation of miRNA expression is not without precedence, and even occurs normally. For example, although miR-138 displays differential expression across different mouse tissues, its precursor, pre-miR-138-2, is ubiquitously expressed. The authors of this study suggest the existence of an inhibitory factor in some tissues but not

others that, for example, prevents the processing of the precursor by the enzyme Dicer (Obernosterer et al., 2006). A criticism of the data presented in Figure 6.7 is that the error bar for the pri-miR-503 expression in *dko* tissue is very large, indicating the need for more biological samples to be included. However, this could not be done because of the difficulty in obtaining 10-week-old male *dko* mice.

In order to assess the change in expression of miR-503 with age, its expression was measured in TA tissue from *dko* and *mdx* mice at the following ages – 4 weeks, 6 weeks, and 10 weeks. The data were plotted in Figure 6.8, and show clearly that miR-503 expression reduced with age. This reduction appears to be more pronounced in the *mdx* mouse than in the *dko* mouse, and the difference in expression became significant only at 10 weeks of age. This divergence in expression occurring late in the dystrophic progression is perhaps indicative that the higher expression of miR-503 in 10-week-old *dko* mice was a response to the higher accumulation of muscle damage seen in *dko* compared to *mdx* mice.

To further examine the role of miR-503 in the dystrophic progression of skeletal muscle in the *dko* mouse, functional validation of two predicted targets, *myb* and *socs6*, was performed. *Myb* is known to play an important role in cell growth and differentiation. It has been recently shown that the overexpression of *myb* results in the significant increase in expression of IGF-I, IGF-II, and IGF-IR, and a significant reduction in insulin-like growth factor binding protein-3 (Kim et al., 2009). Overexpression of IGF-1 in *mdx* mice has been shown to result in reduced pathology most likely caused by a reduction in muscle necrosis. IGF-1 is thought to act via complex signalling pathways involving protein synthesis and degradation, myoblast proliferation and muscle differentiation (Grounds et al., 2008). *Myb* overexpression could therefore possibly result in an amelioration of the dystrophic phenotype via its upregulation of IGF-1. *Socs6* was selected because of its demonstrated role in fibrosis. A major pathological feature of DMD is elevated levels of fibrosis. This unregulated proliferation of connective tissue not only contributes to muscle weakness but also presents an obstacle to potential treatment. DMD muscle is also characterized by the infiltration of inflammatory cells. T lymphocytes are a major constituent of these infiltrates. It had been proposed that these

cells contribute to the elevated levels of fibrosis (and necrosis) via their role in chronic inflammation. This led to the hypothesis that a reduction in the levels of T lymphocytes in the *mdx* mouse would result in reduced fibrosis and an amelioration of the dystrophic phenotype. *mdx* mice were crossed with *scid* mice (these are mice that do not produce B- or T-lymphocytes) to produce *mdx*/*scid* progeny. These heterozygotes displayed marked reduction in fibrosis and levels of TGF-β1, which is known to stimulate collagen synthesis. *Scid*/*mdx* mice displayed better muscle endurance in treadmill exercise compared to *mdx* mice (Farini et al., 2007). It has recently been shown that *socs6* negatively regulates T cell activation. It does so by binding to the T cell-specific tyrosine kinase, $p56^{lck}$, thereby promoting its ubiquitination and targeting to the proteasome for degradation. $p56^{lck}$ plays an important role in enhancing T cell receptor signalling, which contributes to T cell activation (Choi et al., 2010). It therefore seems reasonable to propose that *socs6* overexpression could result in the partial correction of the dystrophic phenotype via its negative regulation of T cell activation and the resulting reduction in fibrosis.

The validation of *myb* and *socs6* as bona fide targets of miR-503 might not only help to further understand the worsened phenotype of the *dko* mouse (if they were targets of miR-503, then the observed overexpression of miR-503 might result in reduced expression of both these genes, thereby possibly contributing to the dystrophic phenotype) but might also present a therapeutic option that would involve the artificial downregulation of miR-503 to increase the expression of both these genes.

Figures 6.10A and B clearly show that miR-503 overexpression resulted in the significant knockdown in expression of *myb* and *socs6*, and that this knockdown was mediated via the predicted target seed regions in the 3' UTR. Figures 6.10C and D indicate that miR-503 did not have an inhibitory effect on the naked psiCheck2.2 vector or on the 3' UTR of a gene (*mgst1*) that is not a predicted target.

Therefore, perhaps miR-503 overexpression in *dko* skeletal muscle contributes to the worsened phenotype due to its inhibitory effects on *myb* and *socs6*. Assuming this to be the case, it follows that the artificial downregulation of miR-503, and the resulting increase in *myb* and *socs6* expression, presents itself as a possible therapeutic option.

In conclusion, the results in this chapter indicate that both the absence of dystrophin and the combined absence of dystrophin and utrophin result in the dysregulation of a range of miRNAs. Considering the numerous predicted targets of each miRNA, this dysregulation could have numerous hitherto unknown influences on the progression of dystrophy in both the *mdx* and *dko* mouse. Further examination of the expression profiles of two important miRNAs, miR-31 and miR-206, were also performed, highlighting their potential use as biomarkers. Finally, the experimental validation of two potentially important targets of miR-503 not only points to a potentially important involvement of this miRNA in the dystrophic progression but also indicates that it might be a therapeutic target whose expression could be artificially modulated to ameliorate the disease. An important follow-up experiment would therefore be to evaluate the effects of knocking down miR-503 in the skeletal muscle of *dko* mice to determine if this knockdown resulted in an amelioration of the dystrophic phenotype.

7 Discussion

7.1 Summary of results

The overarching leitmotif of this thesis is the investigation of therapeutic options for DMD. The results from Chapter 3 indicate that while utrophin serves as an excellent substitute for dystrophin in the skeletal muscle of sedentary mice, functional differences between these two proteins became apparent under conditions of prolonged stress-inducing exercise. In Chapters 4 and 5, the results for two mouse drug trials were presented. These results indicate that both GW501516 (Chapter 4) and C1100 (Chapter 5) partially corrected the dystrophic phenotype of the *mdx* mouse. C1100 was also shown to robustly upregulate utrophin *in vitro* and the mode of this upregulation was deciphered. In Chapter 6 it was shown that both the absence of dystrophin and the combined absence of dystrophin and utrophin in skeletal muscle resulted in a marked alteration in the global miRNA expression profile in this tissue. This chapter also presented results of more comprehensive expression analyses of miR-31, miR-206 and miR-503. Experimental validation of two predicted targets of miR-503 was performed, possibly implicating it in the dystrophic progression seen in the skeletal muscle of *dko* mice and therefore presenting it as a target for therapeutic manipulation.

7.2 Therapeutic implications of the functional differences between dystrophin and utrophin

The results from Chapter 3 indicate that when the *Fiona* transgenic mouse and the wild-type C57Bl/6 mouse were subjected to the same levels of stress-inducing exercise, limb skeletal muscle from the *Fiona* mouse exhibited greater signs of damage and functional impairment. However, damage was significantly more pronounced in the skeletal muscle of exercised *mdx* mice, indicating the retention of some of the protective functions of utrophin under these conditions. We suggest that a reason for this functional difference could be the inability of utrophin to recruit nNOS to the sarcolemma where it is known to prevent vasoconstriction especially during bouts of exercise. The absence of nNOS could therefore result in functional ischaemia which results in impaired muscle function. The

results from this study therefore suggest that any utrophin-based therapy will need to be used in conjunction with a treatment that maintains proper blood flow to the muscle in order to be a cure (Li et al., 2010).

7.3 The therapeutic promise of pharmacological compounds

The results from Chapter 4 show that the PPARδ agonist GW501516 had ameliorative effects on the *mdx* mice via its ability to increase the expression of utrophin in skeletal muscle. These results have been confirmed by others (Miura et al., 2009), who also show that this drug induces a fast-to-slow fibre type switch. Due to overlap in the signalling cascades that are responsible for both this switch and the upregulation of utrophin, treatments that result in this switch are likely to show some level of success. However the observed fold-increase in utrophin expression (~1.7-fold increase in TA and mild, non-significant increase in diaphragm) as a result of treatment falls short of the generally accepted two- to three-fold upregulation of utrophin that is thought be sufficient for successfully combating dystrophic progression in the *mdx* mouse (Khurana and Davies, 2003). Also, as discussed in section 4.6, GW501516 treatment might result in adverse side-effects, thus prompting the development of partial PPARδ agonists. The PPARs have a ligand binding domain that consists of 13 α-helices and 4 β-strands. One of these α-helices contains the AF-2 transcriptional activation domain that plays an important role in the recruitment of co-activators. Two GW501516-based partial agonists were designed to not interact directly with the AF-2 helix, with maximum PPARδ activation of 87% and 39% respectively compared to that of GW501516 (Pettersson et al., 2007). These authors have provided a general strategy for generating even more partial agonists, which could then be tested in the *mdx* mouse.

The experiments described in Chapter 5 indicate that despite the significantly positive effect of the drug C1100 on the utrophin A promoter, its administration resulted in only a mild improvement in the pathology of the *mdx* mouse. However, as discussed in section 5.8, this trial had a number of drawbacks, including poor solubility of the drug, late timing of commencement of administration, and the suboptimal conditions of the animal facility used at the time. It is important to restate that this was one of a number of mouse

trials that tested the effects of C1100 administration. Many of these other trials, carried out in this lab and by others (Summit plc, BioMarin Pharmaceuticals Inc., and Prof. Annamaria De Luca, University of Bari), have yielded more positive results, prompting the carrying forward of C1100 to human trials. Early in 2010, C1100 (under the new name of BMN 195) was administered to the first subject of a Phase I clinical study carried out by the company BioMarin Pharmaceuticals Inc. This was a double-blind, placebo-controlled study involving the oral administration of BMN 195 to healthy volunteers whose objective was to test the safety and pharmacokinetics in these healthy individuals before administration to patients with DMD. Unfortunately, the results of this trial indicated that although BMN 195 was found to be safe according to the toxicology studies carried out, high enough plasma concentrations proposed to be necessary to achieve sufficient increase in utrophin expression were not obtained, therefore further clinical trials have been cancelled. Summit plc are currently in the process of improving the formulation of C1100 to circumvent this problem (http://www.summitplc.com/bmn-dmd.aspx).

In keeping with previous *in vitro* experiments performed by Summit plc, and other mouse trials that confirmed the potent effects of C1100 on utrophin expression, the results presented in sections 5.5 and 5.6 indicate that treatment with C1100 resulted in a significant increase in activity of both the 9.4 kb and 1.3 kb utrophin A promoter fragments.

The mode of action of C1100 on the utrophin A promoter was also deciphered, as this is a requirement for all drugs that are to be eventually used on humans. The N-box, PPRE half site and NFAT motifs were all shown to be essential for C1100 to exert its upregulatory effect. This finding opens the possibility for numerous follow-up experiments, the most important of which would be to discover if, like GW501516, C1100 physically interacts with proteins responsible for the upregulation of utrophin.

GW501516 and C1100 present themselves as particularly attractive therapeutic options because unlike other pharmacological agents (like gentamicin and PTC124), they can be used to treat all patients with DMD, irrespective of the mutations they harbour. The

promising results presented in this thesis and the results of other research groups encourage further research work on both these drugs.

Additional future work includes the development of more sophisticated screening tools for compounds that increase the expression of utrophin. To this end, an *mdx* transgenic mouse with a luciferase reporter gene knocked into exon 7 of one allele of the *utrophin* gene has been generated by Dr. Rebecca Fairclough in this lab. This mouse model will enable the assessment of the efficacy of drugs (by measuring the level of whole-body luminescent emission) at multiple time points of a trial without having to sacrifice the animal. Additionally, a stable cell line derived from the hind limbs of these mice is being developed. This is an ideal cell line to use for high-throughput screening and is superior to the H2K-*mdx*-UtroA cell line as it can be used to test the effects of compounds on both the utrophin A and B promoters instead of only a 9.4 kb fragment of the utrophin A promoter.

7.4 miRNAs – a novel therapeutic option

The results from Chapter 6 highlight the immense changes in the global expression profiles of miRNAs in skeletal muscle of *mdx* and *dko* mice. Considering the numerous predicted mRNA targets of each miRNA, it seems reasonable to posit that these changes could have many deleterious downstream effects. Of these deregulated miRNAs, miR-31, miR-206 and miR-503 were selected for more detailed analysis, leaving open the possibility of pursuing further research on the many other deregulated miRNAs to assess their contribution to the dystrophic process.

A particularly important finding in this chapter is that both miR-31 and miR-206 showed significant overexpression in dystrophic compared to normal muscle very early in the dystrophic process (3 weeks of age), perhaps indicating that misexpression of both these miRNAs is a direct consequence of the absence of dystrophin and not simply a response to general muscle damage. Equally interesting is that both pri-miR-31 and pri-miR-206 also displayed significant overexpression in dystrophic muscle indicating a difference in the levels of transcription of these two miRNA genes in dystrophic and normal muscle.

Therefore, possible future experiments could include the search for factors that regulate the transcription of these genes and determine if they too display differential expression.

As mentioned in section 6.12, because both miR-31 and miR-206 were so highly dysregulated in dystrophic muscle, they could be used as biomarkers to assess the level of dystrophy and therefore, for example, the efficacy of a particular therapy. This is exemplified by the results shown in Figures 6.5A and B which show that the phenotypic correction observed in the muscle of *Fiona* mice was mirrored by the correction of the misexpression of both miR-31 and miR-206 to wild-type levels.

This chapter also presented results that confirm two predicted targets of miR-503 (which was found to be significantly dysregulated in skeletal muscle from *dko* mice) as bona fide targets. It was suggested in section 6.12 that the artificial upregulation of these two targets, *myb* and *socs6*, could yield therapeutic benefits, namely an upregulation of IGF-1 and a decrease in T cell activation and resulting fibrosis, respectively. It was also suggested in this chapter that this upregulation could conceivably be achieved by reducing the expression of miR-503. Currently, the two most promising ways of inhibiting miRNA expression *in vitro* and *in vivo* are the use of locked nucleic acid oligonucleotides (LNAs) and antagomirs. LNAs are oligonucleotides that contain at least one LNA monomer i.e. one 2'-*O*, 4'-*C*-methylene-*β*-D-ribofuranosyl nucleotide. LNAs have been shown to bind efficiently to complementary nucleic acids and induce potent antisense effects both *in vitro* and *in vivo* (Elmen et al., 2008; Vester and Wengel, 2004). Antagomirs are usually chemically modified, cholesterol-conjugated single-stranded RNA molecules complementary to miRNAs. Their administration has been shown to result in potent and long-term reduction in the levels of a number of miRNAs in a range of tissues, including the heart and muscle, in mice (Czech, 2006; Krutzfeldt et al., 2005). Therefore, a follow-up study could involve the administration of miR-503–specific LNAs or antagomirs to the *dko* mouse to test for an amelioration of the dystrophic phenotype, via either the upregulation of IGF-1 or a reduction in fibrosis.

7.5 Conclusion

As discussed in section 1.1.2, the absence of dystrophin at the sarcolemma results in numerous downstream effects that are deleterious to the muscle. It therefore seems likely that the most successful therapeutic strategy would involve the employment of multiple complementary treatment options i.e. those that correct different aspects of the disease phenotype. This thesis has presented an evaluation of different (and potentially complementary) treatment options that could be used to combat DMD.

8 References

Acharyya, S., Butchbach, M.E.R., Sahenk, Z., Wang, H.T., Saji, M., Carathers, M., Ringel, M.D., Skipworth, R.J.E., Fearon, K.C.H., Hollingsworth, M.A*., et al.* (2005). Dystrophin glycoprotein complex dysfunction: A regulatory link between muscular dystrophy and cancer cachexia. Cancer Cell *8*, 421-432.

Adams, M.E., Kramarcy, N., Krall, S.P., Rossi, S.G., Rotundo, R.L., Sealock, R., and Froehner, S.C. (2000). Absence of alpha-syntrophin leads to structurally aberrant neuromuscular synapses deficient in utrophin. J Cell Biol *150*, 1385-1398.

Alter, J., Lou, F., Rabinowitz, A., Yin, H.F., Rosenfeld, J., Wilton, S.D., Partridge, T.A., and Lu, Q.L. (2006). Systemic delivery of morpholino oligonucleotide restores dystrophin expression bodywide and improves dystrophic pathology. Nature Medicine *12*, 175-177.

Amann, K.J., Guo, A.W., and Ervasti, J.M. (1999). Utrophin lacks the rod domain actin binding activity of dystrophin. J Biol Chem *274*, 35375-35380.

Amann, K.J., Renley, B.A., and Ervasti, J.M. (1998). A cluster of basic repeats in the dystrophin rod domain binds F-actin through an electrostatic interaction. Journal of Biological Chemistry *273*, 28419-28423.

Anderson, C., Catoe, H., and Werner, R. (2006). MIR-206 regulates connexin43 expression during skeletal muscle development. Nucleic Acids Res *34*, 5863-5871.

Anderson, J.E., Bressler, B.H., and Ovalle, W.K. (1988). Functional regeneration in the hindlimb skeletal muscle of the mdx mouse. J Muscle Res Cell Motil *9*, 499-515.

Angelini, C. (2007). The role of corticosteroids in muscular dystrophy: a critical appraisal. Muscle Nerve *36*, 424-435.

Angus, L.M., Chakkalakal, J.V., Mejat, A., Eibl, J.K., Belanger, G., Megeney, L.A., Chin, E.R., Schaeffer, L., Michel, R.N., and Jasmin, B.J. (2005). Calcineurin-NFAT signaling, together with GABP and peroxisome PGC-1{alpha}, drives utrophin gene expression at the neuromuscular junction. American Journal of Physiology - Cell Physiology *289*, C908-917.

Araki, E., Nakamura, K., Nakao, K., Kameya, S., Kobayashi, O., Nonaka, I., Kobayashi, T., and Katsuki, M. (1997). Targeted disruption of exon 52 in the mouse dystrophin gene induced muscle Degeneration similar to that observed in Duchenne muscular dystrophy. Biochem Bioph Res Co *238*, 492-497.

Auld, D.S., Thorne, N., Maguire, W.F., and Inglese, J. (2009). Mechanism of PTC124 activity in cell-based luciferase assays of nonsense codon suppression. P Natl Acad Sci USA *106*, 3585-3590.

Baker, P.E., Kearney, J.A., Gong, B., Merriam, A.P., Kuhn, D.E., Porter, J.D., and Rafael-Fortney, J.A. (2006). Analysis of gene expression differences between utrophin/dystrophin-deficient vs mdx skeletal muscles reveals a specific upregulation of slow muscle genes in limb muscles. Neurogenetics *7*, 81-91.

Barclay, C.J., Woledge, R.C., and Curtin, N.A. (2008). Effects of UCP3 genotype, temperature and muscle type on energy turnover of resting mouse skeletal muscle. Pflugers Arch *in press*.

Bartel, D.P. (2004). MicroRNAs: genomics, biogenesis, mechanism, and function. Cell *116*, 281-297.

Barton, E.R., Morris, L., Kawana, M., Bish, L.T., and Toursel, T. (2005). Systemic administration of L-arginine benefits mdx skeletal muscle function. Muscle Nerve *32*, 751-760.

Barton, E.R., Morris, L., Musaro, A., Rosenthal, N., and Sweeney, H.L. (2002). Muscle-specific expression of insulin-like growth factor I counters muscle decline in mdx mice. J Cell Biol *157*, 137-148.

Bassel-Duby, R., and Olson, E.N. (2006). Signaling pathways in skeletal muscle remodeling. Annu Rev Biochem *75*, 19-37.
Benson, M.A., Newey, S.E., Martin-Rendon, E., Hawkes, R., and Blake, D.J. (2001). Dysbindin, a novel coiled-coil-containing protein that interacts with the dystrobrevins in muscle and brain. Journal of Biological Chemistry *276*, 24232-24241.
Beroud, C., Tuffery-Giraud, S., Matsuo, M., Hamroun, D., Humbertclaude, V., Monnier, N., Moizard, M.P., Voelckel, M.A., Calemard, L.M., Boisseau, P.*, et al.* (2007). Multiexon skipping leading to an artificial DMD protein lacking amino acids from exons 45 through 55 could rescue up to 63% of patients with Duchenne muscular dystrophy. Hum Mutat *28*, 196-202.
Betel, D., Wilson, M., Gabow, A., Marks, D.S., and Sander, C. (2008). The microRNA.org resource: targets and expression. Nucleic Acids Res *36*, D149-153.
Biggar, W.D., Harris, V.A., Eliasoph, L., and Alman, B. (2006). Long-term benefits of deflazacort treatment for boys with Duchenne muscular dystrophy in their second decade. Neuromuscular Disorders *16*, 249-255.
Blake, D.J., and Kroger, S. (2000). The neurobiology of duchenne muscular dystrophy: learning lessons from muscle? Trends Neurosci *23*, 92-99.
Blake, D.J., Weir, A., Newey, S.E., and Davies, K.E. (2002). Function and genetics of dystrophin and dystrophin-related proteins in muscle. Physiological Reviews *82*, 291-329.
Bostjancic, E., and Glavac, D. (2008). Importance of microRNAs in skin morphogenesis and diseases. Acta Dermatovenerol Alp Panonica Adriat *17*, 95-102.
Brockington, M., Yuva, Y., Prandini, P., Brown, S.C., Torelli, S., Benson, M.A., Herrmann, R., Anderson, L.V., Bashir, R., Burgunder, J.M.*, et al.* (2001). Mutations in the fukutin-related protein gene (FKRP) identify limb girdle muscular dystrophy 2I as a milder allelic variant of congenital muscular dystrophy MDC1C. Hum Mol Genet *10*, 2851-2859.
Brooks, S.V. (1998). Rapid recovery following contraction-induced injury to in situ skeletal muscles in mdx mice. J Muscle Res Cell Motil *19*, 179-187.
Brooks, S.V., and Faulkner, J.A. (1988). Contractile properties of skeletal muscles from young, adult and aged mice. J Physiol *404*, 71-82.
Buckingham, M. (2006). Myogenic progenitor cells and skeletal myogenesis in vertebrates. Curr Opin Genet Dev *16*, 525-532.
Buckle, V.J., Guenet, J.L., Simon-Chazottes, D., Love, D.R., and Davies, K.E. (1990). Localisation of a dystrophin-related autosomal gene to 6q24 in man, and to mouse chromosome 10 in the region of the dystrophia muscularis (dy) locus. Hum Genet *85*, 324-326.
Burton, E.A., Tinsley, J.M., Holzfeind, P.J., Rodrigues, N.R., and Davies, K.E. (1999). A second promoter provides an alternative target for therapeutic up-regulation of utrophin in Duchenne muscular dystrophy. P Natl Acad Sci USA *96*, 14025-14030.
Byers, T.J., Lidov, H.G., and Kunkel, L.M. (1993). An alternative dystrophin transcript specific to peripheral nerve. Nat Genet *4*, 77-81.
Campanelli, J.T., Roberds, S.L., Campbell, K.P., and Scheller, R.H. (1994). A role for dystrophin-associated glycoproteins and utrophin in agrin-induced AChR clustering. Cell *77*, 663-674.
Carnwath, J.W., and Shotton, D.M. (1987). Muscular dystrophy in the mdx mouse: histopathology of the soleus and extensor digitorum longus muscles. J Neurol Sci *80*, 39-54.
Chakkalakal, J.V., Harrison, M.A., Carbonetto, S., Chin, E., Michel, R.N., and Jasmin, B.J. (2004). Stimulation of calcineurin signaling attenuates the dystrophic pathology in mdx mice. Hum Mol Genet *13*, 379-388.
Chakkalakal, J.V., Michel, S.A., Chin, E.R., Michel, R.N., and Jasmin, B.J. (2006). Targeted inhibition of Ca2+ /calmodulin signaling exacerbates the dystrophic phenotype in mdx mouse muscle. Human Molecular Genetics *15*, 1423-1435.

Chakkalakal, J.V., Stocksley, M.A., Harrison, M.A., Angus, L.M., Deschenes-Furry, J., St-Pierre, S., Megeney, L.A., Chin, E.R., Michel, R.N., and Jasmin, B.J. (2003). Expression of utrophin A mRNA correlates with the oxidative capacity of skeletal muscle fiber types and is regulated by calcineurin/NFAT signaling. P Natl Acad Sci USA *100*, 7791-7796.
Chang, T.C., Yu, D., Lee, Y.S., Wentzel, E.A., Arking, D.E., West, K.M., Dang, C.V., Thomas-Tikhonenko, A., and Mendell, J.T. (2008). Widespread microRNA repression by Myc contributes to tumorigenesis. Nat Genet *40*, 43-50.
Chapman, V.M., Miller, D.R., Armstrong, D., and Caskey, C.T. (1989). Recovery of induced mutations for X chromosome-linked muscular dystrophy in mice. Proc Natl Acad Sci U S A *86*, 1292-1296.
Charge, S.B., and Rudnicki, M.A. (2004). Cellular and molecular regulation of muscle regeneration. Physiol Rev *84*, 209-238.
Chen, C., Ridzon, D.A., Broomer, A.J., Zhou, Z., Lee, D.H., Nguyen, J.T., Barbisin, M., Xu, N.L., Mahuvakar, V.R., Andersen, M.R*., et al.* (2005). Real-time quantification of microRNAs by stem-loop RT-PCR. Nucleic Acids Res *33*, e179.
Chen, J.F., Mandel, E.M., Thomson, J.M., Wu, Q., Callis, T.E., Hammond, S.M., Conlon, F.L., and Wang, D.Z. (2006). The role of microRNA-1 and microRNA-133 in skeletal muscle proliferation and differentiation. Nat Genet *38*, 228-233.
Choi, Y.B., Son, M., Park, M., Shin, J., and Yun, Y. (2010). SOCS-6 negatively regulates T cell activation through targeting p56lck to proteasomal degradation. The Journal of biological chemistry *285*, 7271-7280.
Cohn, R.D., Henry, M.D., Michele, D.E., Barresi, R., Saito, F., Moore, S.A., Flanagan, J.D., Skwarchuk, M.W., Robbins, M.E., Mendell, J.R*., et al.* (2002). Disruption of DAG1 in differentiated skeletal muscle reveals a role for dystroglycan in muscle regeneration. Cell *110*, 639-648.
Consolino, C.M., and Brooks, S.V. (2004). Susceptibility to sarcomere injury induced by single stretches of maximally activated muscles of mdx mice. J Appl Physiol *96*, 633-638.
Cooper, S.T., Lo, H.P., and North, K.N. (2003). Single section Western blot: improving the molecular diagnosis of the muscular dystrophies. Neurology *61*, 93-97.
Cottonham, C.L., Kaneko, S., and Xu, L. (2010). miR-21 and miR-31 converge on TIAM1 to regulate migration and invasion of colon carcinoma cells. J Biol Chem.
Courey, A.J., and Tjian, R. (1988). Analysis of Sp1 in vivo reveals multiple transcriptional domains, including a novel glutamine-rich activation motif. Cell *55*, 887-898.
Czech, M.P. (2006). MicroRNAs as therapeutic targets. N Engl J Med *354*, 1194-1195.
Davies, K.E., and Grounds, M.D. (2006). Treating muscular dystrophy with stem cells? Cell *127*, 1304-1306.
Davies, K.E., and Nowak, K.J. (2006). Molecular mechanisms of muscular dystrophies: old and new players. Nat Rev Mol Cell Biol *7*, 762-773.
De Luca, A., Nico, B., Rolland, J.F., Cozzoli, A., Burdi, R., Mangieri, D., Giannuzzi, V., Liantonio, A., Cippone, V., De Bellis, M*., et al.* (2008). Gentamicin treatment in exercised mdx mice: Identification of dystrophin-sensitive pathways and evaluation of efficacy in work-loaded dystrophic muscle. Neurobiology of Disease *32*, 243-253.
De Luca, A., Pierno, S., Liantonio, A., Cetrone, M., Camerino, C., Fraysse, B., Mirabella, M., Servidei, S., Ruegg, U.T., and Conte Camerino, D. (2003). Enhanced dystrophic progression in mdx mice by exercise and beneficial effects of taurine and insulin-like growth factor-1. J Pharmacol Exp Ther *304*, 453-463.

Deconinck, A.E., Potter, A.C., Tinsley, J.M., Wood, S.J., Vater, R., Young, C., Metzinger, L., Vincent, A., Slater, C.R., and Davies, K.E. (1997a). Postsynaptic abnormalities at the neuromuscular junctions of utrophin-deficient mice. J Cell Biol *136*, 883-894.
Deconinck, A.E., Rafael, J.A., Skinner, J.A., Brown, S.C., Potter, A.C., Metzinger, L., Watt, D.J., Dickson, J.G., Tinsley, J.M., and Davies, K.E. (1997b). Utrophin-dystrophin-deficient mice as a model for Duchenne muscular dystrophy. Cell *90*, 717-727.
Deconinck, N., Rafael, J., Beckers-Bleukx, G., Kahn, D., Davies, K., and Gillis, J.M. (1998). Consequences of the combined deficiency in dystrophin and utrophin on the mechanical properties and myosin composition of limb and respiratory muscles of the mouse. Pflug Arch Eur J Phy *435*, R250-R250.
Dellorusso, C., Crawford, R.W., Chamberlain, J.S., and Brooks, S.V. (2001). Tibialis anterior muscles in mdx mice are highly susceptible to contraction-induced injury. J Muscle Res Cell Motil *22*, 467-475.
Dennis, C.L., Tinsley, J.M., Deconinck, A.E., and Davies, K.E. (1996). Molecular and functional analysis of the utrophin promoter. Nucleic Acids Res *24*, 1646-1652.
DiMario, J.X., Uzman, A., and Strohman, R.C. (1991). Fiber regeneration is not persistent in dystrophic (MDX) mouse skeletal muscle. Dev Biol *148*, 314-321.
Dsouza, V.N., Man, N.T., Morris, G.E., Karges, W., Pillers, D.A.M., and Ray, P.N. (1995). A Novel Dystrophin Isoform Is Required for Normal Retinal Electrophysiology. Human Molecular Genetics *4*, 837-842.
Dynan, W.S., and Tjian, R. (1983). The promoter-specific transcription factor Sp1 binds to upstream sequences in the SV40 early promoter. Cell *35*, 79-87.
Ebihara, S., Guibinga, G.H., Gilbert, R., Nalbantoglu, J., Massie, B., Karpati, G., and Petrof, B.J. (2000). Differential effects of dystrophin and utrophin gene transfer in immunocompetent muscular dystrophy (mdx) mice. Physiol Genomics *3*, 133-144.
Eisenberg, I., Alexander, M.S., and Kunkel, L.M. (2009). miRNAS in normal and diseased skeletal muscle. J Cell Mol Med *13*, 2-11.
Eisenberg, I., Eran, A., Nishino, I., Moggio, M., Lamperti, C., Amato, A.A., Lidov, H.G., Kang, P.B., North, K.N., Mitrani-Rosenbaum, S*., et al.* (2007). Distinctive patterns of microRNA expression in primary muscular disorders.[erratum appears in Proc Natl Acad Sci U S A. 2008 Jan 8;105(1):399]. Proceedings of the National Academy of Sciences of the United States of America *104*, 17016-17021.
Elmen, J., Lindow, M., Schutz, S., Lawrence, M., Petri, A., Obad, S., Lindholm, M., Hedtjarn, M., Hansen, H.F., Berger, U*., et al.* (2008). LNA-mediated microRNA silencing in non-human primates. Nature *452*, 896-899.
Ervasti, J.M. (2007). Dystrophin, its interactions with other proteins, and implications for muscular dystrophy. Bba-Mol Basis Dis *1772*, 108-117.
Ervasti, J.M., and Campbell, K.P. (1993). A role for the dystrophin-glycoprotein complex as a transmembrane linker between laminin and actin. Journal of Cell Biology *122*, 809-823.
Fakhfakh, R., Michaud, A., and Tremblay, J.P. (2010). Blocking the Myostatin Signal With a Dominant Negative Receptor Improves the Success of Human Myoblast Transplantation in Dystrophic Mice. Mol Ther.
Farini, A., Meregalli, M., Belicchi, M., Battistelli, M., Parolini, D., D'Antona, G., Gavina, M., Ottoboni, L., Constantin, G., Bottinelli, R*., et al.* (2007). T and B lymphocyte depletion has a marked effect on the fibrosis of dystrophic skeletal muscles in the scid/mdx mouse. Journal of Pathology *213*, 229-238.
Farini, A., Razini, P., Erratico, S., Torrente, Y., and Meregalli, M. (2009). Cell based therapy for Duchenne muscular dystrophy. J Cell Physiol *221*, 526-534.

Filipowicz, W., Bhattacharyya, S.N., and Sonenberg, N. (2008). Mechanisms of post-transcriptional regulation by microRNAs: are the answers in sight? Nat Rev Genet *9*, 102-114.
Fisher, R., Tinsley, J.M., Phelps, S.R., Squire, S.E., Townsend, E.R., Martin, J.E., and Davies, K.E. (2001). Non-toxic ubiquitous over-expression of utrophin in the mdx mouse. Neuromuscular Disord *11*, 713-721.
Fracasso, C., and Patarnello, T. (1998). Evolution of the dystrophin muscular promoter and 5' flanking region in primates. J Mol Evol *46*, 168-179.
Friedman, R.C., Farh, K.K.H., Burge, C.B., and Bartel, D.P. (2009). Most mammalian mRNAs are conserved targets of microRNAs. Genome Research *19*, 92-105.
Galbiati, F., Razani, B., and Lisanti, M.P. (2001). Caveolae and caveolin-3 in muscular dystrophy. Trends Mol Med *7*, 435-441.
Galvagni, F., Capo, S., and Oliviero, S. (2001). Sp1 and Sp3 physically interact and co-operate with GABP for the activation of the utrophin promoter. J Mol Biol *306*, 985-996.
Galvagni, F., Lestingi, M., Cartocci, E., and Oliviero, S. (1997). Serum response factor and protein-mediated DNA bending contribute to transcription of the dystrophin muscle-specific promoter. Mol Cell Biol *17*, 1731-1743.
Giraldez, A.J., Cinalli, R.M., Glasner, M.E., Enright, A.J., Thomson, J.M., Baskerville, S., Hammond, S.M., Bartel, D.P., and Schier, A.F. (2005). MicroRNAs regulate brain morphogenesis in zebrafish. Science *308*, 833-838.
Glass, D.J. (2005). A signaling role for dystrophin: inhibiting skeletal muscle atrophy pathways. Cancer Cell *8*, 351-352.
Goldfarb, L.G., Park, K.Y., Cerven, x00E, kov, x00E, Gorokhova, S., Lee, H.S., Vasconcelos, O., Nagle, J.W*., et al.* (1998). Missense mutations in desmin associated with familial cardiac and skeletal myopathy. Nature Genetics *19*, 402-403.
Goyenvalle, A., Babbs, A., Powell, D., Kole, R., Fletcher, S., Wilton, S.D., and Davies, K.E. (2010). Prevention of Dystrophic Pathology in Severely Affected Dystrophin/Utrophin-deficient Mice by Morpholino-oligomer-mediated Exon-skipping. Molecular Therapy *18*, 198-205.
Grady, R.M., Grange, R.W., Lau, K.S., Maimone, M.M., Nichol, M.C., Stull, J.T., and Sanes, J.R. (1999). Role for alpha-dystrobrevin in the pathogenesis of dystrophin-dependent muscular dystrophies. Nat Cell Biol *1*, 215-220.
Grady, R.M., Teng, H., Nichol, M.C., Cunningham, J.C., Wilkinson, R.S., and Sanes, J.R. (1997). Skeletal and cardiac myopathies in mice lacking utrophin and dystrophin: a model for Duchenne muscular dystrophy. Cell *90*, 729-738.
Gramolini, A.O., Angus, L.M., Schaeffer, L., Burton, E.A., Tinsley, J.M., Davies, K.E., Changeux, J.P., and Jasmin, B.J. (1999). Induction of utrophin gene expression by heregulin in skeletal muscle cells: role of the N-box motif and GA binding protein. Proc Natl Acad Sci U S A *96*, 3223-3227.
Gramolini, A.O., Belanger, G., Thompson, J.M., Chakkalakal, J.V., and Jasmin, B.J. (2001). Increased expression of utrophin in a slow vs. a fast muscle involves posttranscriptional events. Am J Physiol Cell Physiol *281*, C1300-1309.
Gramolini, A.O., Dennis, C.L., Tinsley, J.M., Robertson, G.S., Cartaud, J., Davies, K.E., and Jasmin, B.J. (1997). Local transcriptional control of utrophin expression at the neuromuscular synapse. Journal of Biological Chemistry *272*, 8117-8120.
Gramolini, A.O., and Jasmin, B.J. (1999). Expression of the utrophin gene during myogenic differentiation. Nucleic Acids Res *27*, 3603-3609.
Granchelli (2000). Pre-clinical screening of drugs using the *mdx* mouse. Neuromuscular Disorders *10*, 235-239.

Greco, S., De Simone, M., Colussi, C., Zaccagnini, G., Fasanaro, P., Pescatori, M., Cardani, R., Perbellini, R., Isaia, E., Sale, P.*, et al.* (2009). Common micro-RNA signature in skeletal muscle damage and regeneration induced by Duchenne muscular dystrophy and acute ischemia. FASEB Journal *23*, 3335-3346.
Griffiths-Jones, S., Grocock, R.J., van Dongen, S., Bateman, A., and Enright, A.J. (2006). miRBase: microRNA sequences, targets and gene nomenclature. Nucleic Acids Res *34*, D140-144.
Grimson, A., Farh, K.K.H., Johnston, W.K., Garrett-Engele, P., Lim, L.P., and Bartel, D.P. (2007). MicroRNA targeting specificity in mammals: Determinants beyond seed pairing. Molecular Cell *27*, 91-105.
Grounds, M.D., Radley, H.G., Lynch, G.S., Nagaraju, K., and De Luca, A. (2008). Towards developing standard operating procedures for pre-clinical testing in the mdx mouse model of Duchenne muscular dystrophy. Neurobiol Dis *31*, 1-19.
Grum, V.L., Li, D., MacDonald, R.I., and Mondragon, A. (1999). Structures of two repeats of spectrin suggest models of flexibility. Cell *98*, 523-535.
Guo, C., Willem, M., Werner, A., Raivich, G., Emerson, M., Neyses, L., and Mayer, U. (2006). Absence of alpha 7 integrin in dystrophin-deficient mice causes a myopathy similar to Duchenne muscular dystrophy. Hum Mol Genet *15*, 989-998.
Gyrd-Hansen, M., Krag, T.O., Rosmarin, A.G., and Khurana, T.S. (2002). Sp1 and the ets-related transcription factor complex GABP alpha/beta functionally cooperate to activate the utrophin promoter. J Neurol Sci *197*, 27-35.
Handschin, C., Kobayashi, Y.M., Chin, S., Seale, P., Campbell, K.P., and Spiegelman, B.M. (2007). PGC-1alpha regulates the neuromuscular junction program and ameliorates Duchenne muscular dystrophy. Genes & Development *21*, 770-783.
Handschin, C., Rhee, J., Lin, J., Tarr, P.T., and Spiegelman, B.M. (2003). An autoregulatory loop controls peroxisome proliferator-activated receptor gamma coactivator 1alpha expression in muscle. Proceedings of the National Academy of Sciences of the United States of America *100*, 7111-7116.
Harper, S.Q., Hauser, M.A., DelloRusso, C., Duan, D., Crawford, R.W., Phelps, S.F., Harper, H.A., Robinson, A.S., Engelhardt, J.F., Brooks, S.V.*, et al.* (2002). Modular flexibility of dystrophin: implications for gene therapy of Duchenne muscular dystrophy.[see comment]. Nature Medicine *8*, 253-261.
He, L., He, X.Y., Lowe, S.W., and Hannon, G.J. (2007). microRNAs join the p53 network - another piece in the tumour-suppression puzzle. Nat Rev Cancer *7*, 819-822.
Hilger-Eversheim, K., Moser, M., Schorle, H., and Buettner, R. (2000). Regulatory roles of AP-2 transcription factors in vertebrate development, apoptosis and cell-cycle control. Gene *260*, 1-12.
Hoffman, E.P., and Dressman, D. (2001). Molecular pathophysiology and targeted therapeutics for muscular dystrophy. Trends Pharmacol Sci *22*, 465-470.
Hondares, E., Pineda-Torra, I., Iglesias, R., Staels, B., Villarroya, F., and Giralt, M. (2007). PPARdelta, but not PPARalpha, activates PGC-1alpha gene transcription in muscle. Biochem Biophys Res Commun *354*, 1021-1027.
Hopf, F.W., Turner, P.R., Denetclaw, W.F., Jr., Reddy, P., and Steinhardt, R.A. (1996). A critical evaluation of resting intracellular free calcium regulation in dystrophic mdx muscle. American Journal of Physiology *271*, C1325-1339.
Ichida, F., Tsubata, S., Bowles, K.R., Haneda, N., Uese, K., Miyawaki, T., Dreyer, W.J., Messina, J., Li, H., Bowles, N.E.*, et al.* (2001). Novel gene mutations in patients with left ventricular noncompaction or Barth syndrome. Circulation *103*, 1256-1263.

Ichim, T.E., Alexandrescu, D.T., Solano, F., Lara, F., Campion, R.D., Paris, E., Woods, E.J., Murphy, M.P., Dasanu, C.A., Patel, A.N*., et al.* (2010). Mesenchymal stem cells as anti-inflammatories: Implications for treatment of Duchenne muscular dystrophy. Cellular Immunology *260*, 75-82.
Imamura, M., Araishi, K., Noguchi, S., and Ozawa, E. (2000). A sarcoglycan-dystroglycan complex anchors Dp116 and utrophin in the peripheral nervous system. Hum Mol Genet *9*, 3091-3100.
Ishikawa-Sakurai, M., Yoshida, M., Imamura, M., Davies, K.E., and Ozawa, E. (2004). ZZ domain is essentially required for the physiological binding of dystrophin and utrophin to beta-dystroglycan. Human Molecular Genetics *13*, 693-702.
Ji, Z., Lee, J.Y., Pan, Z., Jiang, B., and Tian, B. (2009). Progressive lengthening of 3' untranslated regions of mRNAs by alternative polyadenylation during mouse embryonic development. Proc Natl Acad Sci U S A *106*, 7028-7033.
Jimenez-Mallebrera, C., Torelli, S., Feng, L., Kim, J., Godfrey, C., Clement, E., Mein, R., Abbs, S., Brown, S.C., Campbell, K.P*., et al.* (2009). A comparative study of alpha-dystroglycan glycosylation in dystroglycanopathies suggests that the hypoglycosylation of alpha-dystroglycan does not consistently correlate with clinical severity. Brain Pathol *19*, 596-611.
Jovanovic, M., and Hengartner, M.O. (2006). miRNAs and apoptosis: RNAs to die for. Oncogene *25*, 6176-6187.
Karpati, G., and Carpenter, S. (1986). Small-caliber skeletal muscle fibers do not suffer deleterious consequences of dystrophic gene expression. American Journal of Medical Genetics *25*, 653-658.
Khurana, T.S., and Davies, K.E. (2003). Pharmacological strategies for muscular dystrophy. Nat Rev Drug Discov *2*, 379-390.
Khurana, T.S., Rosmarin, A.G., Shang, J., Krag, T.O.B., Das, S., and Gammeltoft, S. (1999). Activation of utrophin promoter by heregulin via the ets-related transcription factor complex GA-binding protein alpha/beta. Molecular Biology of the Cell *10*, 2075-2086.
Khurana, T.S., Watkins, S.C., Chafey, P., Chelly, J., Tome, F.M., Fardeau, M., Kaplan, J.C., and Kunkel, L.M. (1991). Immunolocalization and developmental expression of dystrophin related protein in skeletal muscle. Neuromuscul Disord *1*, 185-194.
Kim, M.S., Kim, S.Y., Arunachalam, S., Hwang, P.H., Yi, H.K., Nam, S.Y., and Lee, D.Y. (2009). c-myb stimulates cell growth by regulation of insulin-like growth factor (IGF) and IGF-binding protein-3 in K562 leukemia cells. Biochem Bioph Res Co *385*, 38-43.
Kim, V.N. (2005). MicroRNA biogenesis: coordinated cropping and dicing. Nat Rev Mol Cell Biol *6*, 376-385.
Kinali, M., Arechavala-Gomeza, V., Feng, L., Cirak, S., Hunt, D., Adkin, C., Guglieri, M., Ashton, E., Abbs, S., Nihoyannopoulos, P*., et al.* (2009). Local restoration of dystrophin expression with the morpholino oligomer AVI-4658 in Duchenne muscular dystrophy: a single-blind, placebo-controlled, dose-escalation, proof-of-concept study. Lancet Neurol *8*, 918-928.
Kobayashi, K., Nakahori, Y., Miyake, M., Matsumura, K., Kondo-Iida, E., Nomura, Y., Segawa, M., Yoshioka, M., Saito, K., Osawa, M*., et al.* (1998). An ancient retrotransposal insertion causes Fukuyama-type congenital muscular dystrophy. Nature *394*, 388-392.
Koenig, M., Monaco, A.P., and Kunkel, L.M. (1988). The complete sequence of dystrophin predicts a rod-shaped cytoskeletal protein. Cell *53*, 219-228.
Koike, S., Schaeffer, L., and Changeux, J.P. (1995). Identification of a DNA element determining synaptic expression of the mouse acetylcholine receptor delta-subunit gene. Proc Natl Acad Sci U S A *92*, 10624-10628.
Krag, T.O.B., Bogdanovich, S., Jensen, C.J., Fischer, M.D., Hansen-Schwartz, J., Javazon, E.H., Flake, A.W., Edvinsson, L., and Khurana, T.S. (2004). Heregulin ameliorates the dystrophic phenotype in mdx mice. P Natl Acad Sci USA *101*, 13856-13860.

Krutzfeldt, J., Rajewsky, N., Braich, R., Rajeev, K.G., Tuschl, T., Manoharan, M., and Stoffel, M. (2005). Silencing of microRNAs in vivo with 'antagomirs'. Nature *438*, 685-689.
Kumar, M.S., Lu, J., Mercer, K.L., Golub, T.R., and Jacks, T. (2007). Impaired microRNA processing enhances cellular transformation and tumorigenesis. Nat Genet *39*, 673-677.
Lagos-Quintana, M., Rauhut, R., Lendeckel, W., and Tuschl, T. (2001). Identification of novel genes coding for small expressed RNAs. Science *294*, 853-858.
Lai, Y., Thomas, G.D., Yue, Y., Yang, H.T., Li, D., Long, C., Judge, L., Bostick, B., Chamberlain, J.S., Terjung, R.L*., et al.* (2009). Dystrophins carrying spectrin-like repeats 16 and 17 anchor nNOS to the sarcolemma and enhance exercise performance in a mouse model of muscular dystrophy. J Clin Invest *119*, 624-635.
Lau, N.C., Lim, L.P., Weinstein, E.G., and Bartel, D.P. (2001). An abundant class of tiny RNAs with probable regulatory roles in Caenorhabditis elegans. Science *294*, 858-862.
Lee, R.C., and Ambros, V. (2001). An extensive class of small RNAs in Caenorhabditis elegans. Science *294*, 862-864.
Lee, R.C., Feinbaum, R.L., and Ambros, V. (1993). The C-Elegans Heterochronic Gene Lin-4 Encodes Small Rnas with Antisense Complementarity to Lin-14. Cell *75*, 843-854.
Levine, B.A., Moir, A.J., Patchell, V.B., and Perry, S.V. (1990). The interaction of actin with dystrophin. FEBS Lett *263*, 159-162.
Li, D., Bareja, A., Judge, L., Yue, Y., Lai, Y., Fairclough, R., Davies, K.E., Chamberlain, J.S., and Duan, D. (2010). Sarcolemmal nNOS anchoring reveals a qualitative difference between dystrophin and utrophin. Journal of Cell Science *123*, 2008-2013.
Li, Z., Colucci-Guyon, E., Pin, x00E, on-Raymond, M., Mericskay, M., Pournin, S., Paulin, D., and Babinet, C. (1996). Cardiovascular lesions and skeletal myopathy in mice lacking desmin. Developmental Biology *175*, 362-366.
Lidov, H.G., Selig, S., and Kunkel, L.M. (1995). Dp140: a novel 140 kDa CNS transcript from the dystrophin locus. Hum Mol Genet *4*, 329-335.
Lim, L.E., Duclos, F., Broux, O., Bourg, N., Sunada, Y., Allamand, V., Meyer, J., Richard, I., Moomaw, C., Slaughter, C*., et al.* (1995). Beta-sarcoglycan: characterization and role in limb-girdle muscular dystrophy linked to 4q12. Nat Genet *11*, 257-265.
Lin, J., Wu, H., Tarr, P.T., Zhang, C.Y., Wu, Z., Boss, O., Michael, L.F., Puigserver, P., Isotani, E., Olson, E.N*., et al.* (2002). Transcriptional co-activator PGC-1 alpha drives the formation of slow-twitch muscle fibres. Nature *418*, 797-801.
Liu, X., Sempere, L.F., Ouyang, H., Memoli, V.A., Andrew, A.S., Luo, Y., Demidenko, E., Korc, M., Shi, W., Preis, M*., et al.* (2010). MicroRNA-31 functions as an oncogenic microRNA in mouse and human lung cancer cells by repressing specific tumor suppressors. Journal of Clinical Investigation *120*, 1298-1309.
Longman, C., Brockington, M., Torelli, S., Jimenez-Mallebrera, C., Kennedy, C., Khalil, N., Feng, L., Saran, R.K., Voit, T., Merlini, L*., et al.* (2003). Mutations in the human LARGE gene cause MDC1D, a novel form of congenital muscular dystrophy with severe mental retardation and abnormal glycosylation of alpha-dystroglycan. Hum Mol Genet *12*, 2853-2861.
Luca, D. (2002). Enhanced dystrophic progression in mdx mice by exercise and beneficial effects of taurine and insulin-like growth factor-1. The Journal of Pharmacology and Experimental Techniques *304*, 453-463.
Luca, D. (2005). A multidisciplinary evaluation of the effectiveness of cyclosporine A in dystrophic mdx mice. American Journal of Pathology *166*, 477-489.
Luquet, S., Lopez-Soriano, J., Holst, D., Fredenrich, A., Melki, J., Rassoulzadegan, M., and Grimaldi, P.A. (2003). Peroxisome proliferator-activated receptor delta controls muscle development and oxidative capability. FASEB Journal *17*, 2299-2301.

Lynch, G.S., Hinkle, R.T., Chamberlain, J.S., Brooks, S.V., and Faulkner, J.A. (2001). Force and power output of fast and slow skeletal muscles from mdx mice 6-28 months old. J Physiol *535*, 591-600.
Lynch, G.S., Hinkle, R.T., and Faulkner, J.A. (2000). Power output of fast and slow skeletal muscles of mdx (dystrophic) and control mice after clenbuterol treatment. Experimental Physiology *85*, 295-299.
Malik, V., Rodino-Klapac, L.R., Viollet, L., Wall, C., King, W., Al-Dahhak, R., Lewis, S., Shilling, C.J., Kota, J., Serrano-Munuera, C*., et al.* (2010). Gentamicin-induced readthrough of stop codons in Duchenne muscular dystrophy. Ann Neurol *67*, 771-780.
Manuvakhova, M., Keeling, K., and Bedwell, D.M. (2000). Aminoglycoside antibiotics mediate context-dependent suppression of termination codons in a mammalian translation system. Rna *6*, 1044-1055.
Manzur, A.Y., and Muntoni, F. (2009). Diagnosis and new treatments in muscular dystrophies. Postgrad Med J *85*, 622-630.
Marin, M., Karis, A., Visser, P., Grosveld, F., and Philipsen, S. (1997). Transcription factor Sp1 is essential for early embryonic development but dispensable for cell growth and differentiation. Cell *89*, 619-628.
Marini, J.F., Pons, F., Leger, J., Loffreda, N., Anoal, M., Chevallay, M., Fardeau, M., and Leger, J.J. (1991). Expression of myosin heavy chain isoforms in Duchenne muscular dystrophy patients and carriers. Neuromuscul Disord *1*, 397-409.
McCarthy, J.J., Esser, K.A., and Andrade, F.H. (2007). MicroRNA-206 is overexpressed in the diaphragm but not the hindlimb muscle of mdx mouse. Am J Physiol Cell Physiol *293*, C451-457.
McClorey, G., Moulton, H.M., Iversen, P.L., Fletcher, S., and Wilton, S.D. (2006). Antisense oligonucleotide-induced exon skipping restores dystrophin expression in vitro in a canine model of DMD. Gene Ther *13*, 1373-1381.
McCullagh, K.J., Edwards, B., Kemp, M.W., Giles, L.C., Burgess, M., and Davies, K.E. (2008). Analysis of skeletal muscle function in the C57BL6/SV129 syncoilin knockout mouse. Mammalian Genome *19*, 339-351.
McNally, E.M., Duggan, D., Gorospe, J.R., Bonnemann, C.G., Fanin, M., Pegoraro, E., Lidov, H.G., Noguchi, S., Ozawa, E., Finkel, R.S*., et al.* (1996). Mutations that disrupt the carboxyl-terminus of gamma-sarcoglycan cause muscular dystrophy. Hum Mol Genet *5*, 1841-1847.
McPherron, A.C., Lawler, A.M., and Lee, S.J. (1997). Regulation of skeletal muscle mass in mice by a new TGF-beta superfamily member. Nature *387*, 83-90.
Megeney, L.A., Kablar, B., Garrett, K., Anderson, J.E., and Rudnicki, M.A. (1996). MyoD is required for myogenic stem cell function in adult skeletal muscle. Genes Dev *10*, 1173-1183.
Megeney, L.A., Kablar, B., Perry, R.L., Ying, C., May, L., and Rudnicki, M.A. (1999). Severe cardiomyopathy in mice lacking dystrophin and MyoD. Proc Natl Acad Sci U S A *96*, 220-225.
Michalik, L., Desvergne, B., and Wahli, W. (2004). Peroxisome-proliferator-activated receptors and cancers: complex stories. Nat Rev Cancer *4*, 61-70.
Miska, E.A., Alvarez-Saavedra, E., Townsend, M., Yoshii, A., Sestan, N., Rakic, P., Constantine-Paton, M., and Horvitz, H.R. (2004). Microarray analysis of microRNA expression in the developing mammalian brain. Genome Biol *5*, R68.
Miura, P., Chakkalakal, J.V., Boudreault, L., Belanger, G., Hebert, R.L., Renaud, J.M., and Jasmin, B.J. (2009). Pharmacological activation of PPARbeta/delta stimulates utrophin A expression in skeletal muscle fibers and restores sarcolemmal integrity in mature mdx mice. Hum Mol Genet *18*, 4640-4649.
Miura, P., and Jasmin, B.J. (2006). Utrophin upregulation for treating Duchenne or Becker muscular dystrophy: how close are we? Trends Mol Med *12*, 122-129.

Mizuno, Y., Thompson, T.G., Guyon, J.R., Lidov, H.G., Brosius, M., Imamura, M., Ozawa, E., Watkins, S.C., and Kunkel, L.M. (2001). Desmuslin, an intermediate filament protein that interacts with alpha -dystrobrevin and desmin. P Natl Acad Sci USA *98*, 6156-6161.
Moens, P., Baatsen, P.H., and Marechal, G. (1993). Increased susceptibility of EDL muscles from mdx mice to damage induced by contractions with stretch. J Muscle Res Cell Motil *14*, 446-451.
Morrison, J., Lu, Q.L., Pastoret, C., Partridge, T., and Bou-Gharios, G. (2000). T-cell-dependent fibrosis in the mdx dystrophic mouse. Lab Invest *80*, 881-891.
Mu, x00F, oz, M., x00E, rmol, A.M., Strasser, G., Isamat, M., Coulombe, P.A., Yang, Y., Roca, X*., et al.* (1998). A dysfunctional desmin mutation in a patient with severe generalized myopathy. P Natl Acad Sci USA *95*, 11312-11317.
Narkar, V.A., Downes, M., Yu, R.T., Embler, E., Wang, Y.X., Banayo, E., Mihaylova, M.M., Nelson, M.C., Zou, Y., Juguilon, H*., et al.* (2008). AMPK and PPARdelta agonists are exercise mimetics. Cell *134*, 405-415.
Newey, S.E., Howman, E.V., Ponting, C.P., Benson, M.A., Nawrotzki, R., Loh, N.Y., Davies, K.E., and Blake, D.J. (2001). Syncoilin, a novel member of the intermediate filament superfamily that interacts with alpha-dystrobrevin in skeletal muscle. Journal of Biological Chemistry *276*, 6645-6655.
Nigro, V., de Sa Moreira, E., Piluso, G., Vainzof, M., Belsito, A., Politano, L., Puca, A.A., Passos-Bueno, M.R., and Zatz, M. (1996a). Autosomal recessive limb-girdle muscular dystrophy, LGMD2F, is caused by a mutation in the delta-sarcoglycan gene. Nat Genet *14*, 195-198.
Nigro, V., Piluso, G., Belsito, A., Politano, L., Puca, A.A., Papparella, S., Rossi, E., Viglietto, G., Esposito, M.G., Abbondanza, C*., et al.* (1996b). Identification of a novel sarcoglycan gene at 5q33 encoding a sarcolemmal 35 kDa glycoprotein. Hum Mol Genet *5*, 1179-1186.
Nowak, K.J., and Davies, K.E. (2004). Duchenne muscular dystrophy and dystrophin: pathogenesis and opportunities for treatment. EMBO Rep *5*, 872-876.
O'Brien, K.F., and Kunkel, L.M. (2001). Dystrophin and muscular dystrophy: past, present, and future. Mol Genet Metab *74*, 75-88.
Obernosterer, G., Leuschner, P.J., Alenius, M., and Martinez, J. (2006). Post-transcriptional regulation of microRNA expression. Rna-A Publication of the Rna Society *12*, 1161-1167.
Ohlendieck, K., Ervasti, J.M., Matsumura, K., Kahl, S.D., Leveille, C.J., and Campbell, K.P. (1991). Dystrophin-related protein is localized to neuromuscular junctions of adult skeletal muscle. Neuron *7*, 499-508.
Ojuka, E.O., Jones, T.E., Han, D.H., Chen, M., and Holloszy, J.O. (2003). Raising Ca2+ in L6 myotubes mimics effects of exercise on mitochondrial biogenesis in muscle. Faseb J *17*, 675-681.
Olaru, A.V., Selaru, F.M., Mori, Y., Vazquez, C., David, S., Paun, B., Cheng, Y., Jin, Z., Yang, J., Agarwal, R*., et al.* (2010). Dynamic changes in the expression of MicroRNA-31 during inflammatory bowel disease-associated neoplastic transformation. Inflamm Bowel Dis.
Olson, E.N. (1993). Regulation of muscle transcription by the MyoD family. The heart of the matter. Circ Res *72*, 1-6.
Olson, E.N., and Williams, R.S. (2000). Remodeling muscles with calcineurin. Bioessays *22*, 510-519.
Orom, U.A., and Lund, A.H. (2010). Experimental identification of microRNA targets. Gene *451*, 1-5.
Ozawa, E., Hagiwara, Y., and Yoshida, M. (1999). Creatine kinase, cell membrane and Duchenne muscular dystrophy. Molecular & Cellular Biochemistry *190*, 143-151.
Ozawa, E., Mizuno, Y., Hagiwara, Y., Sasaoka, T., and Yoshida, M. (2005). Molecular and cell biology of the sarcoglycan complex. Muscle Nerve *32*, 563-576.

Park, B.H., Vogelstein, B., and Kinzler, K.W. (2001). Genetic disruption of PPARdelta decreases the tumorigenicity of human colon cancer cells. Proc Natl Acad Sci U S A *98*, 2598-2603.
Partridge, T. (2010). The potential of exon skipping for treatment for Duchenne muscular dystrophy. J Child Neurol *25*, 1165-1170.
Pastoret, C., and Sebille, A. (1995). mdx mice show progressive weakness and muscle deterioration with age. Journal of the Neurological Sciences *129*, 97-105.
Pearce, M., Blake, D.J., Tinsley, J.M., Byth, B.C., Campbell, L., Monaco, A.P., and Davies, K.E. (1993). The utrophin and dystrophin genes share similarities in genomic structure. Hum Mol Genet *2*, 1765-1772.
Perkins, K.J., Burton, E.A., and Davies, K.E. (2001). The role of basal and myogenic factors in the transcriptional activation of utrophin promoter A: implications for therapeutic up-regulation in Duchenne muscular dystrophy. Nucleic Acids Res *29*, 4843-4850.
Perkins, K.J., and Davies, K.E. (2002). The role of utrophin in the potential therapy of Duchenne muscular dystrophy. Neuromuscul Disord *12 Suppl 1*, S78-89.
Peters, M.F., Adams, M.E., and Froehner, S.C. (1997). Differential association of syntrophin pairs with the dystrophin complex. J Cell Biol *138*, 81-93.
Peters, M.F., Sadoulet-Puccio, H.M., Grady, R.M., Kramarcy, N.R., Kunkel, L.M., Sanes, J.R., Sealock, R., and Froehner, S.C. (1998). Differential membrane localization and intermolecular associations of alpha-dystrobrevin isoforms in skeletal muscle. Journal of Cell Biology *142*, 1269-1278.
Petrof, B.J., Stedman, H.H., Shrager, J.B., Eby, J., Sweeney, H.L., and Kelly, A.M. (1993). Adaptations in myosin heavy chain expression and contractile function in dystrophic mouse diaphragm. Am J Physiol *265*, C834-841.
Pettersson, I., Ebdrup, S., Havranek, M., Pihera, P., Korinek, M., Mogensen, J.P., Jeppesen, C.B., Johansson, E., and Sauerberg, P. (2007). Design of a partial PPARdelta agonist. Bioorganic & Medicinal Chemistry Letters *17*, 4625-4629.
Piccolo, F., Roberds, S.L., Jeanpierre, M., Leturcq, F., Azibi, K., Beldjord, C., Carrie, A., Recan, D., Chaouch, M., Reghis, A*., et al.* (1995). Primary adhalinopathy: a common cause of autosomal recessive muscular dystrophy of variable severity. Nat Genet *10*, 243-245.
Pillai, R.S., Bhattacharyya, S.N., and Filipowicz, W. (2007). Repression of protein synthesis by miRNAs: how many mechanisms? Trends Cell Biol *17*, 118-126.
Pons, F., Nicholson, L.V., Robert, A., Voit, T., and Leger, J.J. (1993). Dystrophin and dystrophin-related protein (utrophin) distribution in normal and dystrophin-deficient skeletal muscles. Neuromuscul Disord *3*, 507-514.
Poon, E., Howman, E.V., Newey, S.E., and Davies, K.E. (2002). Association of syncoilin and desmin: linking intermediate filament proteins to the dystrophin-associated protein complex. Journal of Biological Chemistry *277*, 3433-3439.
Prochniewicz, E., Henderson, D., Ervasti, J.M., and Thomas, D.D. (2009). Dystrophin and utrophin have distinct effects on the structural dynamics of actin. P Natl Acad Sci USA *106*, 7822-7827.
Qiao, C., Li, J., Jiang, J., Zhu, X., Wang, B., and Xiao, X. (2008). Myostatin propeptide gene delivery by adeno-associated virus serotype 8 vectors enhances muscle growth and ameliorates dystrophic phenotypes in mdx mice. Hum Gene Ther *19*, 241-254.
Rafael, J.A., Townsend, E.R., Squire, S.E., Potter, A.C., Chamberlain, J.S., and Davies, K.E. (2000). Dystrophin and utrophin influence fiber type composition and post-synaptic membrane structure. Human Molecular Genetics *9*, 1357-1367.

Rao, P.K., Kumar, R.M., Farkhondeh, M., Baskerville, S., and Lodish, H.F. (2006). Myogenic factors that regulate expression of muscle-specific microRNAs. Proc Natl Acad Sci U S A *103*, 8721-8726.
Rapaport, D., Fuchs, O., Nudel, U., and Yaffe, D. (1992). Expression of the Duchenne Muscular-Dystrophy Gene-Products in Embryonic Stem-Cells and Their Differentiated Derivatives. Journal of Biological Chemistry *267*, 21289-21292.
Reiser, P.J., Moss, R.L., Giulian, G.G., and Greaser, M.L. (1985). Shortening velocity and myosin heavy chains of developing rabbit muscle fibers. Journal of Biological Chemistry *260*, 14403-14405.
Ridgley, J.A., Pinniger, G.J., Hamer, P.W., and Grounds, M.D. (2009). The physiological effects of IGF-1 (class 1:Ea transgene) over-expression on exercise-induced damage and adaptation in dystrophic muscles of mdx mice. Pflugers Arch *457*, 1121-1132.
Roberds, S.L., Leturcq, F., Allamand, V., Piccolo, F., Jeanpierre, M., Anderson, R.D., Lim, L.E., Lee, J.C., Tome, F.M., Romero, N.B.*, et al.* (1994). Missense mutations in the adhalin gene linked to autosomal recessive muscular dystrophy. Cell *78*, 625-633.
Roberts, R.G., and Bobrow, M. (1998). Dystrophins in vertebrates and invertebrates. Human Molecular Genetics *7*, 589-595.
Rosenberg, M.I., Georges, S.A., Asawachaicharn, A., Analau, E., and Tapscott, S.J. (2006). MyoD inhibits Fstl1 and Utrn expression by inducing transcription of miR-206. J Cell Biol *175*, 77-85.
Royuela, M., Chazalette, D., Hugon, G., Paniagua, R., Guerlavais, V., Fehrentz, J.A., Martinez, J., Labbe, J.P., Rivier, F., and Mornet, D. (2003). Formation of multiple complexes between beta-dystroglycan and dystrophin family products. J Muscle Res Cell Motil *24*, 387-397.
Rybakova, I.N., Amann, K.J., and Ervasti, J.M. (1996). A new model for the interaction of dystrophin with F-actin. J Cell Biol *135*, 661-672.
Rybakova, I.N., and Ervasti, J.M. (2005). Identification of spectrin-like repeats required for high affinity utrophin-actin interaction. J Biol Chem *280*, 23018-23023.
Rybakova, I.N., Humston, J.L., Sonnemann, K.J., and Ervasti, J.M. (2006). Dystrophin and utrophin bind actin through distinct modes of contact. Journal of Biological Chemistry *281*, 9996-10001.
Rybakova, I.N., Patel, J.R., Davies, K.E., Yurchenco, P.D., and Ervasti, J.M. (2002). Utrophin binds laterally along actin filaments and can couple costameric actin with sarcolemma when overexpressed in dystrophin-deficient muscle. Molecular Biology of the Cell *13*, 1512-1521.
Rybakova, I.N., Patel, J.R., and Ervasti, J.M. (2000). The dystrophin complex forms a mechanically strong link between the sarcolemma and costameric actin. Journal of Cell Biology *150*, 1209-1214.
Sampaolesi, M., Blot, S., D'Antona, G., Granger, N., Tonlorenzi, R., Innocenzi, A., Mognol, P., Thibaud, J.L., Galvez, B.G., Barthelemy, I.*, et al.* (2006). Mesoangioblast stem cells ameliorate muscle function in dystrophic dogs. Nature *444*, 574-579.
Sarkar, S., Dey, B.K., and Dutta, A. (2010). MiR-322/424 and-503 Are Induced during Muscle Differentiation and Promote Cell Cycle Quiescence and Differentiation by Down-Regulation of Cdc25A. Molecular Biology of the Cell *21*, 2138-2149.
Schaeffer, P.J., Wende, A.R., Magee, C.J., Neilson, J.R., Leone, T.C., Chen, F., and Kelly, D.P. (2004). Calcineurin and calcium/calmodulin-dependent protein kinase activate distinct metabolic gene regulatory programs in cardiac muscle. J Biol Chem *279*, 39593-39603.
Schiaffino, S., and Reggiani, C. (1996). Molecular diversity of myofibrillar proteins: gene regulation and functional significance. Physiol Rev *76*, 371-423.

Sicinski, P., Geng, Y., Ryder-Cook, A.S., Barnard, E.A., Darlison, M.G., and Barnard, P.J. (1989). The molecular basis of muscular dystrophy in the mdx mouse: a point mutation. Science *244*, 1578-1580.
Skuk, D. (2004). Myoblast transplantation for inherited myopathies: a clinical approach. Expert opinion on biological therapy *4*, 1871-1885.
Stupka, N., Plant, D.R., Schertzer, J.D., Emerson, T.M., Bassel-Duby, R., Olson, E.N., and Lynch, G.S. (2006). Activated calcineurin ameliorates contraction-induced injury to skeletal muscles of mdx dystrophic mice. Journal of Physiology *575*, 645-656.
Talts, J.F., Andac, Z., x00F, hring, W., Brancaccio, A., and Timpl, R. (1999). Binding of the G domains of laminin alpha1 and alpha2 chains and perlecan to heparin, sulfatides, alpha-dystroglycan and several extracellular matrix proteins. EMBO Journal *18*, 863-870.
Tanaka, T., Yamamoto, J., Iwasaki, S., Asaba, H., Hamura, H., Ikeda, Y., Watanabe, M., Magoori, K., Ioka, R.X., Tachibana, K.*, et al.* (2003). Activation of peroxisome proliferator-activated receptor delta induces fatty acid beta-oxidation in skeletal muscle and attenuates metabolic syndrome. Proc Natl Acad Sci U S A *100*, 15924-15929.
Tinsley, J., Deconinck, N., Fisher, R., Kahn, D., Phelps, S., Gillis, J.M., and Davies, K. (1998). Expression of full-length utrophin prevents muscular dystrophy in mdx mice. Nat Med *4*, 1441-1444.
Tinsley, J.M., Blake, D.J., Roche, A., Fairbrother, U., Riss, J., Byth, B.C., Knight, A.E., Kendrickjones, J., Suthers, G.K., Love, D.R.*, et al.* (1992). Primary Structure of Dystrophin-Related Protein. Nature *360*, 591-593.
Tonino, P., Pappas, C.T., Hudson, B.D., Labeit, S., Gregorio, C.C., and Granzier, H. (2010). Reduced myofibrillar connectivity and increased Z-disk width in nebulin-deficient skeletal muscle. J Cell Sci *123*, 384-391.
Trollet, C., Athanasopoulos, T., Popplewell, L., Malerba, A., and Dickson, G. (2009). Gene therapy for muscular dystrophy: current progress and future prospects. Expert Opin Biol Ther *9*, 849-866.
Turk, R., Sterrenburg, E., de Meijer, E.J., van Ommen, G.J., den Dunnen, J.T., and t Hoen, P.A. (2005). Muscle regeneration in dystrophin-deficient mdx mice studied by gene expression profiling. Bmc Genomics *6*, 98.
Turner, P.R., Fong, P.Y., Denetclaw, W.F., and Steinhardt, R.A. (1991). Increased calcium influx in dystrophic muscle. J Cell Biol *115*, 1701-1712.
Vaillend, C., and Ungerer, A. (1999). Behavioral characterization of mdx3cv mice deficient in C-terminal dystrophins. Neuromuscular Disord *9*, 296-304.
Venema, V.J., Ju, H., Zou, R., and Venema, R.C. (1997). Interaction of neuronal nitric-oxide synthase with caveolin-3 in skeletal muscle. Identification of a novel caveolin scaffolding/inhibitory domain. J Biol Chem *272*, 28187-28190.
Vester, B., and Wengel, J. (2004). LNA (locked nucleic acid): high-affinity targeting of complementary RNA and DNA. Biochemistry *43*, 13233-13241.
Voisin, V., Sebrie, C., Matecki, S., Yu, H., Gillet, B., Ramonatxo, M., Israel, M., and De la Porte, S. (2005). L-arginine improves dystrophic phenotype in mdx mice. Neurobiology of Disease *20*, 123-130.
Wang, Y.X., Zhang, C.L., Yu, R.T., Cho, H.K., Nelson, M.C., Bayuga-Ocampo, C.R., Ham, J., Kang, H., and Evans, R.M. (2004). Regulation of muscle fiber type and running endurance by PPARdelta. PLoS Biol *2*, e294.
Webster, C., Silberstein, L., Hays, A.P., and Blau, H.M. (1988). Fast muscle fibers are preferentially affected in Duchenne muscular dystrophy. Cell *52*, 503-513.

Wehling, M., Spencer, M.J., and Tidball, J.G. (2001). A nitric oxide synthase transgene ameliorates muscular dystrophy in mdx mice. J Cell Biol *155*, 123-131.
Welch, E.M., Barton, E.R., Zhuo, J., Tomizawa, Y., Friesen, W.J., Trifillis, P., Paushkin, S., Patel, M., Trotta, C.R., Hwang, S.W.*, et al.* (2007). PTC124 targets genetic disorders caused by nonsense mutations. Nature *447*, 87-U86.
Williams, T., and Tjian, R. (1991). Characterization of a dimerization motif in AP-2 and its function in heterologous DNA-binding proteins. Science *251*, 1067-1071.
Williamson, R.A., Henry, M.D., Daniels, K.J., Hrstka, R.F., Lee, J.C., Sunada, Y., Ibraghimov-Beskrovnaya, O., and Campbell, K.P. (1997). Dystroglycan is essential for early embryonic development: disruption of Reichert's membrane in Dag1-null mice. Hum Mol Genet *6*, 831-841.
Willmann, R., Possekel, S., Dubach-Powell, J., Meier, T., and Ruegg, M.A. (2009). Mammalian animal models for Duchenne muscular dystrophy. Neuromuscul Disord *19*, 241-249.
Winder, S.J., Hemmings, L., Maciver, S.K., Bolton, S.J., Tinsley, J.M., Davies, K.E., Critchley, D.R., and Kendrick-Jones, J. (1995). Utrophin actin binding domain: analysis of actin binding and cellular targeting. J Cell Sci *108 (Pt 1)*, 63-71.
Yang, N., Kaur, S., Volinia, S., Greshock, J., Lassus, H., Hasegawa, K., Liang, S., Leminen, A., Deng, S., Smith, L.*, et al.* (2008). MicroRNA microarray identifies Let-7i as a novel biomarker and therapeutic target in human epithelial ovarian cancer. Cancer Research *68*, 10307-10314.
Yuasa, K., Hagiwara, Y., Ando, M., Nakamura, A., Takeda, S., and Hijikata, T. (2008). MicroRNA-206 is highly expressed in newly formed muscle fibers: implications regarding potential for muscle regeneration and maturation in muscular dystrophy. Cell Struct Funct *33*, 163-169.
Zhang, J., Bang, M.L., Gokhin, D.S., Lu, Y., Cui, L., Li, X., Gu, Y., Dalton, N.D., Scimia, M.C., Peterson, K.L.*, et al.* (2008). Syncoilin is required for generating maximum isometric stress in skeletal muscle but dispensable for muscle cytoarchitecture. American Journal of Physiology - Cell Physiology *294*, C1175-1182.